Spring 2001

SPICE-Based Heat Transport Model for Non-Intrusive Thermal Diagnostic Applications

Michael Stelzer
Old Dominion University

SPICE BASED HEAT TRANSPORT MODEL FOR

NON-INTRUSIVE THERMAL DIAGONSTIC APPLICATIONS

by
Michael Stelzer
B.S. in Electrical Engineering Technology
DeVry Institute of Technology, Columbus, Ohio.

A Thesis submitted to the faculty of
Old Dominion University in Partial Fulfillment of the
Requirement for the Degree of

MASTER OF SCIENCE

ELECTRICAL ENGINEERING

OLD DOMINION UNIVERSITY
MAY 2001

Approved by:

Dr. Ravindra P. Joshi (Director)

Dr. Linda Vahala (Member)

Dr. Frederic McKenzie (Member)

ABSTRACT

SPICE BASED HEAT TRANSPORT MODEL FOR NON-INTRUSIVE THERMAL DIAGONSTIC APPLICATIONS

Michael Stelzer

Old Dominion University

Director: Dr. Ravindra P. Joshi

Nondestructive material testing and diagnostics play an important role in reliability analysis, component wear-out testing, life-cycle estimates, and safety inspections. Of the several techniques available for nondestructive inspections, thermal analysis has been chosen to be the focus of this thesis research. An equivalence between the system of equations for the heat flow problem, and the variables of circuit theory suggests that an electrical model can be constructed to represent the actual thermal system. This electrical model is constructed based upon a finite difference discretization of the heat flow equation. Using these associations a basic one-dimensional electrical model has been constructed and linked with a circuit simulator (such as SPICE) to simulate the transient, steady state and ac heating scenarios of a sample thermal system. The basic model has been proven to accurately represent the thermal system. It has then been expanded to include temperature dependence of the conductivity parameter (with the aid of voltage controlled resistors) and multidimensional heat flow by extending the one-dimensional circuit along various directions. Finally, this SPICE-based model has been applied for thermal analysis of samples containing surface material defects such as cracks. It is shown that the model can adequately locate such cracks based upon the electro-thermal

relationships between time delay and voltage (temperature) magnitudes. It would thus be a useful simulation tool in the analysis of defects and for investigating non-intrusive thermal diagnostic response.

ACKNOWLEDGEMENTS

I would like to thank Dr. Ravindra Joshi for his guidance and support as my academic and thesis advisor. I would also like to take this opportunity to thank Dr. Linda Vahala and Dr. Frederic McKenzie for their time and consideration in serving on my thesis guidance committee. Finally, I want to thank Timothy Matich and Edward Gossman for introducing me to computer office software.

TABLE OF CONTENTS

LIST OF TABLES

Table **Page**

LIST OF FIGURES

Figure **Page**

CHAPTER 1

INTRODUCTION

1.1 THERMAL ISSUES AND THEIR ROLE IN ENGINEERING

Heat and thermal conduction play an important role consideration in several engineering fields. The production of heat is often a desirable product, such as in the case of welding, to produce energy such as the result of fuel combustion, to drive chemical reactions and affect their kinetics, and so on. At other times, it exists as an undesirable by-product, such as in friction, power dissipation in electrical components, and material property alterations. Thermal transport can similarly be beneficial in applications such as forced cooling to prevent over-heating, to contain thermal breakdown in semiconductor electronics, or to supply directed energy from a supply source to a receiving element. For such purposes, heat is usually removed from the system through an air or fluid cooling system. An example of a fluid cooling system will be presented in the heat convection section of this text. Transport can also be detrimental in that it leads to losses through undesirable thermal leakage and reduces the efficiency of thermal systems.

Heat induced by friction occurs when two objects in contact rub together. The continuous rubbing of the materials creates a heat build up at the area of contact. When an electrical current experiences a resistance, energy is lost in the form of heat. This heat is usually radiated from the component directly or is transferred via conduction to an attached heat sink. The heat sink absorbs a great portion of the heat and transfers it to its surroundings through radiation. Such transfer is necessary to curtail excessive heating

---

The journal model for this work is the *IEEE journal*

and damage in the electrical circuit. Conduction and radiation heat transfer mechanisms will also be modeled in this text.

The heating and/or thermal transport of materials is characterized by a number of important parameters. These values dictate the thermal behavior and properties of the material. A property of utmost importance is a material's thermal expansion coefficient, which quantifies material expands or contraction with changes in temperature. Serious problems can result by not giving due consideration to this property. For example, if two materials of vastly different thermal expansion coefficients were joined together and heated, a large stress possibly leading to buckling or breakage at the junction can result due to unequal expansions of the two constituent materials. Another is the thermal conductivity coefficient, which is the measure of a material's ability to transport heat through conduction. This property is of utmost important in devising thermal sinks and heat exchangers, or to evaluate thermal losses of high-temperature environments and chambers. As discussed later in this thesis, the thermal conductivity can itself depend on the local temperature since the ability to carry heat is impeded by "phonon scattering" at high temperatures.

In the context of electrical engineering, the self-heating of electronic devices and thermal management issues have begun to take on increasing importance in integrated circuit technology for a variety of reasons. Device down scaling, functional integration, and increases in the on-chip density naturally give rise to higher energy generation. The need to develop reliable active devices for a variety of specific high-power, high-voltage applications has also enhanced the interest in thermal analysis and heat management issues. The applications can range from high power RF generation, solid-state broadband

amplifiers for microwave communications including mobile phones, phased array radars, and high voltage semiconductor switches for power factor control in transmission load networks. The thermal problem is compounded by the need for high-speed electronics, which invariably leads to GaAs as the material of choice. Unfortunately, the thermal conductivity of GaAs (~ 0.46 W/K/cm) is an order of magnitude smaller than SiC, and is lower by factors of 5 and 3, respectively, as compared to GaN and Si. It, therefore, becomes more difficult to conduct away the heat from the active regions of high-power, high-speed GaAs circuits. As a consequence, internal temperature increases need to be taken into account for all device optimization and design procedures.

Temperature increases produced by the internal heat generation affect several parameters of electronic devices that collectively alter the overall response characteristics. Fundamentally, the increased temperature has two main effects: (a) It alters the carrier transport properties by modifying the carrier-phonon interactions, and (b) it leads to an increase in the vibrational kinetic energies of the lattice atoms. The effects on the electronic sub-system tend to reduce mobilities, carrier drift velocities, and the overshoot characteristics. Other effects, often associated with the velocity reductions, typically include reductions in the ac gain, lower transconductances in FET structures, reductions in the cut-off frequency arising from increased transit times, decreases in the characteristic breakdown voltage, increased leakage currents, higher shot-noise, larger channel and series resistances which adversely affect the "RC" time constants, and enhanced carrier emission from traps and defects. Increases in the atomic vibrational energy lead to several consequences as well, some of which can be detrimental for the stability and reliability of the overall circuits. For example, higher atomic kinetic energies

can enhance electromigration, facilitate the propagation of defects and dislocations, and cause the build up of internal stresses and strains. In a perfect lattice containing no imperfections, the temperature rise would not have as dramatic an effect, since the internal symmetry would help in maintaining a balance between the inter-atomic forces. If anything, the lower electron mobility would help reduce the "electron-wind" contributions to electromigration. However, in the presence of defects or asymmetries (including those at the metallization-semiconductor boundaries), increased temperatures make it easier for atoms to hop over localized potential minima and migrate within the lattice. Macroscopically, such atomic movement is characterized in terms of activation energy and the migration rate is typically expressed by an Arrhenium-type formula. The resulting effects, such as defect propagation and internal stress, can in turn influence the trapping-detrapping characteristics. This can potentially lead to instability either by enhancing the internal electric fields through localized space charge formation, or by providing a source of recombination heating which could then possibly lead to a positive feedback action.

1.2 HEAT TRANSPORT SIMULATIONS AND THEIR ADVANTAGES

Computer simulations provide a method to study the response and behavior of real world systems through numerical evaluations based on software that is designed to mimic the system's operational behavior or characteristics. There are several advantages of undertaking such simulation studies. An important advantage is that simulations provide the ability to deal with very complicated models and systems. Next, the development of graphical user interfaces has made it possible to visualize the results,

often in real time. The visualization helps in gaining insights into the phenomena of interest and its dynamic evolution. The computational approaches also provide a cost-effective tool for the study and analysis without the need for costly equipment or experimental facilities. Furthermore, a large number of scenarios and test cases can easily and quickly be analyzed. In this thesis, computer simulations will be employed to gauge an understanding of thermal transport and heat flow, both under transient and steady state conditions. An electrical analogue to the thermal system will be constructed for improved efficiency and computational speed. The advantage of setting up an electrical equivalent to the thermal system will be that all the electrical circuit simulation tools currently available will easily be brought to bear for the thermal problems.

In general, simulation uses methods and applications to mimic the behavior of real systems. A system is usually studied to measure its performance, improve its operation, or design it if it doesn't already exist. It might be possible to experiment with the actual system to observe its response to parameter changes introduced by the analyst. However, in many cases, it may be too difficult, costly, or dangerous to experiment on the actual system. It is these situations in which it would prove beneficial to construct a model for studying the system. The model allows the analyst to experiment with a representation of the system and produce safe and cost effective results.

In general, simulation models are generally classified into three categories: (i) Static vs. Dynamic: A static model is time independent, but a dynamic model uses time as a parameter. Most operational models are dynamic. (ii) Continuous vs. Discrete: Continuous systems change continuously over time. A discrete model has change occurring only at sets of distinct points in time. (iii) Deterministic vs. Stochastic: Models

that use no random inputs are said to be deterministic. Stochastic models, however, operate with random inputs and produce uncertain results. The heat transfer mechanism models may be classified as static (since the results are not time dependant), discrete (since the results do not vary over the simulation), and deterministic (since no random inputs are considered).

1.3 REVIEW OF SCHEMES FOR THERMAL ANALYSES

Thermal modeling is not a new problem area, and an abundant literature exists on the subject [for example, 1-11]. It is perhaps instructive to start with a summarizing survey of the various contributions in this field. Quite generally, there appear to be five main techniques for analyzing the self-heating problems. These are listed below, with brief discussions pertaining to their applicability, merits, and relative disadvantages. These theoretical approaches are a good starting point for selecting an appropriate procedure for the thermal analysis of electronic devices.

1.3.1 Computer Aided Finite Difference Techniques

Heat flow is assumed to be adequately represented by a non-linear diffusion equation in accordance to Fick's law. This inherently assumes an internal quasi-equilibrium between the various phonon modes, and is clearly applicable over dimensions exceeding the thermal mean-free path. For simplicity, the finite difference scheme will be discussed only for the one-dimensional (1D) case, though it can easily be generalized to three dimensions. The 1D heat flow equation is given as:

$$k(T)\,[\delta^2 T(x,t)/\delta x^2] + P(x) = \rho\, C(T)\,[\delta T(x,t)/\delta t]\ , \qquad (1.1)$$

where P (x) is the power generation density, ρ the density of the material, while k (T) and C (T) are the temperature dependent thermal conductivity and specific heat. Discretizing the above equation over a uniform grid of length Δx then leads to the following balance equation:

$$k_n A\,[(T^*_{n-1} - T^*_n)/\Delta x] - k_n A\,[(T^*_n - T^*_{n+1})/\Delta x] + P_n A\,\Delta x = \rho_n C_n \Delta x\,[(T^*_n - T_n)/\Delta t]\ , \quad (1.2)$$

where k_n, ρ_n, and C_n are the thermal conductivity, density and specific heat over the n^{th} discretized box, T^*_n the temperature within the n^{th} box at time $t + \Delta t$, T_n the corresponding temperature at time "t", and P_n the power dissipation density in the n^{th} box. The time step Δt has to be smaller than half the thermal time constant τ, which is given as: $\tau = [2\Delta x/\pi]^2\ [\rho_n\ C_n/K_n]_{max}$. This discretization scheme of equation (1.2) is conditionally stable [12, 13], and leads to the following straightforward expressions for the temperatures T^*_n:

$$T^*_{n-1} - (2+M)\,T^*_n + T^*_{n+1} = -M_n T_n - \Delta x^2 P_n / K_n\ , \qquad (1.3)$$

where $Mn = \Delta x^2 \rho_n C_n / [\,k_n\ \Delta t\,]$. The above gives rise to a tri-diagonal matrix for the temperatures T^*_n at the "n" discretized nodes for the time instant $t + \Delta t$. This problem can easily be solved by matrix inversion, Gauss-Jordan elimination or by employing an iterative relaxation technique.

For boundaries between two separate materials, the same scheme can still be used with a minor modification. For an interface between the (n+1) and (n+2) nodes, the expression (1.3) is replaced by the pair of equations (1.4a, 1.4b) as given below:

$$T^{*}_{n-1} - (3+M-2G_{12})\, T^{*}_{n+1} + 2G_{21}T^{*}_{n+2} = - M_{n+1}\, T_{n+1} - \Delta x^2\, P_{n+1} / K_{n+1} \ , \qquad (1.4a)$$

and

$$T^{*}_{n+3} - (3+M-2G_{21})\, T^{*}_{n+2} + 2G_{12}T^{*}_{n+1} = - M_{n+2}\, T_{n+2} - \Delta x^2\, P_{n+2} / K_{n+2} \ , \qquad (1.4b)$$

where the factors G_{12} and G_{21} are:

$$G_{12} = [A_{n+1}\, k_{n+1}]/[A_{n+1}\, k_{n+1}+A_{n+2}\, k_{n+2}] \ , \qquad (1.4c)$$

and

$$G_{21} = 1 - G_{12} \ . \qquad (1.4d)$$

For two-dimensional (or three-dimensional) problems, the computations boil down to solutions of penta-diagonal (or hepta-diagonal) matrices. Though simple in concept, this finite difference scheme is not a very fast and accurate method. As compared to the finite-element method, a larger number of nodes are required for comparable accuracy [14]. This increase in the matrix size for accuracy then increases the computational burden. Also, as the final solution is not explicitly expressed in terms of an equation, the technique does not provide physical insight and is not very intuitive.

There is a more serious problem with this technique for simulations of power pulses of high magnitude and short durations. This difficulty is associated with the finite

order discretization of the boundary condition at the source regions. For example, the boundary condition: $k\ (x=0)\ [\delta T\ (x=0,t)/\delta x]_{x=0} = -\ P\ (x=0) = -\ P_0$ for a source of power density P_0 at the surface, is discretized as: $[T_0\ (t) - T_1\ (t)]/\Delta x = P_0/k$. This implies that the temperature $T_1(t)$ can and will react to the power inflow and change value in accordance to the value P_0. However, if the rise time of the power source is shorter than the thermal time constant, then physically there may not be enough time for heat flow to occur from the surface to the region below. In such a case, the value of T_1 in the numerical solution should hardly change to accurately reflect this physical reality. However, an attempt at developing a more physical model requires smaller time steps, and will lead to significant increases in the computation time.

1.3.2 Computer Based Finite Element Techniques

Another classical method of solving thermal problems in semiconductors is the finite element technique that is based on a variational approximation of the heat equation [15]. The approximated solution T(x, t) to the 1D heat flow equation with power inflow at the surface is generally expressed as [1.15]: $T(x, t) = {}^{m}\Sigma_{i=1}\ \zeta_i\ (t)\ Wi(x)$, where $W_i(x)$ are the decomposition functions, and $\zeta_i(t)$ the co-ordinates of the temperature approximation in the functional basis formed by the decompositional functions. Solutions recently presented by Ammous et al. [14] indicate that the method inherently overcomes most of the drawbacks of the finite difference scheme.

The primary difficulty with the FE method is that it requires a great deal of personal expertise and experience to decompose the geometry into finite elements and set up the trial solutions. The use of software packages would help alleviate the problem of

this complicated and cumbersome technique. However, the method is not very transparent, and does not lend itself to simple predictions of scaling behavior. It could be pursued if rigorous solutions to complicated geometric structures are desired. However, for simple geometries, and as a quick design aid, some of the analytical techniques discussed later would be far more efficient.

1.3.3 The Transmission Line Matrix Method

The transmission line matrix (TLM) approach was first proposed by Johns [15] and Lohse et al. [16] as an alternative for overcoming the shortcomings of the finite difference (FD) scheme. As discussed above, stability of the FD scheme requires that the time step be less than half the thermal time constant. This can potentially result in excessively long computational times or increases in the matrix storage requirements. The TLM method, on the other hand, which relies on an equivalent RC transmission line model, proves to be conditionally stable. Its main utility lies in the time dependent domain of heat flow analysis.

The TLM method was originally introduced to solve Maxwell's equations, and problems in the field of electromagnetics and transmission lines [17,18]. Its application to thermal flow analysis stems from the fact that the form of the wave equations of electromagnetics and the transmission line expressions, both reduce to the heat diffusion equation as the permittivity (or distributed inductance) become vanishingly small. This correspondence between the electromagnetic and the thermal systems sets up an equivalence between the voltages of transmission line theory and the temperature at an internal node of the discretized semiconductor space. A discretized segment of the

semiconductor material can then be represented in terms of a differential element of a transmission-line circuit. The resistance "R_{tran}" and capacitance "C_{tran}" associated with such an analogous transmission line model are then given as: $R_{tran} = \Delta x / [k\ A]$ and Ctran $= C\ \rho\ A\ \Delta x$. The parameters k, C, and ρ are the thermal conductivity, specific heat, and material density parameters, respectively. As a result, the issue of determining the heat flow problem is transformed to an equivalent problem of evaluating the time dependent propagation of voltage waveforms across the nodes of a distributed transmission line network. Since the equivalent network problem has only capacitors and resistors, it represents a lossy system and is inherently stable. It thus ensures that any spurious oscillations arising in this passive-network would quickly die away.

The TLM method provides an exact time-domain solution for the network by considering the propagation of delta pulses from the various source nodes. The source nodes represent regions of actual power dissipation within the physical semiconductor device. The essence of the technique is to launch pulses from every source node and propagate them down the elemental transmission line segments in all directions. After propagating down a differential transmission line segment, the voltage pulses scatter and are reflected. The time delays between all adjacent transmission line segments are set equal, so that pulses arrive at all successive scattering zones simultaneously. In a sense, the cumulative addition of the voltage at each node following collective propagation and scattering is paramount to a discretization of Huygen's principle. Secondary sources are thus continually created at every time step as the wave interacts with successive transmission line segments. The temporal development of voltage in response to the

initial set of pulses then yields the equivalent temperature as a function of position and time.

The obvious advantage of the TLM technique is the ease with which even the most complicated geometric structures can be analyzed. There are no convergence or stability problems. Also, a large amount of information is made available by the TLM approach. For example, the technique can yield the impulse response for a given semiconductor structure. This can, in principle, allow for the computation of the time-dependent response of the system to any excitation provided the system was linear. Furthermore, the characteristics of the dominant and higher order modes can be assessed through a Fourier transform.

It is also important to state some of the drawbacks and potential sources of error in applying the TLM method for thermal analysis. First, the technique requires that all pulses propagating through the various transmission line segments arrive with perfect synchronization. This implies that the thermal velocity is constant and uniform. In practice, this would be difficult to achieve due to internal inhomogeneities, defects, and temperature dependent material characteristics. Sloping boundaries would cause mis-alignments between the physical geometry and the simulated elemental regions leading to timing errors. The temperature dependence of the material parameters that would become especially important at the higher power dissipation levels would work to invalidate the premise of system linearity. This would bring into question the applicability of the Fourier transform. Apart from the velocity errors, timing offsets, and misalignment effects, truncation of the impulse response to a finite time duration would also contribute to the errors. This effectively would lead to the Gibb's phenomena. In

view of the above problems, the TLM is perhaps not very well suited for steady state thermal analysis. It would best be used for simulations of transient response, especially for fast rising input pulses.

1.3.4 Thermal Analysis Using The SPICE Circuit Simulator

The equivalence between the thermal system of equations and the variables of circuit theory immediately suggests the use of circuit simulators for the solution of the thermal problem. Based on a finite difference discretization of the heat flow equation, an equivalence between the following variables can be shown to result. Details of this are discussed in Chapter 3.

As a result, a differential element of volume within the semiconductor material denoting a unit cell for the thermal problem may be presented in terms of an equivalent electrical building block. This repetitive block would consist of two serial resistors with a parallel combination of a current source and a capacitor connected between them. Obviously, for 2D or 3D analysis, one would have four- or six- resistors, respectively. These building blocks would be interconnected to yield the volume of the entire structure. This equivalent electrical network could be solved for a given set of current excitations, using the commercially available SPICE simulator yielding all node voltages as a function of time. Since SPICE programs are available, and are capable of handling a large number of nodes, the thermal problem could be solved exactly.

Such equivalent electrical circuit simulations have been used for thermal analysis [19, 20]. This approach can easily be generalized to include the temperature dependence of the thermal conductivity and specific heat by employing voltage controlled resistor and

capacitor elements. Since voltage controlled elements are available within the SPICE simulator, this extension should be trivial. The added advantage is that in addition to time-domain analysis, the technique would easily furnish the frequency response characteristics based on the built-in capability of the SPICE simulation tool.

1.3.5 Analytical Techniques and Fourier Series Solutions

This final class of techniques is the least intensive computationally, and provides closed form expressions for the internal device temperature. Quantities of interest such as the thermal resistance and peak surface temperature can easily be obtained. As such, these methods appear to be best suited for quick device optimization or to ascertain the thermal implications for competing layout schemes. Most of the methods are intended for analysis under steady state operating conditions.

1.4 CURRENT RESEARCH OBJECTIVES

The primary goal of this study is to analyze the problem of heat flow and thermal transport in solids through numerical simulations. There are a number of numerical modeling approaches to this problem based on the thermal equations. However, multi-purpose software packages and simulation tools for a variety of operating conditions are not easily available for the thermal problem. Simulators of electrical circuits, on the other hand, are widely available and capable of performing dc, transient, and ac analysis. The SPICE tool is one example with which all electrical engineers have a great deal of familiarity. Consequently, one of the primary objectives of this research was to explore

the feasibility of utilizing such electrical circuit simulators for the solution of thermal problems by establishing electrical analogues.

The focused objectives were the following: (1) Determine whether electrical analogues could be constructed to represent both the transient and steady-state conditions of heat flow in solids. It was necessary and important to have a one-to-one correspondence between the variables of the thermal and electrical systems. (2) Ascertain the equivalent electrical circuit elements (such as capacitors and conductors) required for such a task. (3) Incorporate temperature dependence of parameters such as the thermal conductivity. (4) Demonstrate the validity of such a SPICE-based equivalent electrical simulator for heat flow problems through careful comparisons.

The overall, long-term objective of developing an alternate SPICE-based approach is to be able to carry out steady-state, transient, and frequency-response analysis of both pure (i.e., defect–free), and defective solids. The application to fatigue and defect analysis from such simulations would be very important and useful for non-destructive evaluation (NDE) and testing purposes. Laser-based spanning of samples is currently being pursued as a superior fast, jitter-free technique for such NDE activity. It also has the advantage of good spatial resolution. From this NDE standpoint, it is important for this thesis work to also successfully carry out the following tasks. (a) To demonstrate that clear differences exist in the results of simulated heat flow between pure samples and those containing defects and/or cracks. (b) Identify the parameters that can best carry information on the defects. These are likely to be time-delays or magnitudes of the local temperature in response to a laser-generated heat span. (c) Show at least one simple test example of a SPICE-based method for irrefutable demonstration. (d) Eventually, based

on the success of the results obtained in this research, more detailed analysis could be developed for a more comprehensive and quantitative analysis. Recommendations and suggestions on enhancing the applicability of this mathematical model could also be made.

1.5 THESIS OUTLINE

The contents of the following chapters of this thesis are described next in a brief summarizing form. Chapter 2 comprises an overview of thermal transport and the various heat flow processes. This chapter basically provides a literature review and forms the background for this thesis work. Details on the various conduction mechanisms are provided. In addition to the relevant mathematical models, alternate electrical equivalents are also discussed. Since the eventual goal of this thesis is to gauge the suitability of thermal analysis through equivalent electrical circuit simulations, the electrical equivalents have been introduced where possible. The importance and role of the conduction, convection and radiative processes is brought out and discussed in this chapter. However, for thermal analyses in solids, only the conduction process is important.

In chapter 3, the electrical circuit equivalent for thermal transport is discussed in detail. The equivalence between the various thermal parameters and the corresponding electrical elements such as resistors, capacitors, etc., is brought out, based on the mathematical form of the underlying equations. A basic procedure for setting up the electrical analogue, which is valid under both transient and steady-state conditions, is given. Next, a case is made for using commercially available circuit analysis software

packages, such as SPICE, for numerical modeling. It is shown that due to the existence of an electrical analog for the thermal system, all the numerical techniques for circuit analysis can be brought to bear for quantifying multi-dimensional heat flow problems in general. The issue of temperature dependent thermal conductivity is also discussed. It is shown that such aspects can easily be incorporated through the use of voltage-dependent resistances/conductances in the equivalent electrical circuit. Next, a validation of the SPICE-based electrical circuit based technique is carried out through careful comparisons of temperature predictions from pure thermal solutions. Steady-state conditions, as well as heating and cooling transient, are analyzed. The predicted results match the thermal baseline values very well, thereby demonstrating validity and correct numerical implementation of the SPICE-based electrical circuit method. A number of examples for 2-D and 3-D structures are presented, in addition to simple 1-D SPICE-based analysis.

Chapter 4 presents the main results of this research work with accompanying discussions. Transient heating and cooling characteristics in response to scanned heating by a moving laser is chosen to be the external heat source. This choice has been based on the use of such laser heating for non-intrusive analysis and non-destructive testing of samples in actual experiments. The simulation results clearly demonstrate the relationship in the magnitude of the local temperature changes and the temporal variations due to the sequential nature of the heat flow from a "hot spot." It is agued that such variations can be used to uncover spatial inhomogeneities, defects, and underlying cracks within samples to be tested. Consequently, laser based spanning can be used for non-destructive evaluations (NDE) of the sample integrity. Related literature on the subject of NDE is also, therefore, presented in this chapter. The results clearly demonstrate the potential for

using transient temperature characterization of samples, subjected to pulsed laser scans, for NDE and predictions of internal cracks.

Chapter 5 presents the concluding summary for the entire thesis. This chapter summaries the salient accomplishment and contributions. The primary conclusion in favor of using a SPICE-based electrical simulator for any class of general heat flow problem is presented. The benefits and applicability of using this technique for defect detection and laser-scanning based crack diagnostic is also highlighted. Finally, the scope for future work that could be carried out to further utilize the advantages of this technique for non-destructive diagnostics and analysis is listed. This would serve as the key for extended follow-up work in this area.

CHAPTER 2

BACKGROUND REVIEW ON HEAT TRANSPORT

2.1 INTRODUCTION

In this chapter some of the background material pertaining to heating in solids, details of the various physical mechanisms, and associated thermal effects are discussed. These discussions provide a good starting basis for understanding the phenomena of heating and to identify the processes germane to any subsequent analysis. The chapter also helps lay down groundwork for constructing mathematical models for quantitative analysis of heating in solids. After this basic review, details of the simulation scheme used in this thesis research and results obtained are presented in subsequent chapters.

2.2 HEAT TRANSFER MECHANISMS

Heat transfer occurs through the mechanisms of conduction, convection, and radiation. Each of these mechanisms is presented individually, and it is shown that an electrical equivalent model can be constructed to describe the thermal transport physics for each process. First, the underlying theory and physical models for each heat transport process are presented. Next, the electrical equivalent model is derived using modifications of the analytical equations. This process may be automated with the aid of a suitable computer code to obtain thermal results and electrical equivalent components based upon user-defined heat transfer parameters.

2.3 THERMAL CONDUCTION

The random motion of molecules causes heat energy. Heat occurs due to the presence of internal frictional forces, which continually dissipate the kinetic energies of the vibrating atoms. This dissipated energy can most easily and simply be visualized in terms of a kinetic picture that invokes energy packets called phonons [21-22]. The vibrating atoms give off (or produce) phonons when they release their energy. Conversely, the atoms can also absorb energy from the phonons through the reverse mechanism. For equilibrium to be attained, the atoms on an average give off and accept equal numbers of phonons, thus maintaining a time invariant "phonon bath." However, during periods of external heating (say by a laser, or heater), energy is supplied to the atoms of the constituent material. The atoms begin to oscillate more strongly, and give off the excess energy by producing additional phonons. This net emission of phonons increases the population of the local phonon bath. The excess phonon population, then in turn, begins to diffuse to other lower-population areas, thus giving rise to "heat-flow" or "net thermal conduction." Alternatively, without invoking the "phonon" concept, one can simply view heat flow in terms of the following picture: The faster moving, high kinetic-energy atoms come in contact with the slower moving (and hence, less energetic) atoms within a material. Energy is exchanged causing the slower atoms to vibrate more rapidly (and hence, posses a higher energy), while the faster atoms slow down. The net result is that the warmer/energetic molecules lose energy and decline in temperature, while the cooler objects gain energy and increase their characteristic temperature. Thus, heat always travels from warmer objects to cooler objects. This method of heat transfer is called thermal conduction.

Metals are good conductors because they transfer heat quickly, and air is a poor conductor because it transfers heat slowly. Materials that conduct heat poorly are called insulators. The coefficient k of heat conduction indicates a materials' relative rate of conduction as compared to silver. Silver is taken to have a heat conduction coefficient value of 100. The composition of a material affects its conduction rate. If a copper rod and an iron rod are joined together end to end and heated, the heat will conduct through the copper end more quickly than the iron end because copper has a thermal conductivity of 92, whereas, the value for irons is only 11. Due to this bottleneck effect at the junction, the temperature is expected to be non-uniform within such a bar.

Fourier (1768-1830) summarized these properties and presented them in Fourier's law of heat conduction. This law is expressed mathematically as

$$\phi = -k \frac{\Delta T}{\Delta L}, \tag{2.1}$$

where ΔT is the differential temperature across a length segment ΔL.

2.3.1 THE MODEL

The physical model in this analysis for heat conduction is chosen to be a bar with constant cross sectional area (A). This bar exists in one-dimensional space for x = 0 to x = L. The left end of the bar is subjected to a constant heat source and the right end of the bar is held constant at ambient temperature.

2.3.2 SECTIONAL ANALYSIS

This problem is analyzed by dividing the length of the bar into equal sections to discretize the physical sample. Dividing a 2-meter bar into ten equal sections, yields a

length of 0.2 meters for each section. Assuming that the left end of the bar is heated while the right end is maintained at 300 degrees Kelvin, the heat will travel to the right. Conservation of energy in the steady state, ensures that the heat flowing out of one section is the same as that flowing into the next section. This fundamental theorem may be expressed as

$$\phi_{right} A = \phi_{left} A , \tag{2.2}$$

where ϕ is the heat flux.

An analysis of the above equation states that the net change of energy due to heat transfer across the boundary between sections is zero in steady-state. By substituting Fourier's Law into the conservation of energy equation, we have

$$-k_{left} \frac{\Delta T_{left}}{\Delta L_{left}} A + k_{right} \frac{\Delta T_{right}}{\Delta L_{right}} A = 0. \tag{2.3}$$

Replacing $\Delta T_{left} = T_c - T_w$ and $\Delta T_{right} = T_s - T_c$ and dividing the expression by its area, equation (2.3) becomes

$$-k_{left} \frac{T_c - T_w}{\Delta L_{left}} + k_{right} \frac{Ts - T_c}{\Delta L_{right}} = 0. \tag{2.4}$$

Here, T_w = temperature at the entrance of the section, T_s = temperature at the end of the next section, and T_c = temperature that exists between the sections. Solving this equation for T_c yields

$$Tc = \frac{\frac{k_{left}}{\Delta L_{left}} T_w + \frac{k_{right}}{\Delta L_{right}} T_s}{\frac{k_{left}}{\Delta L_{left}} + \frac{k_{right}}{\Delta L_{right}}} . \tag{2.5}$$

If $k_{left} = k_{right} = k_o$, then the thermal conductivity (k_o) may be factored out of equation [2.5] to yield

$$Tc = \frac{\frac{T_w}{\Delta L_{left}} + \frac{T_s}{\Delta L_{right}}}{\frac{1}{\Delta L_{left}} + \frac{1}{\Delta L_{right}}} . \qquad (2.6)$$

If $\Delta L_{right} = \Delta L_{left} = \Delta L$, we obtain

$$Tc = \frac{k_{left} T_w + k_{right} T_s}{k_{left} + k_{right}} . \qquad (2.7)$$

This equation may be applied to a bar composed of two or more materials, such as in the previous example of iron and copper. To assure correct calculations it is important that the junction between the different materials occurs between section boundaries.

If $k_{left} = k_{right}$, and $\Delta L_{left} = \Delta L_{right}$, a further simplification results:

$$T_c = \frac{T_w + T_s}{2} . \qquad (2.8)$$

These equations may be used repeatedly to calculate the junction temperature (Tc) between every section by shifting the temperature references as illustrated in figure 2-1.

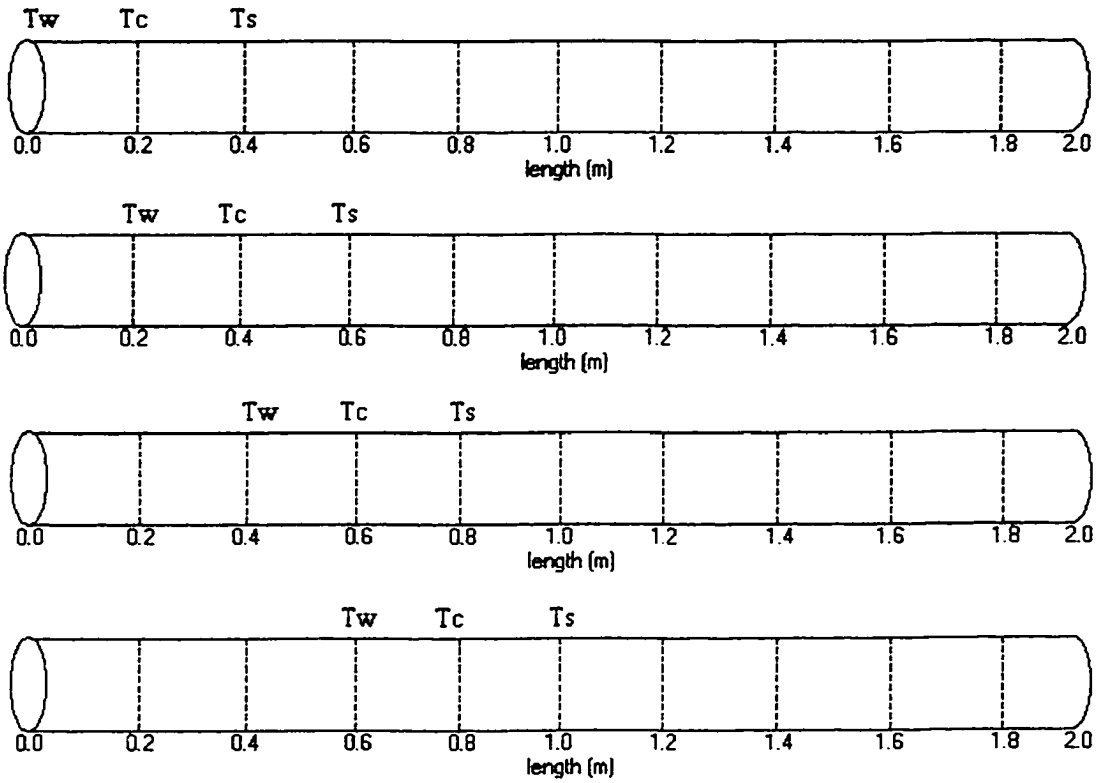

Figure 2-1: Shifting temperature references to calculate junction temperatures.

The electrical model represents each section of the bar as an electrical resistance and the temperatures as voltage sources. This model is presented schematically as figure 2-2.

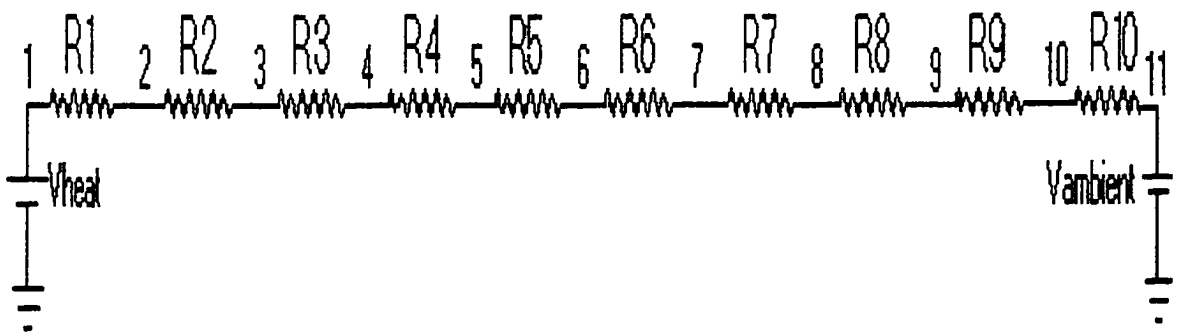

Figure 2-2: Electrical model for conduction heat transfer.

Resistance values are computed according to the length and material properties of the corresponding section. The magnitudes of these resistance values assure the proper distribution of the potential difference between V_{heat} and $V_{ambient}$ at the voltage nodes (representing the section junctions). Details on this electrical analogue will be presented and discussed in the next chapter.

2.4 HEAT CONVECTION

Convection heat transfer through gases and liquids from a solid boundary results from the fluid motion along the surface. Newton's Equation may quantify the rate of energy transfer from the system to the fluid as

$$\phi = h\,(T_s - T_f), \tag{2.9}$$

where, T_f = fluid temperature, T_s = surface temperature, and h = the convection coefficient.

In order to elaborate on this mechanism, an analysis is presented that examines heat transfer between a gas and a coolant through a cylinder wall. This problem consists of three heat transfer functions, a conduction transfer through the cylinder wall, and two convection heat transfers between the wall surface and the moving mediums. In order to derive the total heat flux, one needs to calculate the total convection heat transfer coefficient and temperature change across all three mediums. The total heat flux (ϕ) may be calculated as

$$\phi = Q_{total}\,(T_{gas} - T_{coolant}) = \frac{(T_{gas} - T_{coolant})}{\frac{1}{h_{gas}} + \frac{1}{h_{wall}} + \frac{1}{h_{coolant}}}, \tag{2.10}$$

with h_{wall} = k/L being the conduction heat transfer through the cylinder wall, h_{gas} = convection heat transfer coefficient for the gas, T_{gas} = gas temperature, $h_{coolant}$ = convection heat transfer coefficient for the coolant, $T_{coolant}$ = coolant temperature, and Q_{total} = the total heat transfer occurring through all three mediums.

It is now possible to calculate the temperatures on the cylindrical wall. The heat travels from the heat source (gas), through the cylinder wall, to the heat sink (coolant), and moves from left to right. This temperature profile forces the left side of the cylinder wall to be at a lower temperature than the gas, and the temperature on the right side of the wall to be greater than that of the coolants. In order to calculate the temperature on the left side of the cylinder wall, we first determine the surface temperature from the gas temperature and heat flux.

If

$$\phi = h\,(T_{gas} - T_{l\text{-}wall}), \tag{2.11}$$

then,

$$T_{l\text{-}wall} = T_{gas} - \phi / h_{gas}. \tag{2.12}$$

The cylinder's right wall heats the coolant. This temperature may be derived by the coolants' temperature through the application of Newton's Equation by

$$T_{r\text{-}wall} = T_{coolant} + \phi / h_{coolant}\ . \tag{2.13}$$

One can also calculate the same result by using Fourier's' equation to obtain ΔT across the cylinders' wall from the heat flux. Once this value is derived, it must be subtracted from the left-side wall temperature (since temperature is decreasing from left to right) to obtain the temperature, which exists on the right side.

If

$$\phi = k\,(\Delta T/L). \tag{2.14}$$

Then

$$\Delta T = (L\,\phi)\,/\,k\ . \tag{2.15}$$

Therefore,

$$T_{r\text{-}wall} = T_{i\text{-}wall} - \Delta T \tag{2.16}$$

The temperature profile may now be displayed as in figure 2-3.

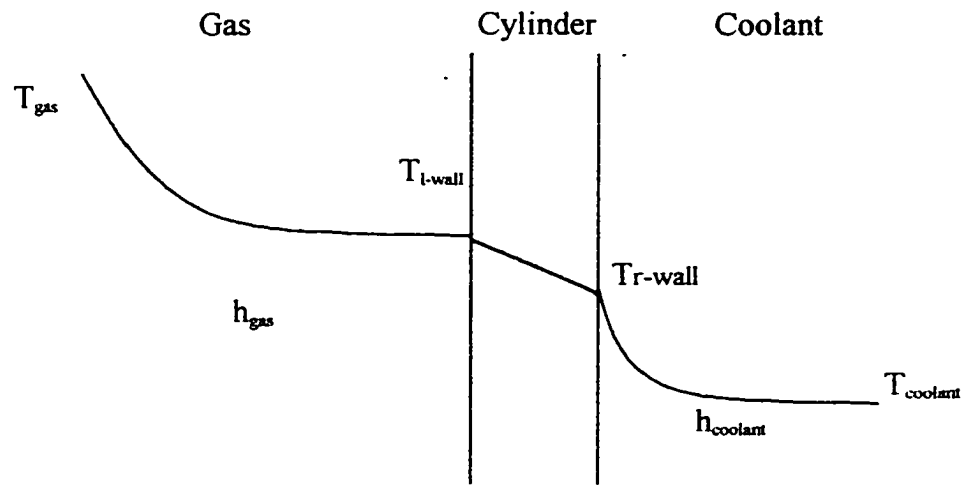

Figure 2-3: Analytical temperature profile.

The heat transfer through the cylinder wall occurs via the conduction process. We can translate the conduction heat transfer equation to the convection form through the following procedures. Since,

$$\phi = h\,\Delta T = \frac{\Delta T,}{1/h} \tag{2.17}$$

and

$$I = \phi A = \Delta V G. \tag{2.18}$$

The thermal expression for convection heat transfer can be transformed into the electrical equivalent expression

$$\phi A = \Delta V G, \tag{2.19}$$

where, $G = h = G_{cond}$. By replacing G_{cond} with its' equivalent derivation equation, one obtains

$$\phi A = \Delta V ([A k] / L). \tag{2.20}$$

Upon dividing both sides of the equation by its area, the heat flux of the thermal model is obtained, which represents the current for the electrical model. This flux is given by

$$\phi = \Delta V \, Gcond = \Delta V (k / L). \tag{2.21}$$

Since,

$$G_{cond} = 1/R_{cond} , \tag{2.22}$$

the resistance may now be computed as

$$R_{wall} = 1/G_{conduction} = L / k . \tag{2.23}$$

The second type of heat transfer action occurs through the gas layer, which lies between the surface of the wall and the moving medium. This heat transfer process is illustrated as figure 2-4.

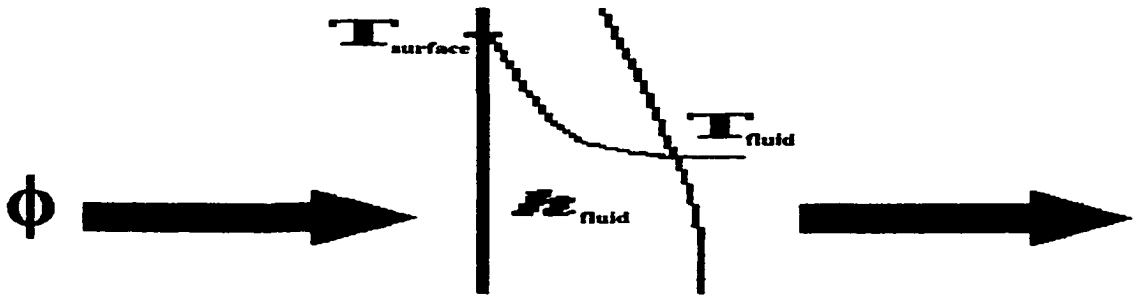

Figure 2-4: Convection heat transfer.

The heat transfer coefficient (h) depends on the type of fluid and the fluid velocity. If we relate Fourier's Law of heat conduction to Newton's equation, we obtain

$$\frac{k\Delta T}{L} = h\Delta T. \tag{2.24}$$

The value of h may now be derived by dividing both sides of the equation by ΔT, to obtain

$$h = k/L\,. \tag{2.25}$$

Comparing this function to the previously derived equation for conduction resistance (equation [2.23]), leads to

$$R = 1/h. \tag{2.26}$$

Consequently, resistances on both sides of the cylinder wall can now be computed as

$$R_{gas} = 1/_{hgas}\ , \text{ and} \tag{2.27}$$

$$R_{coolant} = 1/h_{coolant}\ . \tag{2.28}$$

In order to model the heat transfer through the cylinder wall electrically, a series resistance circuit is created. The temperatures of the gas and coolant are modeled by DC voltage sources. Series connected resistors model the thermal resistance of the gas layer,

cylinder wall, and coolant. Using this relationship, the electrical model presented as figure 2-5 may be used to model the convection heat transfer system.

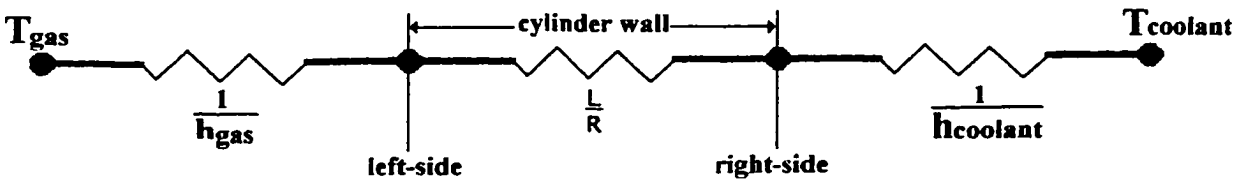

Figure 2-5: Electrical model for convection heat transfer.

These components are then connected as per figure 2-6 and can be simulated with a circuit simulation tool such as SPICE.

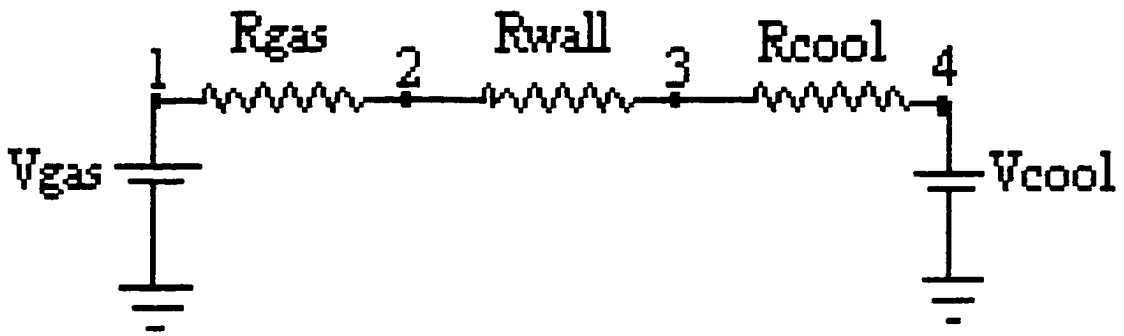

Figure 2-6: SPICE equivalent model for heat convection.

In the equivalent electrical circuit of figure 1-6, the various node voltages denote temperatures at various locations. Specifically, NODE (1) = T_{gas}, NODE (2) = $T_{left\text{-}side\ of}$

$_{\text{cylinder wall}}$, NODE (3) = $T_{\text{right-side of cylinder wall}}$, NODE (4) = T_{coolant}, and $I_{gas} = I_{wall} = I_{cool}$ = heat flux.

2.5 HEAT RADIATION

Thermal radiation is energy emitted by matter at a finite temperature as a result of changes in the electron configuration of the atoms or molecules. Electromagnetic waves or photons transport radiation energy. Heat transfer by radiation is proportional to the fourth power of the absolute material temperature.

The radiative heat flux emitted by a real surface may be determined by the Stefan-Boltzmann law, which may be expressed by the equation

$$\phi = \varepsilon \sigma Ts^4, \tag{2.29}$$

where, ϕ = heat flux (in W/m^2) , ε = emissivity constant, σ = Stefan-Boltzmann constant = 5.67×10^{-8} [in $Wm^{-2} K^{-4}$], and T_s is the surface temperature (K). The emissivity constant ε, is the radiative property of a surface and has a value between zero and one. This ratio is the proportion of radiative energy relative to an ideal radiator or blackbody (i.e. $\varepsilon = 1.0$).

The radiation from a surface has different intensities in different directions. The intensity of radiation along a "normal to the surface" is termed the intensity of normal radiation, I_n. Lamberts' cosine law states that the intensity of radiation along a direction of angle θ with the normal to the surface may be computed according to the equation:

$$I_\theta = I_n * \cos\theta. \tag{2.30}$$

The Lamberts' cosine law is illustrated in figure 2-7.

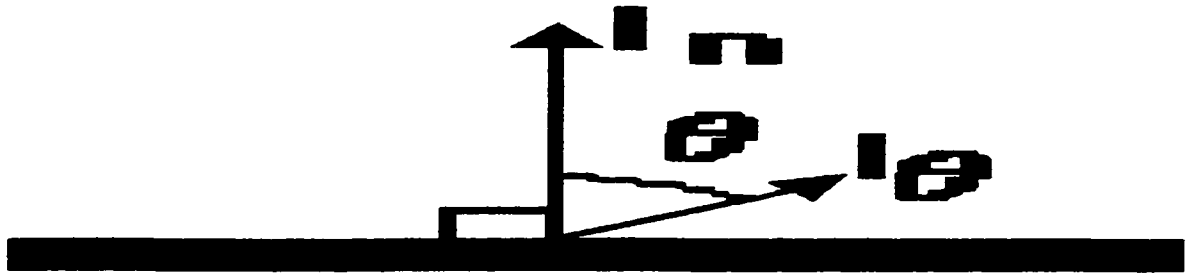

Figure 2-7: Lambert's cosine law.

By combining both Lamberts' cosine law and Stefan-Boltzmann law, one can derive the intensity of normal radiation as

$$I_n = [\varepsilon \sigma (T_s^4)] / \pi . \qquad (2.31)$$

The radiated heat is transferred to its surroundings in the form of electromagnetic radiation, which is usually in the infrared (IR) regime. This radiated heat process is illustrated as figure 2-8.

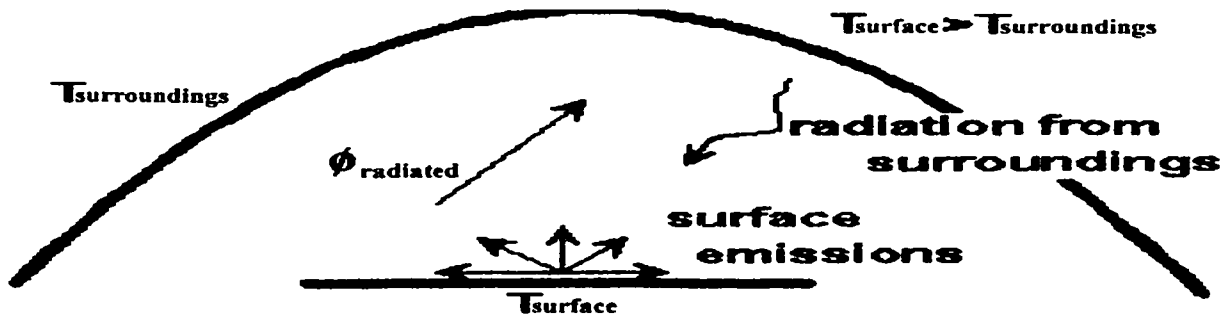

Figure 2-8: Heat radiated from a surface.

A portion of this emitted heat will be absorbed by its surroundings. The rate of energy absorbed per unit surface area may be defined as

$$\phi_{abs} = \alpha \phi, \qquad (2.32)$$

where α is the absorptivity constant. This proportionality constant is a dimensionless value representing the fraction of incident radiation that is absorbed by its surroundings.

As the object's surface temperature rises, it emits greater radiation and warms its surroundings. As the emitted radiation increases, so does the absorbed radiation. Therefore, the net radiated heat is a function of both its surface and surrounding temperatures. The radiation equations are now presented as

$$R_{emitted} = \varepsilon \sigma (T_{object}^4), \tag{2.33}$$

$$R_{absorbed} = \varepsilon \sigma (T_{surroundings}^4), \tag{2.34}$$

$$R_{net} = R_{emitted} - R_{absorbed}, \text{ and} \tag{2.35}$$

$$R_{net} = \varepsilon \sigma (T_{object}^4 - T_{surrondings}^4). \tag{2.36}$$

A simple voltage divider circuit such as in figure 2-9 may model the net radiated heat electrically.

Figure 2-9: Electrical model equivalent for heat absorbed/emitted.

where

$$V_{emit} = \varepsilon \sigma T^4 \text{ volts}, \tag{2.37}$$

$$R_{absorb} = \alpha R_{arbitrary}, \text{ and} \tag{2.38}$$

$$R_{net} = (1 - \alpha) R_{arbitrary} . \tag{2.39}$$

The value of the arbitrary resistance is of little significance, since it just ensures the proper voltage to heat flux ratio. Maximum emitted heat occurs when the surrounding temperature is zero degrees Kelvin ($\alpha = 0$). Calculating the voltage at R_{net} using the voltage divider rule may derive the heat emitted to the surroundings as

$$V_{net} = V_{emit} \frac{R_{net}}{R_{absorb} + R_{net}} \quad . \tag{2.40}$$

When thermal radiation strikes a body, it is either absorbed (α), reflected (ρ), or transmitted (τ) through the body. Therefore,

$$\alpha + \rho + \tau = 1 \quad . \tag{2.41}$$

Reflectivity and transmissivity are properties of the body's surface and are dependent on the temperature of the body and the wavelength of the incident radiation. Reflectivity is a fractional value, which represents the portion of incident radiation, which is reflected from the body. Rough surfaces are better absorbers and emitters than smooth surfaces. Transmissivity is that portion of incident radiation, which is transmitted through the body. We can now expand our circuit to model the reflected and transmitted thermal radiation. A portion (ρ) of the emitted radiation is reflected from the body and the remaining is transmitted through the body. Therefore, the equivalent electrical circuit of figure 2-10 may be used to accurately represent the thermal radiated heat.

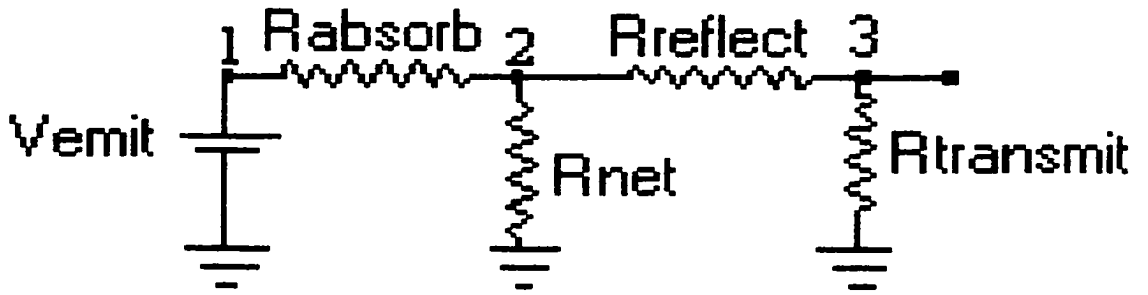

Figure 2-10: Electrical model equivalent for radiated heat.

This circuit forms a series-parallel network, with Rabsorb in series with R_{net} in parallel, with the series combination of $R_{reflect}$ and $R_{transmit}$. The reflected and transmitted radiations are products of the emitted radiation, and therefore, should not affect the quantity of radiation to be absorbed or emitted. In order to effectively isolate $R_{reflect}$ and $R_{transmit}$ from the emission circuit, one must choose a value of $R_{isolated}$, which is much, much greater than the value of $R_{arbritary}$.

The maximum resistance of a parallel network cannot exceed that of the smallest resistance of the network. By using a very large value of $R_{isolated}$ with respect to $R_{arbritary}$, the series combination of $R_{reflect}$ and $R_{transmit}$ places a large resistance in parallel with R_{net}, so that the parallel resistor combination is approximately equal to R_{net}. Since R_{net} resistance remains approximately the same, the emitted voltage does not vary. The heat transmitted through the body may be derived similarly as the emitted heat by another application of the voltage divider rule. This yields:

$$V_{transmit} = V_{net} * \frac{R_{transmit}}{R_{transmit} + R_{reflect}}. \qquad (2.42)$$

CHAPTER III

METHODOLOGY AND IMPLEMENTATION

3.1 INTRODUCTION

The equivalence between the thermal system of equations and the variables of circuit theory, immediately suggests the use of circuit simulators for the solution of the thermal problem. Based on a finite difference discretization of the heat flow equation, an equivalence between the electrical and thermal systems can be shown.

As a result, a differential element of volume within the semiconductor material denoting a unit cell for the thermal problem can be presented in terms of an equivalent electrical building block. This repetitive block would consist of two serial resistors with a parallel combination of a current source and a capacitor connected between them. Obviously, for 2D or 3D analysis, one would have four- or six- resistors, respectively. These building blocks would be interconnected to yield the volume of the entire structure. This equivalent electrical network could be solved for a given set of current excitations, using the commercially available SPICE simulator yielding all nodal voltages as a function of time. Since SPICE programs are available, and are capable of handling a large number of nodes, the thermal problem could be solved exactly.

Such equivalent electrical circuit simulations have been used for thermal analysis [23, 24]. This approach can easily be generalized to include the temperature dependence of the thermal conductivity and specific heat by employing voltage controlled resistor and capacitor elements. Since voltage controlled elements are available within the SPICE simulator, this extension should be trivial. The added advantage is that in addition to time-domain analysis, the technique would easily furnish the frequency response

characteristics based on the built-in capability of the SPICE simulation tool. Details of this technique and the mathematics leading to the SPICE based analysis are presented and discussed next in this chapter.

3.2 ELECTRICAL ANALOG OF THE THERMAL SYSTEM

The heat flow equation for a one-dimensional sample with uniform thermal conductivity may be expressed by the equation

$$k\,(dT^2/dx^2) + g = \rho Cp\,(dT/dt). \tag{3.1}$$

Assigning a new variable $\Delta T = T - T_o$, the equation becomes:

$$k\,(d^2\Delta T/dx^2) + g = \rho Cp\,(\Delta T/dt). \tag{3.2}$$

Equivalence between the variables of the thermal system and an electrical circuit can be invoked through the following transformations:

$$V(x) = T(x), \tag{3.3}$$
$$I_s(x) = A\,\Delta x\,g(x), \tag{3.4}$$
$$C(x) = A\,\Delta x\,\rho\,Cp, \tag{3.5}$$
$$\Delta V(x) = \Delta T(x) = T(x) - To, \tag{3.6}$$
$$G(x) = A\,(k/\Delta x), \text{ and} \tag{3.7}$$
$$R(x) = 1/G(x) = \Delta x/\{A\,k\}\,. \tag{3.8}$$

In the above equations (3.3)-(3.8), A is the cross-sectional area, Δx the length of each discretized segment, $I_s(x)$ a position-dependent equivalent current source, C a capacitance, $\Delta V(x)$ a potential difference between segments of the equivalent circuit, G(x) a conductance element, and R(x) the electrical resistance of each segment. Using this equivalent transformation, the governing equation for thermal transport (3.2) can be expressed in terms of current flow within an electrical circuit. The resulting equation is:

$$G \Delta^2 (d^2 V/dx^2) + I_s (x) = C (dV(x)/dt) \quad (3.9)$$

3.2.1 THERMAL RESISTANCE

Thermal resistance is the reciprocal of its conductance and can be used as a measure of the insulation quality. The thermal (R_t) and electrical resistance (R_e) equations are given as

$$R_t = \Delta x/\{A\ k\}, \text{ and} \quad (3.10)$$

$$R_e = (\rho\ \Delta x)/A. \quad (3.11)$$

The units for equation (3.10) are expressed in degrees Kelvin per Watt. In the electrical model, 1 Watt of energy relates to 1 Ampere of electrical current and one degree Kelvin corresponds to one Volt of electrical potential. So by replacing Watts with Amperes and degrees Kelvin with volts, the correct expression for electrical resistance (the Ohm) is obtained as Volts per Ampere.

Since the heat flow equation is a second-order differential equation, one needs to impose two boundary conditions for a solution. A Dirichlet boundary condition for a constant temperature translates into a fixed node voltage at the appropriate boundary. This can easily be implemented by assigning a very small electrical resistance value between the boundary node and its neighbor(s). Here, for instance, in a one-dimensional (1D) analysis with the Dirichlet boundary taken to be at the $x = 0$ endpoint, a resistance R_1 of 10^{-5} Ohms was assigned for a numerical implementation. This low resistance would ensure (as shown later through actual simulation results), that nodes 1 and 2 were sustained at approximately the same voltage. Boundary conditions of the Neumann type, $dT/dx\ |_{(0,\ t)} = 0$ correspond to adiabatic conditions, and essentially require zero heat flux.

In the electrical equivalent, this corresponds to an adequate representation of zero current. For these purposes, the electrical resistance between such a boundary node and its neighbors was taken to have a very large value. Here, a resistance termed R_{open} of 10^{11} Ohms magnitude was assumed to adequately represent this desired condition. The large value of R_{open} would cause very little current flow, essentially leading to an electrically open circuit at the boundary.

3.2.2 CAPACITANCE

The specific heat of the bar needs to be modeled electrically as a capacitance in the equivalent electrical analogue. A material's specific heat defines the number of Joules required to raise the temperature of one gram of the material one degree Kelvin, and is mathematically defined as

$$Q = m\, Cp\, \Delta T. \tag{3.12}$$

Dividing both sides of the equation by ΔT and replacing the temperature with its electrical equivalent of a voltage, the new equation becomes

$$Q/V = m\, Cp. \tag{3.13}$$

The mass is the product of the material's area, subsection length Δx, and density ρ, i.e. $m = A\, \Delta x\, \rho$. Since the capacitance is defined to be the ratio of the charge to voltage (i.e. $C = Q/V$), one gets

$$C = Q/V = m\, Cp = A\, \Delta x\, \rho\, Cp\,, \tag{3.14}$$

in direct verification of equation (3.5) given previously.

3.2.3 CURRENT SOURCES

The current sources in the electrical model simulate the conduction heat flow. Heat flows in the direction of high to low temperature. Thus for a simple 1D case with the left end maintained at a higher temperature, heat travels from x = 0 to x = L. The total heat applied to the bar is the product of the applied heat per unit volume (g) and the volume of the bar. Since the heat is evenly distributed along the length of the bar, the amount of current added per sub-section is such that the total current flowing out of a particular node is the summation of the currents from all previous nodes.

A conversion from heat flux to an electrical current can be applied to validate the relationship between the models. The amount of heat flux per sub-section may be derived through Fourier's Law of heat conduction by the equation

$$\phi = -k\,(\Delta T/\Delta L). \tag{3.15}$$

Conservation of energy ensures that no heat loss occurs when flowing between sub-sections (between nodes of the electrical circuit). As the heat flow continues down the length of the bar, each sub-section contributes its own amount of heat flow (represented electrically as the current sources) which is cumulative between sub-sections. Therefore, the heat flux and electrical current are at their maximum at the final sub-section. The electrical current is given by Ohm's Law as

$$I = \Delta V\ G. \tag{3.16}$$

Replacing G with its' thermal equivalent expression (equation 3.7), one obtains

$$I = \Delta V\ \{A\,(k/\Delta x)\}. \tag{3.17}$$

By converting Fourier's Law into its electrical equivalent components, equation (3.17) may be expressed in terms of the flux, ϕ, as

$$\phi = -k\,(\Delta V/\Delta x). \qquad (3.18)$$

3.2.4 VOLTAGE SOURCE

The voltage source in the electrical schematic represents the boundary temperature of the bar. Its' magnitude in volts is equivalent to the constant boundary temperature in degrees Kelvin.

Table 3-1 presents a summary of conversions between the models. The remaining substitutions must be calculated according to the physical characteristics of the material.

Thermal model	Electrical Model
Temperature (K)	Voltage (V)
Energy (W)	Current (A)
Thermal conductivity ([W/(m K)])	Resistance (Ω)
Specific heat ([J/(kg K)]	Capacitance (F)
Heat flux ([W/m^2])	Current source (A)

Table 3-1: Equivalent Model Substitutions.

3.3 EQUIVALENT LUMPED ELEMENT CIRCUIT

Based on the equivalent model discussed above, circuit–based thermal analysis can be carried out for one-, two- and three-dimensional cases. The details are presented in this section.

3.3.1 ONE DIMENSIONAL (1-D) EQUIVALENT ELECTRICAL ANALYSIS

The electrical equivalent circuit for a two-meter, 10 sub-section bar is presented as shown in figure 3-1 below for a concrete discussion.

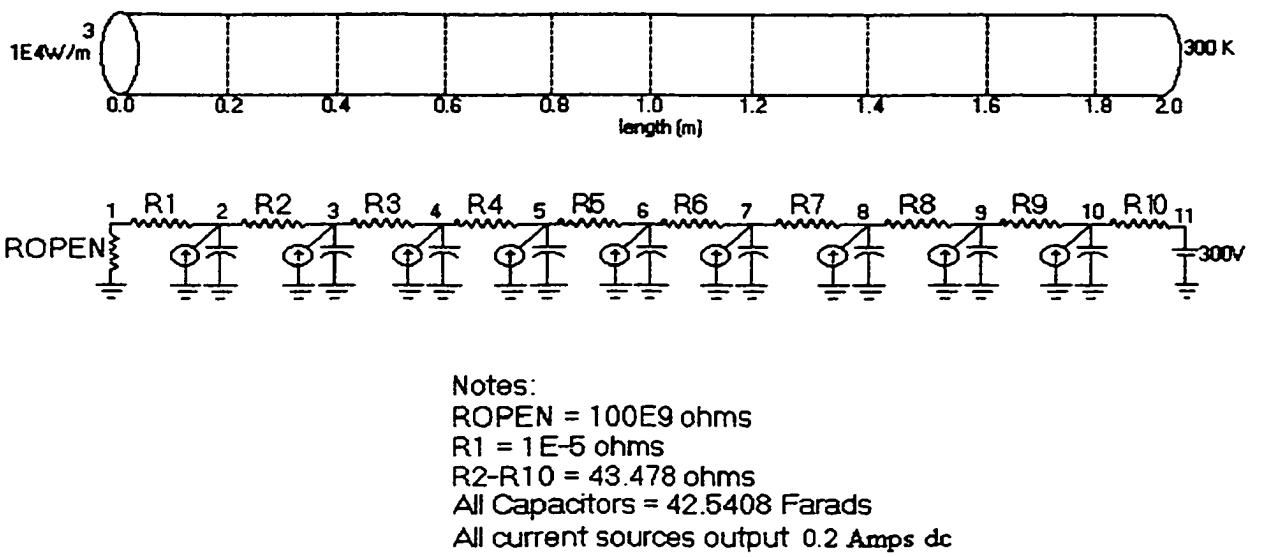

Figure 3-1. Example one-dimensional electrical equivalent of the thermal model.

Note that in the above, there are a total of 11 nodes that need to be used for representing the 10 subsections of the length of the bar. The physical distance between each node relates to 0.2 meters along the length of the bar.

3.3.2 ANALYTICAL SOLUTION FOR THE 1-D THERMAL SYSTEM

The equivalent circuit corresponding to the problem of 1-D heat flow in a solid was derived and discussed in the preceding section. Here, the analytical solution for the same problem is given for comparison based on the actual heat diffusion equation of heat flow. The governing heat flow equation for a bar (one-dimensional analysis) is

$$\frac{d}{dx}\left[k\frac{dT}{dx}\right] + g = \rho Cp\frac{dT}{dt} \tag{3.19}$$

where,

g = heat generation per unit volume,
ρ = density of material,
Cp = specific heat, and
k = thermal conductivity.

For a constant/uniform "k," the above equation becomes

$$k\frac{d^2T}{dx^2} + g = \rho Cp\frac{dT}{dt} \tag{3.20}$$

Assigning: u(x, t) = X(x) * T(t), the following differential equation results:

$$k\,X''\,T + g = \rho\,Cp\,X\,T'. \tag{3.21}$$

Solving this equation by separation of variables under the boundary conditions of

$$dT/dx\,(0, t) = 0, \text{ and } T(L, t) = T_o, \tag{3.22}$$

yields

$$X(x) = \cos\left[\frac{(2m+1)\pi}{2L}\right] \tag{3.23}$$

and

$$T(t) = \exp\left[\frac{-\alpha(2m+1)^2\pi^2 t}{4L^2}\right] \tag{3.24}$$

Since u(x, t) = X(x) * T(t), multiplying these two functions together yields the transient solution:

$$u(x, t) = \exp\left[\frac{-\alpha(2m+1)^2\pi^2 t}{4L^2}\right]\cos\left[\frac{(2m+1)\pi x}{2L}\right] . \tag{3.25}$$

The initial steady-state condition has a uniform temperature, T_o throughout the bar, therefore

$$T(x, 0) = T_o . \tag{3.26}$$

Since the partial differential equation and boundary conditions are linear and homogeneous, the function

$$u(x,0) = B_n \cos\left[\frac{(2m+1)\pi x}{2L}\right] \quad , \tag{3.27}$$

satisfies the solution for arbitrary constants B_n at $t = 0$.

Solving for the Fourier Coefficients yields

$$B_n = \frac{-16gL^2}{k\pi^3} \sum_{m=0}^{m=\infty} \frac{(-1)^m}{(2m+1)} \quad . \tag{3.28}$$

If we now insert this coefficient into our equation, the resulting transient expression becomes

$$u(x, t) = \frac{-16gL^2}{k\pi^3} \sum_{m=0}^{m=\infty} \frac{(-1)^m}{(2m+1)} \exp\left[\frac{-\alpha(2m+1)^2\pi^2 t}{4L^2}\right] \cos\left[\frac{(2m+1)\pi x}{2L}\right] \quad . \tag{3.29}$$

We can now solve for the steady state function. At steady state the rate of change of time is zero, thereby reducing equation (3.20) to

$$k\frac{d^2T}{dx^2} + g = 0 \, . \tag{3.30}$$

Solving this differential equation under the boundary conditions of equation (3.22) yields the steady state bar temperatures of

$$T(x) = \frac{g}{2k}(L^2 - X^2) + T_o \, . \tag{3.31}$$

The complete heat expression is the summation of the transient and steady state equations. Adding these two equations together, yields the final equation for temperature as a function of x and t as

$$T(x, t) = \frac{g}{2k}(L^2 - X^2) + T_o - \frac{16L^2g}{k\pi^3} \sum_{m=0}^{m=\infty} \frac{(-1)^m}{(2m+1)^3} \exp\left[\frac{-\alpha(2m+1)^2\pi^2 t}{4L^2}\right] \cos\left[\frac{(2m+1)\pi x}{2L}\right] \tag{3.32}$$

If the heat source is removed (g = 0) at time t = t_{off}, the bar begins to cool. The cooling heat flow equation now becomes

$$T(x, t) = T_o + \sum_{m=0}^{m=\infty} \exp\left[\frac{-\alpha(2m+1)^2 \pi^2 (t-t_{off})}{4L^2}\right] C_m \cos\left[\frac{(2m+1)\pi x}{2L}\right]. \qquad (3.33)$$

The magnitude of C_m is the temperature above ambient at the instant the heat source is removed ($t = t_{off}$) and is derived from the equation

$$C_m = \frac{2}{L} \int_0^L [T(x, t) - T_o] \cos\left[\frac{(2m+1)\pi x}{2L}\right] . \qquad (3.34)$$

The above equations will be used later in this chapter to obtain analytical solutions for the temperature distribution across a 1-D bar. These results, which represent the exact solution for the actual thermal problem, will be compared with the predictions of the equivalent electrical model developed here. Through these comparisons, it will be shown that the electrical analogue yields identical results and hence, is a valid scheme for numerical calculations for general problems in heat conduction.

3.3.3 TWO-DIMENSIONAL ANALYSIS

Placing a vast quantity of parallel lines side-by-side (zero distance between them) intersecting an equal number of perpendicular lines of the same length and spacing, forms a solid 2-dimensional plane. This methodology is used to model a two-dimensional sample. Each line represents a one-dimensional sample analyzed previously. The points at which the lines intersect are where a common node is shared along both axes. This

newly created two-dimensional sample has lines of equal lengths. The length of each line represents the sub-section length and has a corresponding resistance value. One could minimize the error of the test by minimizing the sub-section lengths, but this would require far too many one-dimensional samples to simulate. Since capacitors in parallel summate to form an equal capacitance value, all capacitor values have doubled at the intersections. Also, due to the dispersion of heat over a larger area in the two-dimensional sample, the temperature increases are not expected to be as significant as predicted for a 1D situation.

Figure 3-2 presents the electrical equivalent circuit for a two-dimensional material. No heat flow (i.e. zero current) occurs between nodes 13 through 16 since they are all attached to a common heat sink and maintain the same constant temperature (voltage). Therefore, the circuit that would represent the fourth horizontal line may be removed from the model without causing any misrepresentation of the physical sample.

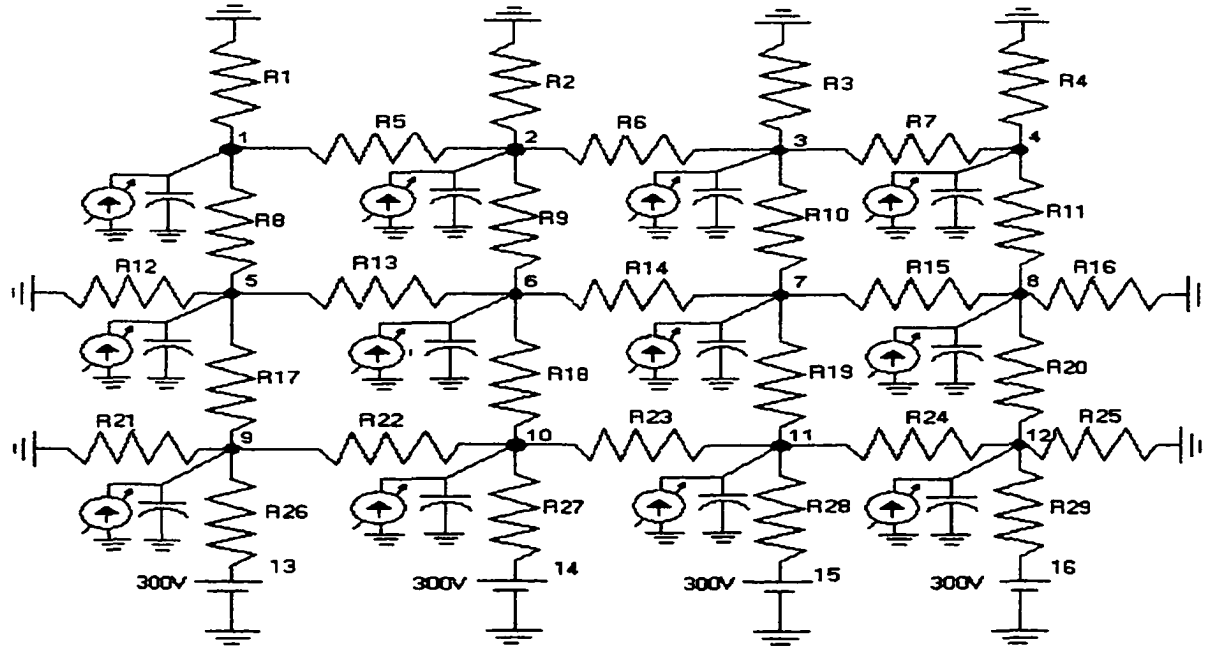

Figure 3-2: Electrical equivalent circuit for a two-dimensional sample.

3.3.4 THREE-DIMENSIONAL ANALYSIS

A three-dimensional sample may be constructed as several stacked two-dimensional planes. This principal is illustrated below as figure 3-3.

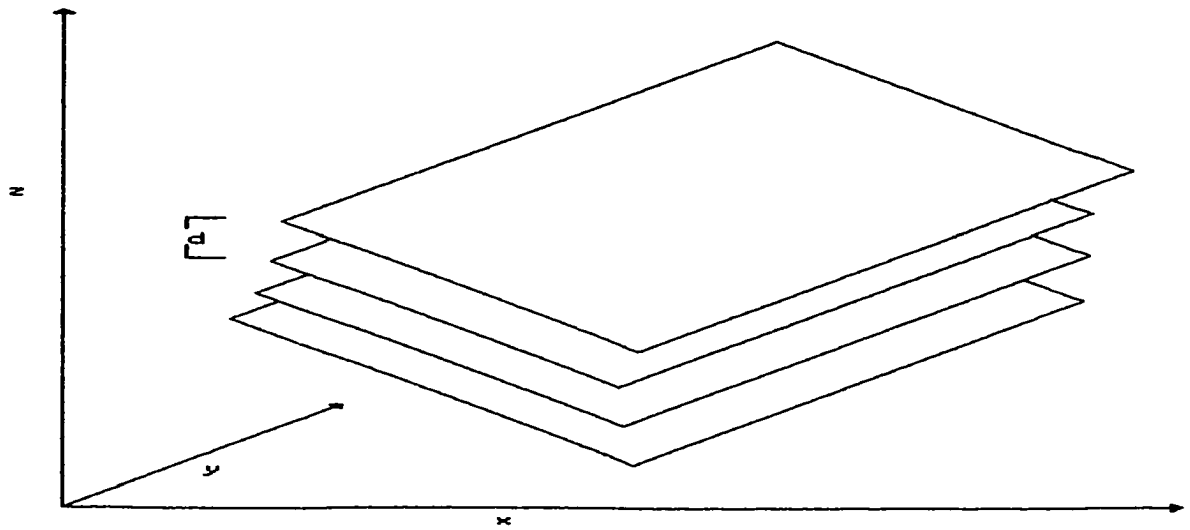

Figure 3-3. Creating a three-dimensional sample by stacking planes.

Each plane is assumed to possess some thickness d, which is the distance between stacked planes. Since no measurement device may be inserted into the solid structure of the device, only one sub-section of length d connects the top plane to the bottom plane. Figure 3-4 displays the electrical attachment circuit that may be connected to the bottom of the two-dimensional circuit to create a three-dimensional representation. Isolation resistors exist along the z-axis at the voltage nodes of each plane, but have been removed for clarity.

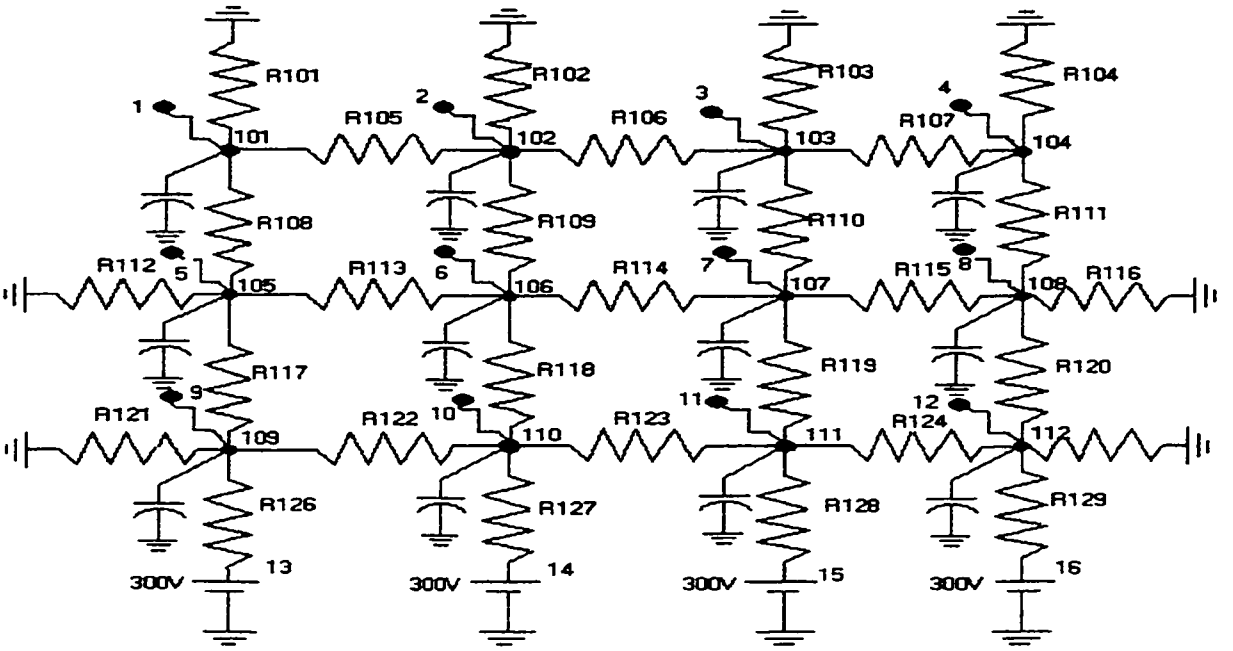

Figure 3-4: Electrical schematic attachment for three-dimensional analysis.

The thickness, d of the sample is assumed to be 0.1m, causing the resistance and capacitance between planes to be equivalent in magnitude to the one-dimensional sample. Capacitors connected to the bottom of the sample have a magnitude increased by a factor of three times normal to account for the third dimension in heat transfer. Top capacitors are only twice as large as that for the one-dimensional analysis to represent surface (two-dimensional) heat flow.

3.4 TEMPERATURE DEPENDANT FEATURES

The thermal conductivity presented thus far has been assigned a constant temperature-independent value. This technique was used to introduce general heat transport behavior through a material. Real materials, however, possess a thermal

conductivity that varies as a function of temperature. This action occurs because of increased internal scattering due to phonons as the temperature increases [25-34]. This essentially leads to a reduced propagation of the thermal energy and lowers the material's ability to conduct heat. From a macroscopic standpoint, this manifests as a reduction in the thermal conductivity parameter. For example, the behavior of silicons' thermal conductivity k(T) is inversely proportional to its temperature and may be expressed by the equation [35]

$$k(T) = \frac{32{,}000}{T-80} . \qquad (3.35)$$

By incorporating this temperature dependence to the one-dimensional sample, for example, it is found that the conductance of both the entire bar and each sub-section vary with temperature. Figure 3-5 plots the conductance values for both the entire bar and each sub-section for a 2-meter/20 sub-section bar with a cross-sectional area of 10^{-4} m^2.

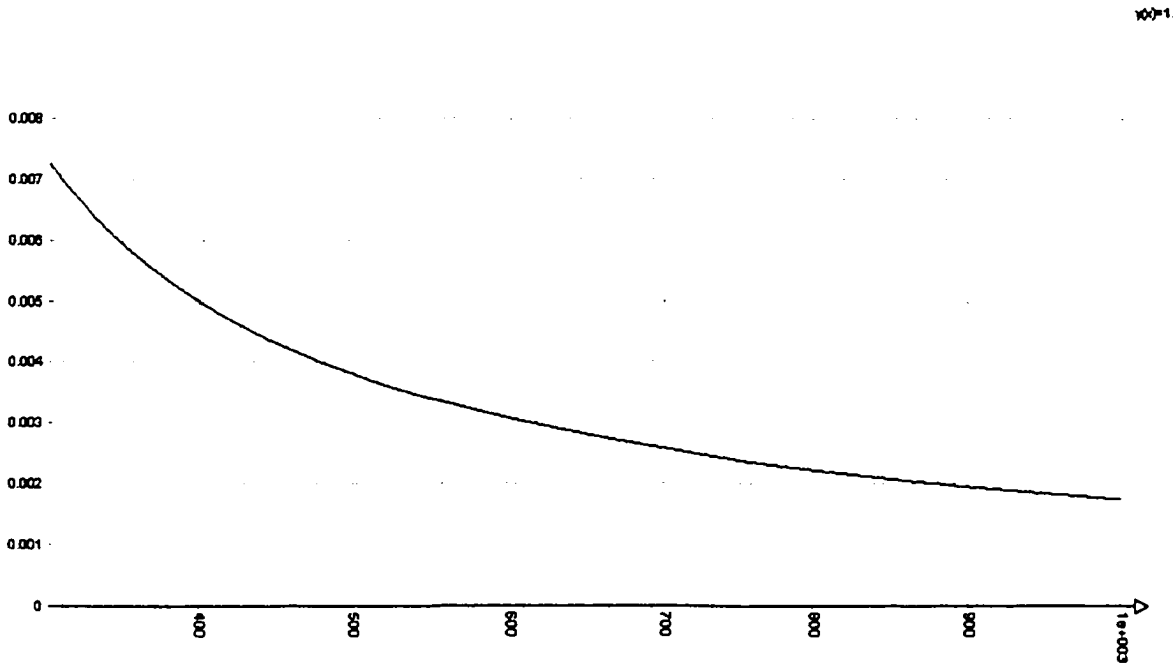

Fig. 3-5(a): Bar conductance as a function of voltage.

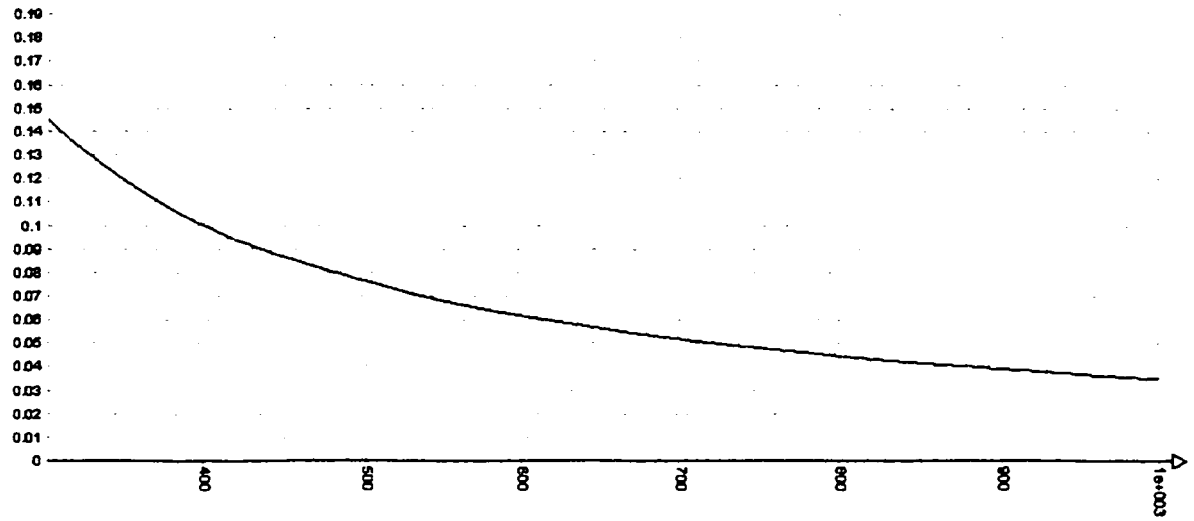

Figure 3-5(b): Sub-section conductance as a function of voltage.

Under these general conditions, the resistance is a function of position as the internal temperature varies with distance within the sample. The overall thermal resistance of the bar (or sample) R_{bar} is then derived as the reciprocal of the total conductance G_{bar}. This, in turn, is simply a collective summation of the conductances for each discretized sub-section $G_{subsection}[i]$. An expression for R_{bar} thus works out be

$$1/R_{bar} = G_{bar} = \sum_{i=1}^{i=n} G_{sub\text{-}section}[i] = \sum_{i=1}^{i=n} \{(A_i/dx_i)\, k\,[T_i]\}\,. \qquad (3.36)$$

During a transient response, the resistance of each sub-section will change with time. The above formula can still be applied. However, the conductivity becomes a temperature and time-dependent entity $k\,[T_i\,(t)]$, which will evolve as the transient proceeds towards a final steady state.

3.5 SPICE-BASED IMPLEMENTATION OF NONUNIFORM CONDUCTIVITY

The electrical circuits for the temperature independent models simulated by SPICE are obtained from figures 3-1 and 3-2 for the one- and two-dimensional models. A three-dimensional circuit is created by connecting the two-dimensional circuit of figure 3-2 to the electrical attachment circuit of figure 3-4.

The temperature dependant models require the sub-section resistances to be converted into voltage dependant variable resistors. To perform this operation, it is first necessary to convert the sub-section conductance equation into a form usable by SPICE. The conductance, in general, is temperature dependent. Hence, for the electrical analog being applied here, the electrical conductance must effectively become voltage dependent. SPICE allows voltage dependent conductors and resistors, provided they are expressed as a suitable polynomial. The primary task, therefore, is to convert the conductances into appropriate voltage dependent polynomials. This is accomplished by assigning the following third-degree polynomial:

$$P_3 T^3 + P_2 T^2 + P_1 T + P_0 = (A/\Delta x)\, k\,[T], \qquad (3.37)$$

As a specific example, letting the area $A = 10^{-4}$ m^2, $\Delta x = 0.1$ m, and $k = 32{,}000/(T-80)$ as given for silicon, and solving equation (3.37) for three temperatures chosen to be 300K, 600K, and 900K, the following set of simultaneous equations result:

$$27{,}000{,}000\, P_3 + 90{,}000\, P_2 + 300\, P_1 + P_0 = 0.14545 \qquad (3.37a)$$

$$216{,}000{,}000\, P_3 + 360{,}000\, P_2 + 600\, P_1 + P_0 = 0.06154 \qquad (3.37b)$$

$$729{,}000{,}000\, P_3 + 810{,}000\, P_2 + 900\, P_1 + P_0 = 0.03902 \qquad (3.37c)$$

Solving, yields: $P_3 = 1.79 \times 10^{-9}$, $P_2 = -2.89 \times 10^{-6}$, $P_1 = 1.19 \times 10^{-3}$, and $P_0 = 43.64 \times 10^{-3}$.

Conductances, instead of resistance values, are calculated so that a voltage-controlled current source may be utilized to model a voltage-controlled resistance. The voltage drop that occurs between nodes is used to calculate a conductance, which in turn controls the magnitude of current output of a voltage-controlled current source. This variable current source is placed in parallel across each sub-section resistance to control the quantity of current flowing through it, thus simulating a non-linear resistance. This process is pictured schematically as figure 3-6.

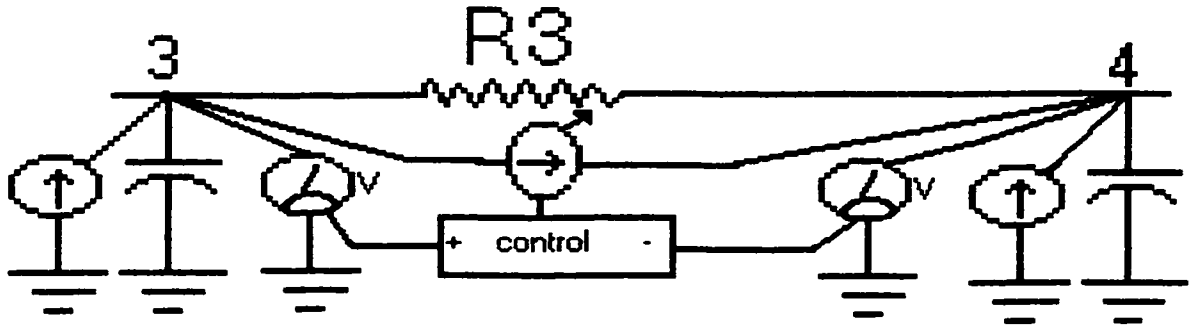

Figure 3-6: Nonlinear sub-section resistance.

The voltage-controlled conductance is implemented in SPICE through the use of a double-variable voltage-controlled current source by invoking the following built-in SPICE function. Thus, for example,

GK3 3 4 POLY (2) (3,0) (4,0) 43.64M 1.19M -1.19M -2.89U 2.89U 1.79N -1.79N

Here, GK3 is the name of the voltage-controlled current source. The next two digits (3 and 4) correspond to the connected circuit nodes. Next, the POLY (2) statement indicates that the voltage to control the current source is obtained from two reference locations. The two sets of numbers enclosed within parenthesis indicate the circuit nodes from

where the controlling voltages are to be obtained. Finally, the string of numbers that follow correspond to the magnitude at which to adjust the current source as determined by the conductance difference between the nodes. This voltage controlled current source is placed across each sub-section resistance to model a voltage-controlled resistor (temperature dependant thermal conductivity) along each axis of every model.

3.6 SIMPLE TEST CASE FOR A VALIDITY CHECK

Validation of the electrical model begins by comparing the results of a 2-meter, 10-node electrical model presented in figure 3-1 to the equivalent thermal model.

3.6.1 INITIAL CONDITIONS

Initially, the bar is in an environment with a uniform temperature of 300K. In the equivalent electrical model, the capacitors are fully charged to that of the voltage source (i.e. a constant 300V representing the 300 K temperature). When the capacitors are fully charged, no current flows in the electrical circuit. The initial condition is displayed in the partial schematic of figure 3-7 between circuit nodes 9 through 11. Notice that the current sources are represented as open circuits indicating that they are turned off in the absence of any external excitation or thermal input.

Applying Kirchoff's current law at each loop of the circuit yields the nodal voltages at this time. Figures 3-8 and 3-9 verify this steady-state condition with the SPICE simulator.

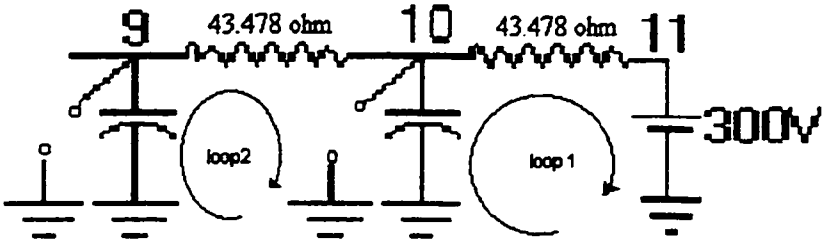

Figure 3-7: Calculating capacitor voltages for the initial condition.

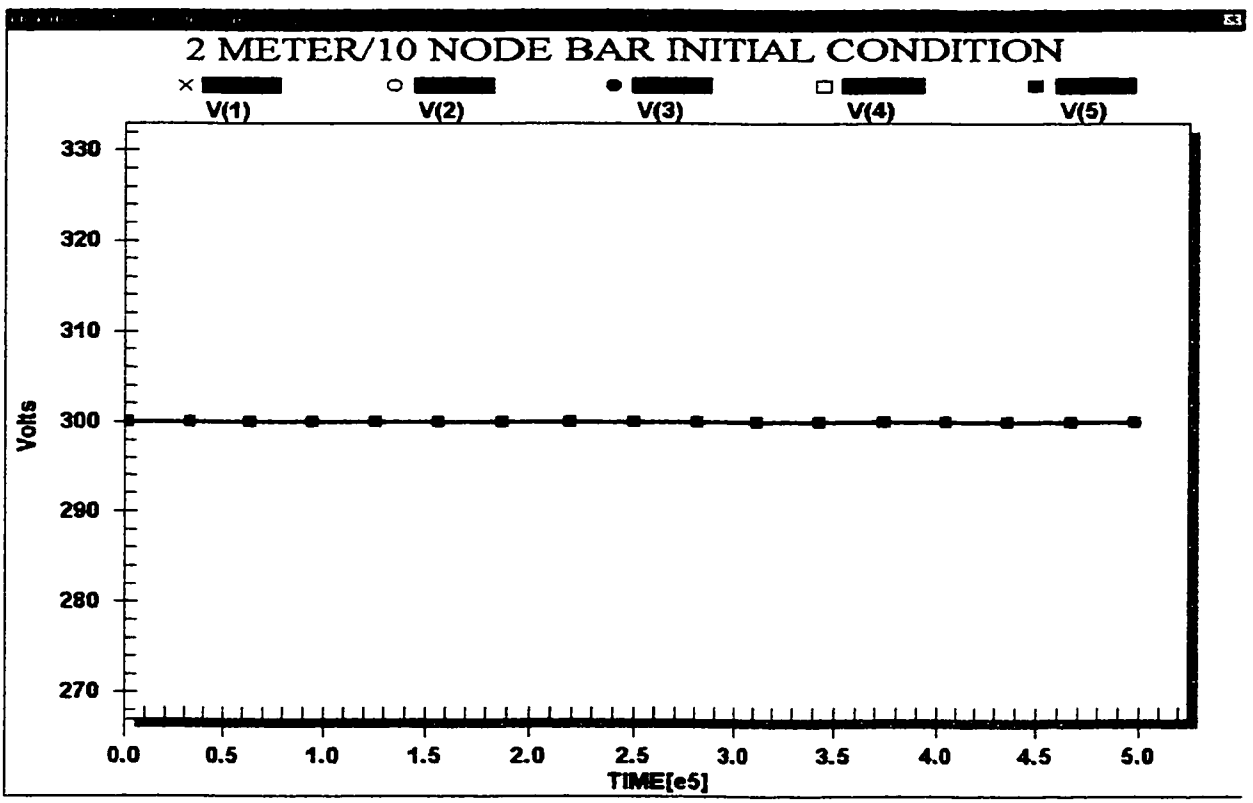

Figure 3-8: Voltage nodes 1-5 for initial condition.

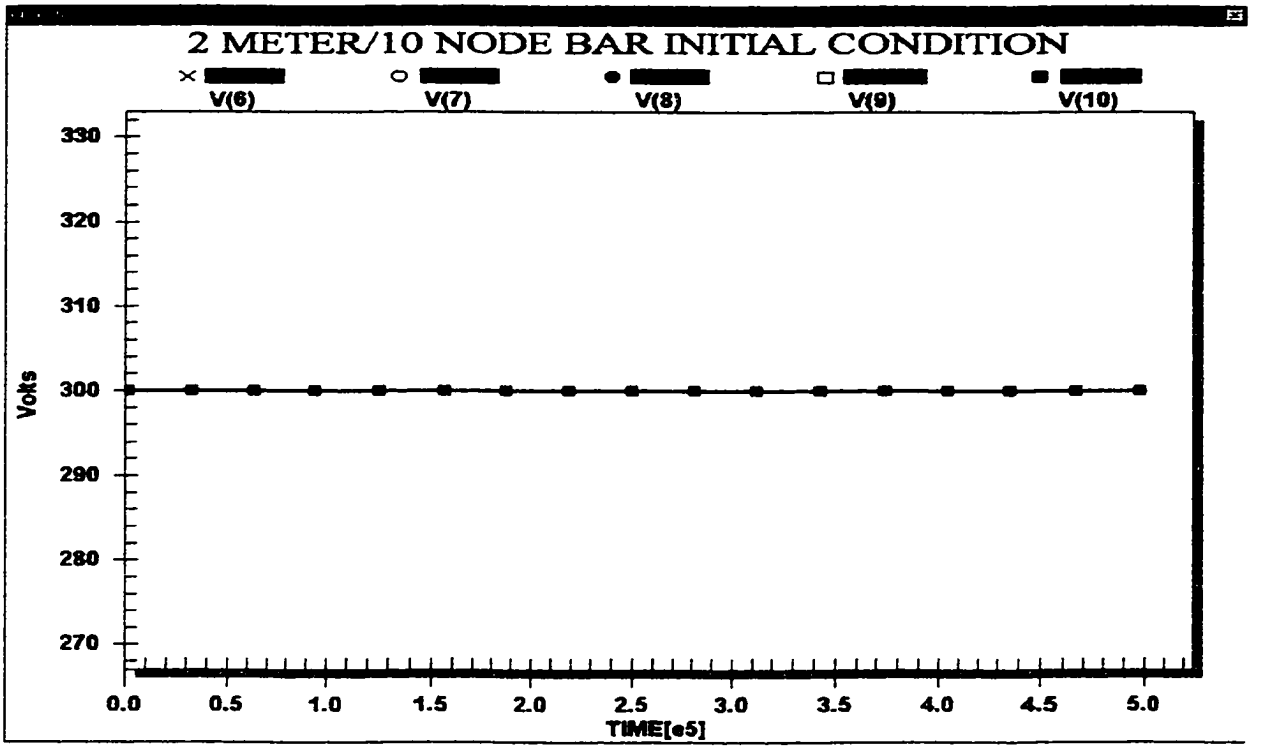

Figure 3-9: Voltage nodes 6-10 for initial condition.

3.6.2 HEATING TRANSIENT ANALYSIS

The electrical circuit simulates the procedure of heating the bar by activating the current sources. When the current sources are turned on, current flows through the electrical equivalent resistance of the bar and produces a voltage imbalance. This unbalanced voltage situation causes current to flow through the circuit to charge the capacitors to a new steady-state value. In thermal terms, this implies a flow of heat due to an internal temperature imbalance at the nodes.

When the current sources are turned on (heat is applied to the bar), 1.4 Amperes from the previous seven current sources adds to the 0.2-Ampere generated at node 9 to produce 1.6 Ampere of current flowing between nodes 9 and 10. This current generates a voltage of 69.565V across R9. Finally, the 1.6-ampere current combines with the 0.2-

ampere source at node 10 to produce 1.8 ampere flowing between nodes 10 and 11. This 1.8-ampere generates a voltage of 78.26V across R10. The resulting schematic representing this scenario is depicted in figure 3-10.

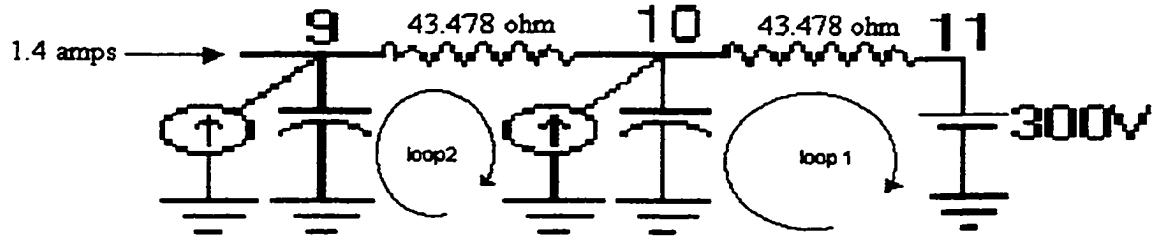

Figure 3-10: Calculating final capacitor voltages for the charging cycle.

Repeating the nodal analysis at the remaining nodes yields the steady state (fully charged) capacitor voltages. Notice that the voltage of each capacitor rises as one draws away from the voltage source, representing an increasing temperature closer to the heat source. The change in voltage across the capacitors does not occur instantaneously, but is delayed due to the circuit component values as determined by each RC time constant. This delay is cumulative between sub-circuits, such that VC9 charges and reaches steady state the fastest and VC1 the slowest. These charging transients correspond with the heating transients of the analytical model. As the bar is heated, the greatest temperature change occurs at the end of the bar that is nearest the heat source (i.e., first sub-section.) However, the heat flux and thermal conduction at the last sub-section of the bar are the largest. The charging transients of the heating cycle are presented in figures 3-11 and 3-12.

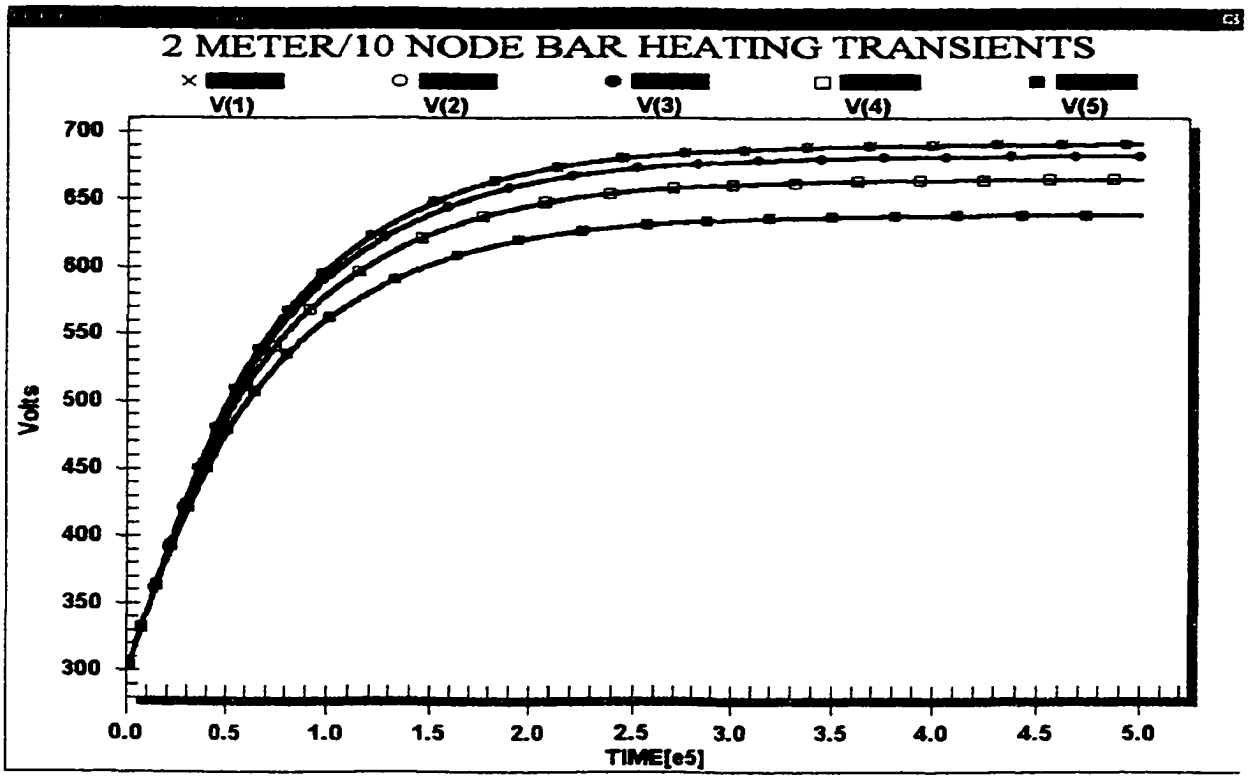

Figure 3-11: Voltage nodes 1-5 for heating transient.

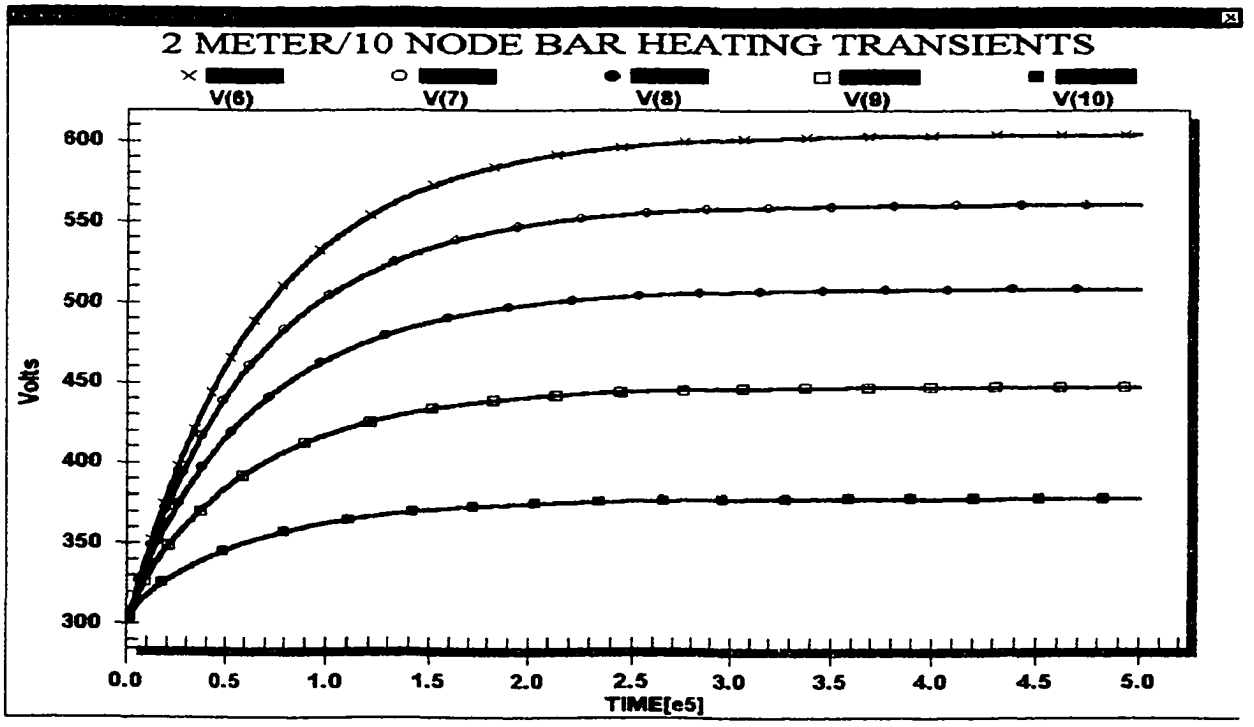

Figure 3-12: Voltage nodes 6-10 for heating transient.

3.6.3 STEADY-STATE CONDITIONS

Steady state is reached in the analytical model when the temperature at each point along the length of the bar remains constant with respect to time. The electrical model of the steady-state situation occurs once all capacitors are fully charged and retain a fixed voltage with respect to time. Once steady state has occurred, voltage and current values for the circuit may be derived through simple applications of Ohm's Law. Figures 3-13 and 3-14 present the steady-state temperatures at the voltage nodes.

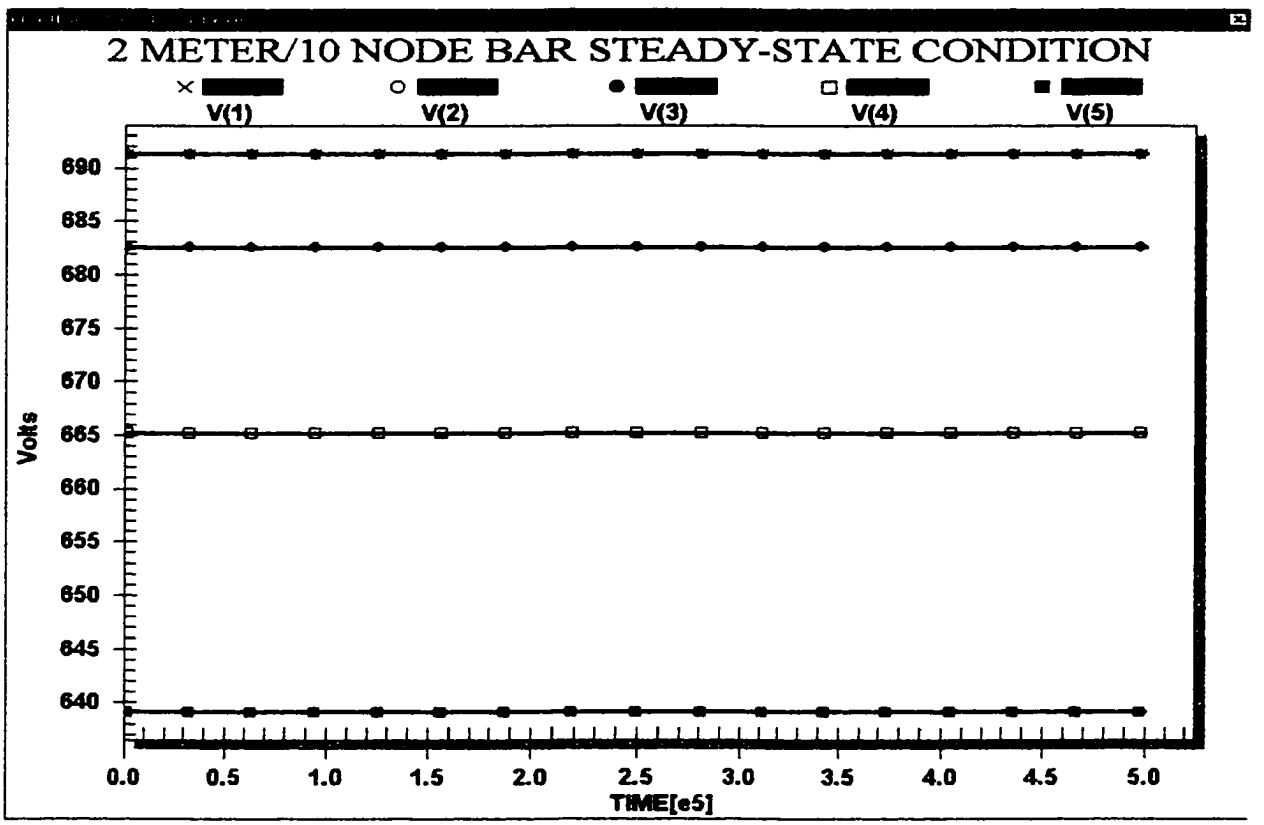

Figure 3-13: Steady-state temperatures for nodes 1-5.

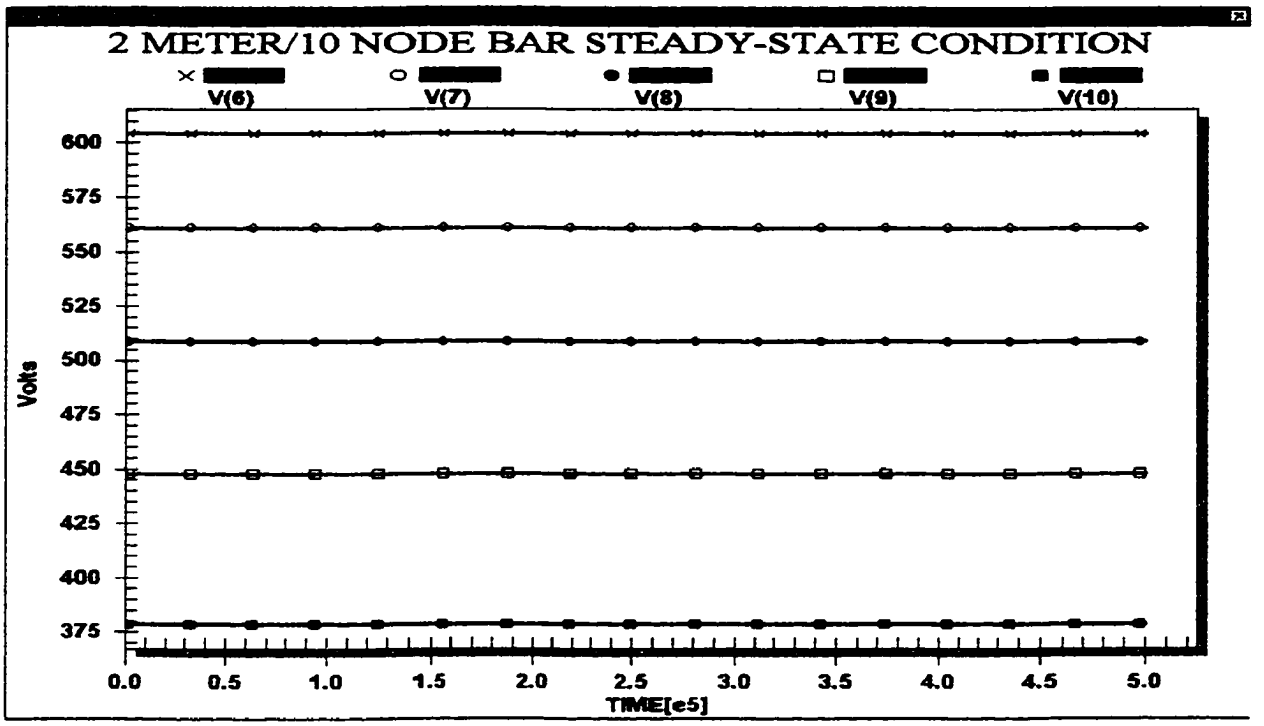

Figure 3-14: Steady-state temperatures for nodes 6-10.

3.6.4 COOLING TRANSIENT ANALYSIS

The bar should begin to cool down to ambient temperature (300K) once the heat source has been removed (electrically equivalent to turning off the current sources). Once the current sources are turned off, the voltages across the resistors drop to zero. This situation presents another voltage imbalance (i.e., a temperature imbalance in the thermal model) that is presented schematically in figure 3-15. Similar voltage imbalances exist throughout the circuit, causing all of the capacitors to discharge to the same voltage as that of the capacitor to its right. This cascade of voltages will reduce the voltage of all capacitors to that of the voltage source (300V). The discharge (cooling) curves express an exponential decay with the same characteristics as the heating cycle. These discharge (cooling) curves are depicted in figures 3-16 and 3-17.

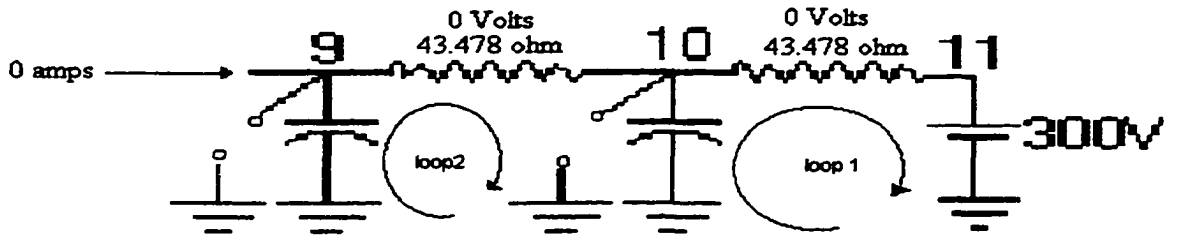

Figure 3-15: Calculating final capacitor voltages for discharge cycle.

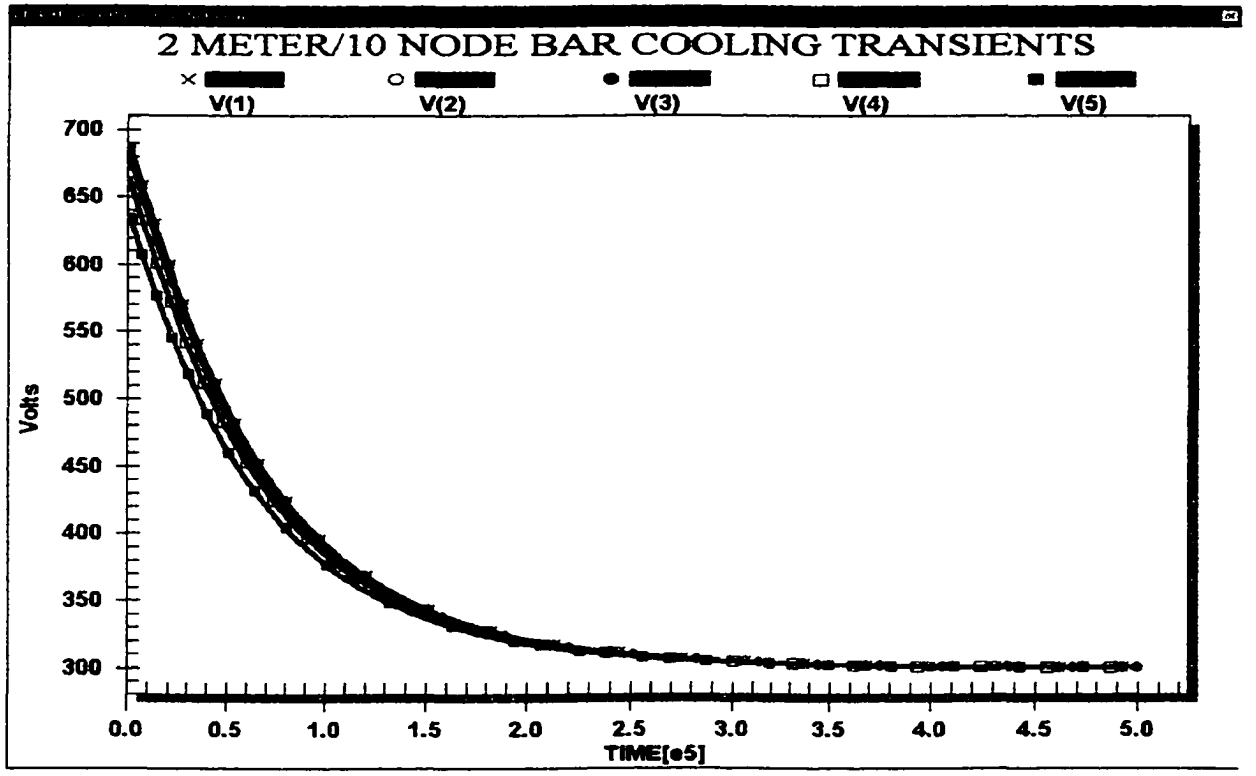

Figure 3-16: Cooling transients for nodes 1-5.

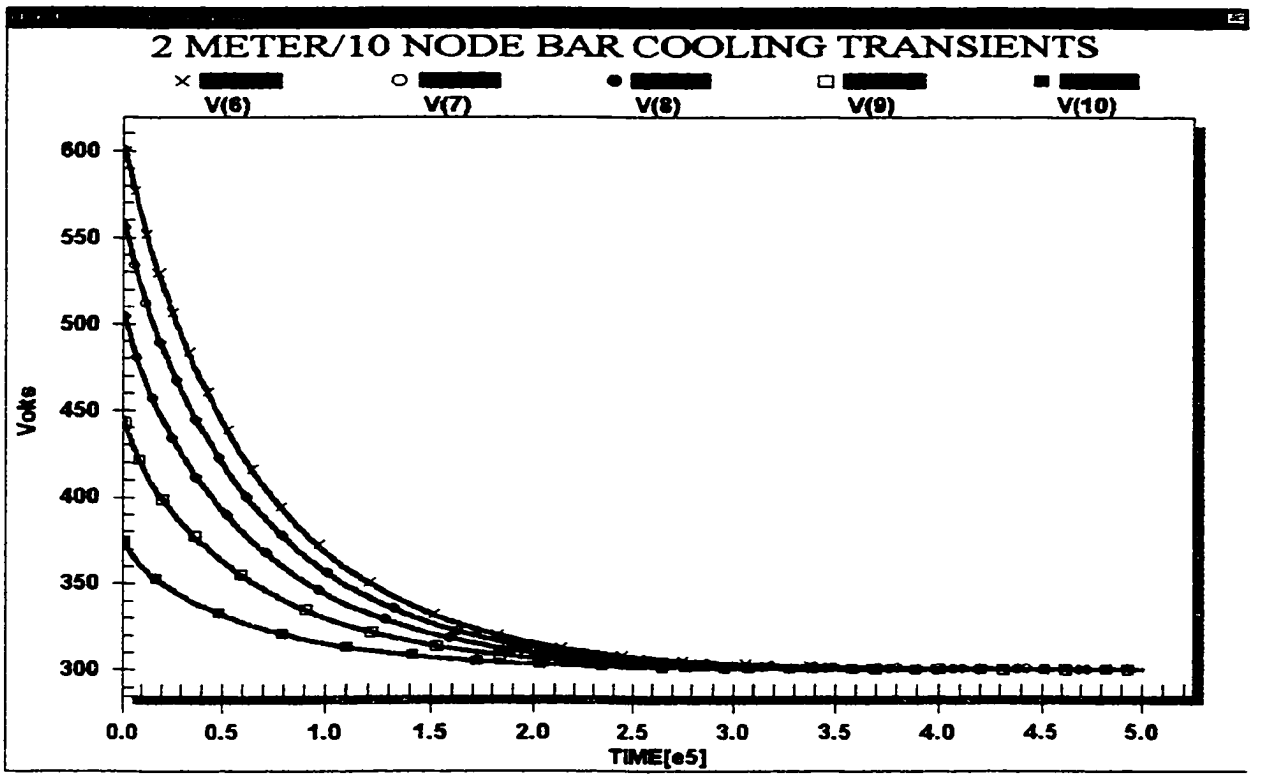

Figure 3-17: Cooling transients for nodes 6-10.

3.6.5 FINAL STATE

The final condition of the bar occurs when it has completely cooled to ambient temperature. This situation can be once again modeled physically and electrically as the initial condition. No SPICE analysis has been presented for this state since it is apparent from the cooling curves that the voltage (temperature) remains at 300V (300K) after approximately 350,000 seconds.

3.7 THE 20-NODE BAR

Discussion thus far has analyzed a 2-meter, 10-node bar. This sample was chosen to illustrate basic concepts and for ease of presentation. Since SPICE only allows up to

five voltage nodes to be plotted at a time, two simulation runs were required to display all of the nodal voltages. This basic model, however, does sacrifice accuracy. For the 10-node sample, each sub-section size was 0.2 meters long. The 20-node model has each sub-section of length 0.1 meters. Since the length of each sub-section is now reduced to half, the accuracy of the model is improved. Table 3-2 verifies the improvement in accuracy of the model with a reduction in sub-section length for the steady state temperatures. This improvement in accuracy does, however, present a trade-off in simulation run time.

Simulation results for both the heating and cooling transients for the 20-node case were obtained from the SPICE-based electrical analog model. Figures 3-18 through 3-27 show the time-dependent heating for the bar from ambient to steady-state temperatures. For simplicity and compactness, the "cool-down" plots have been shown in Figs. 3.28-3.29 for only the first two and the last two grid points.

X (m)	Analytical (K)	SPICE (K)	Error (%)
0.0	732.0	691.3	5.6
0.2	727.7	691.3	5.0
0.4	714.7	682.6	4.5
0.6	693.1	665.2	4.0
0.8	662.9	639.1	3.6
1.0	624.0	604.4	3.1
1.2	576.5	560.8	2.7
1.4	520.3	508.7	2.2
1.6	455.5	447.8	1.7
1.8	382.1	378.2	1.0
2.0	300.0	300.0	0.0
0.0	723.8	706.6	2.4
0.1	722.8	706.6	2.2
0.2	719.6	704.5	2.1
0.3	714.5	700.3	2.0
0.4	707.2	693.9	1.9
0.5	697.4	685.3	1.7

0.6	685.8	674.7	1.6
0.7	679.1	667.4	1.6
0.8	662.9	652.2	1.6
0.9	644.5	634.8	1.5
1.0	618.2	610.6	1.2
1.1	595.9	589.2	1.1
1.2	571.7	565.7	1.1
1.3	549.5	543.5	1.1
1.4	520.3	515.2	1.0
1.5	489.0	484.8	0.9
1.6	455.5	452.2	0.7
1.7	419.9	417.4	0.6
1.8	382.1	380.4	0.4
1.9	342.1	341.3	0.2
2.0	300.0	300.0	0.0

Table 3-2: Accuracy as a function of sub-section size at steady state.

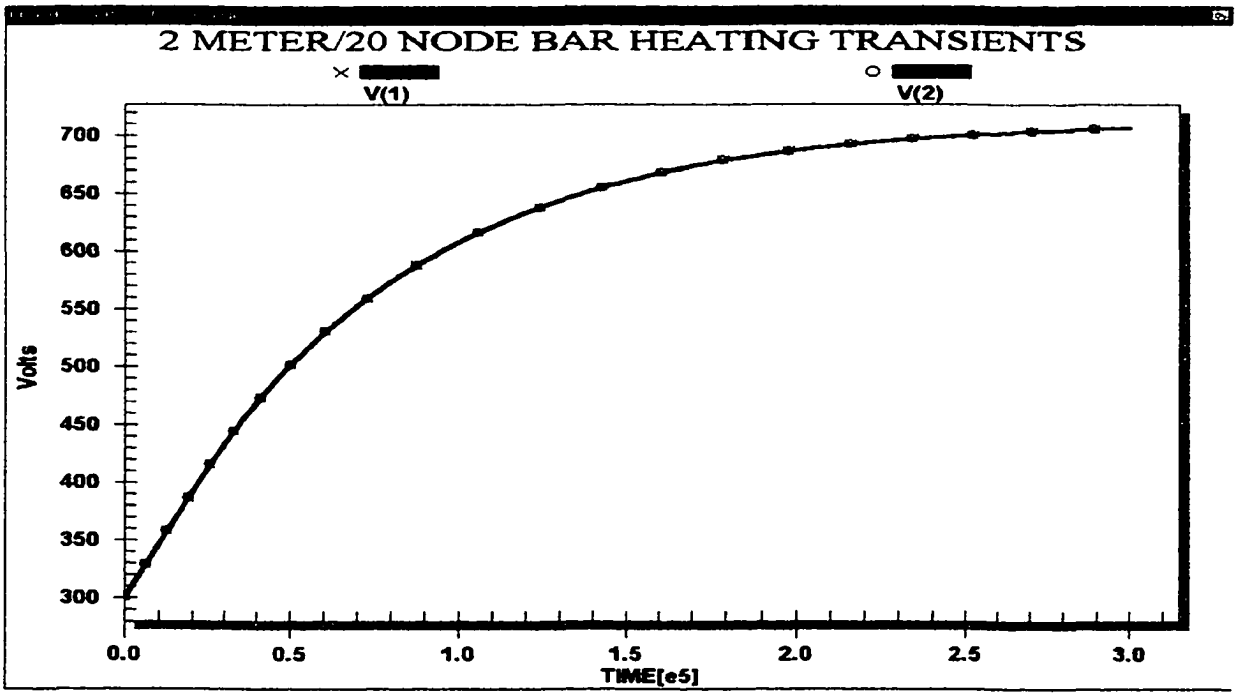

Figure 3-18: Voltage nodes 1 and 2 charging transients.

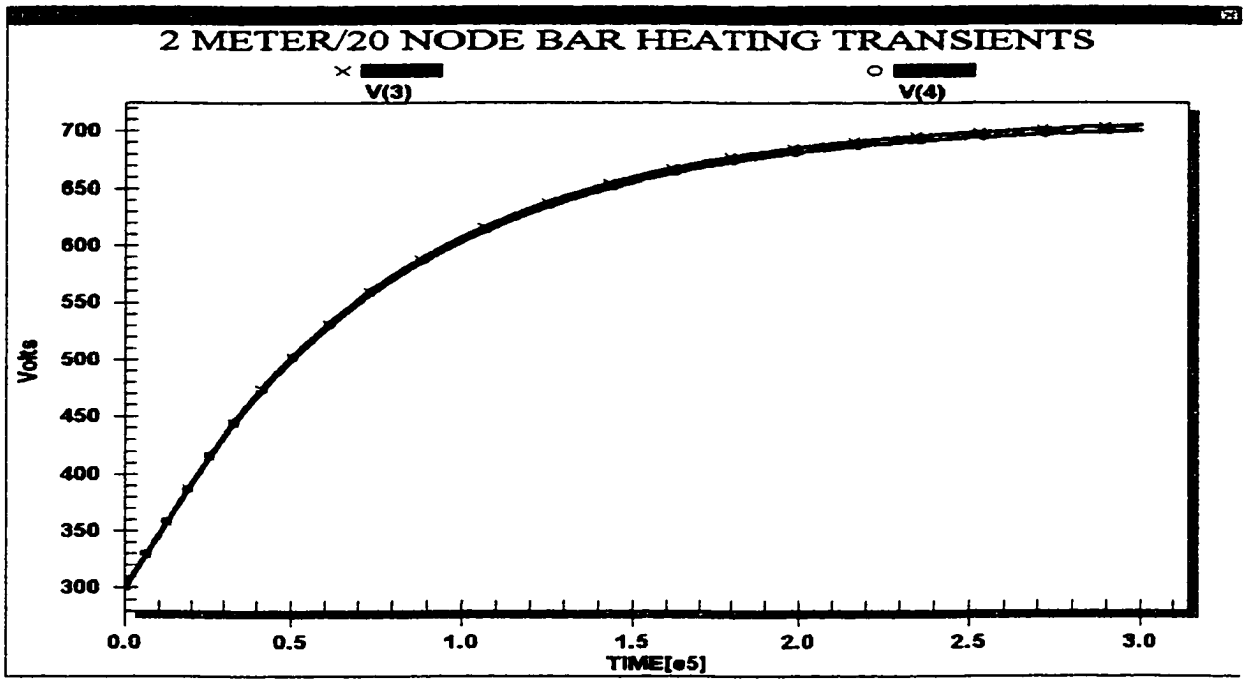

Figure 3-19: Voltage nodes 3 and 4 charging transients.

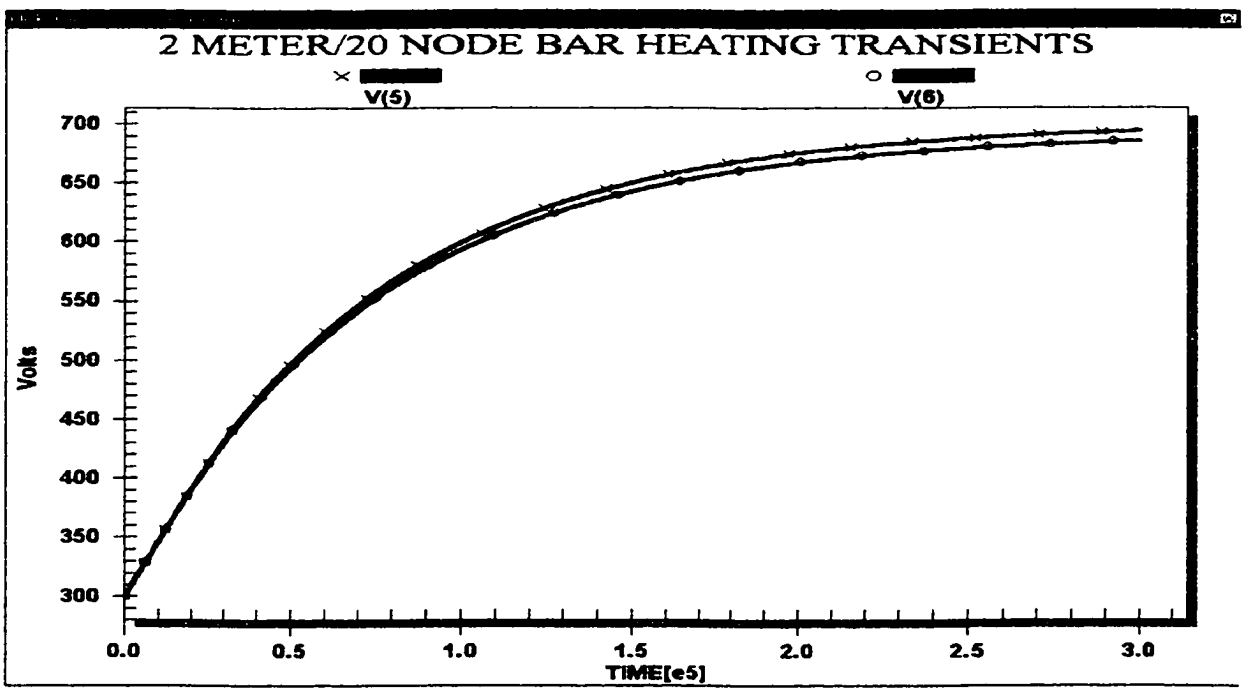

Figure 3-20: Voltage nodes 5 and 6 charging transients.

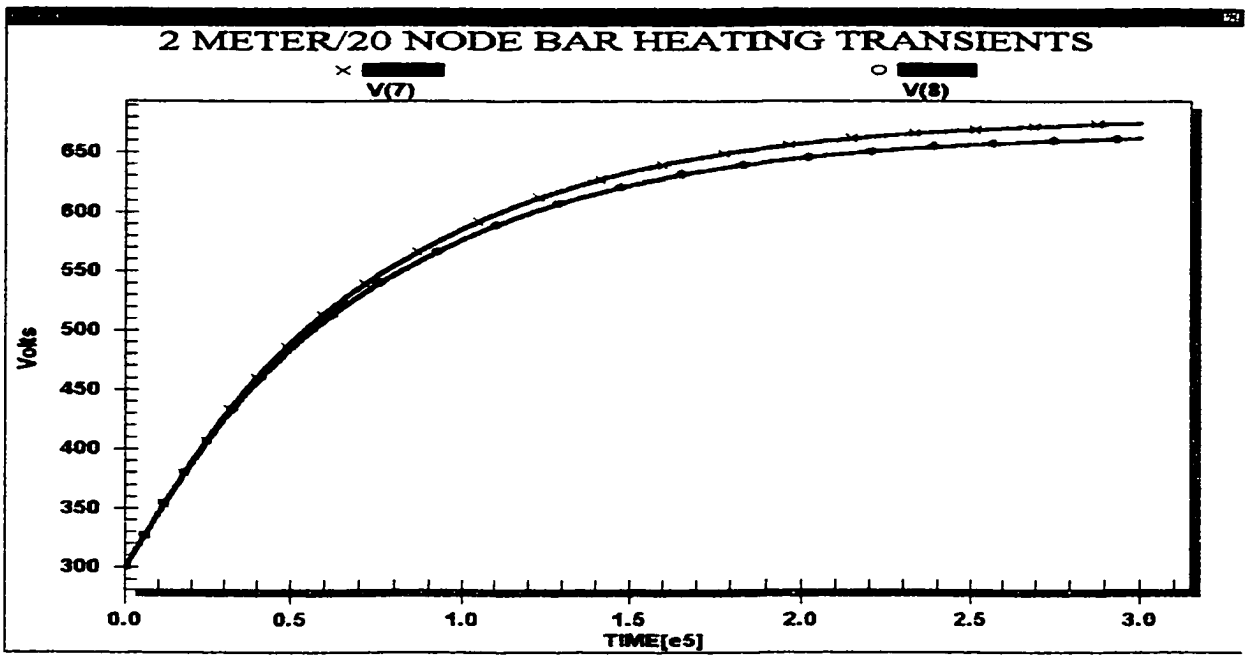

Figure 3-21: Voltage nodes 7 and 8 charging transients.

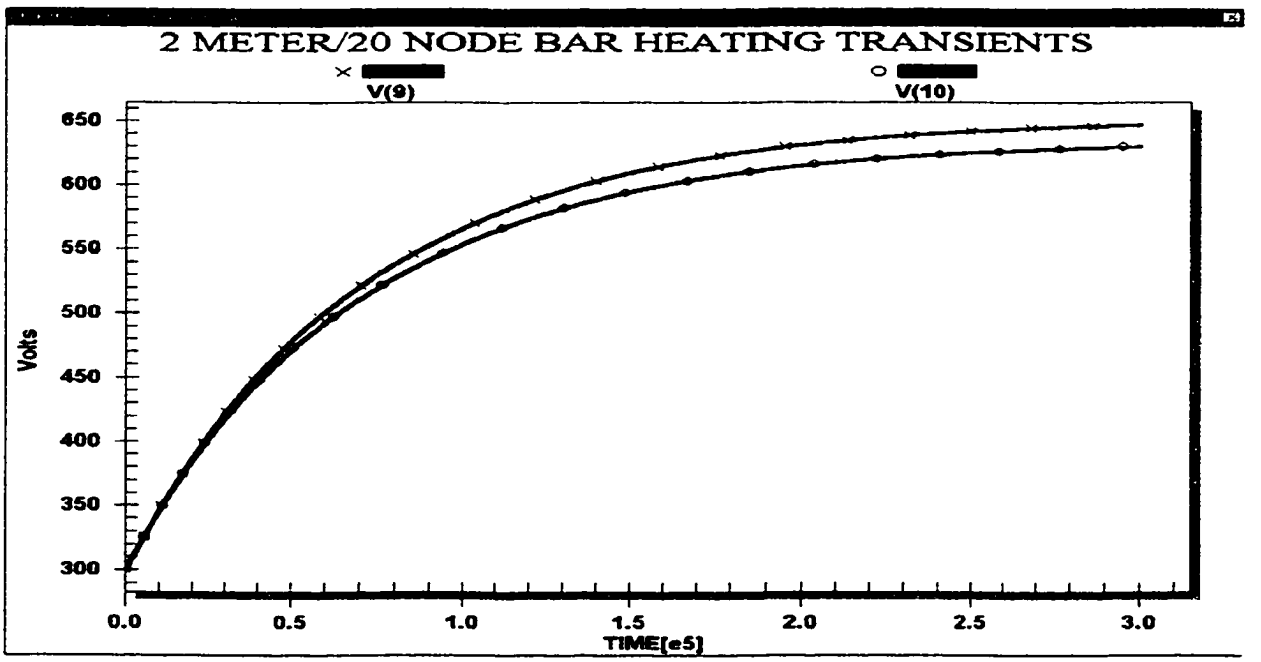

Figure 3-22: Voltage nodes 9 and 10 charging transients.

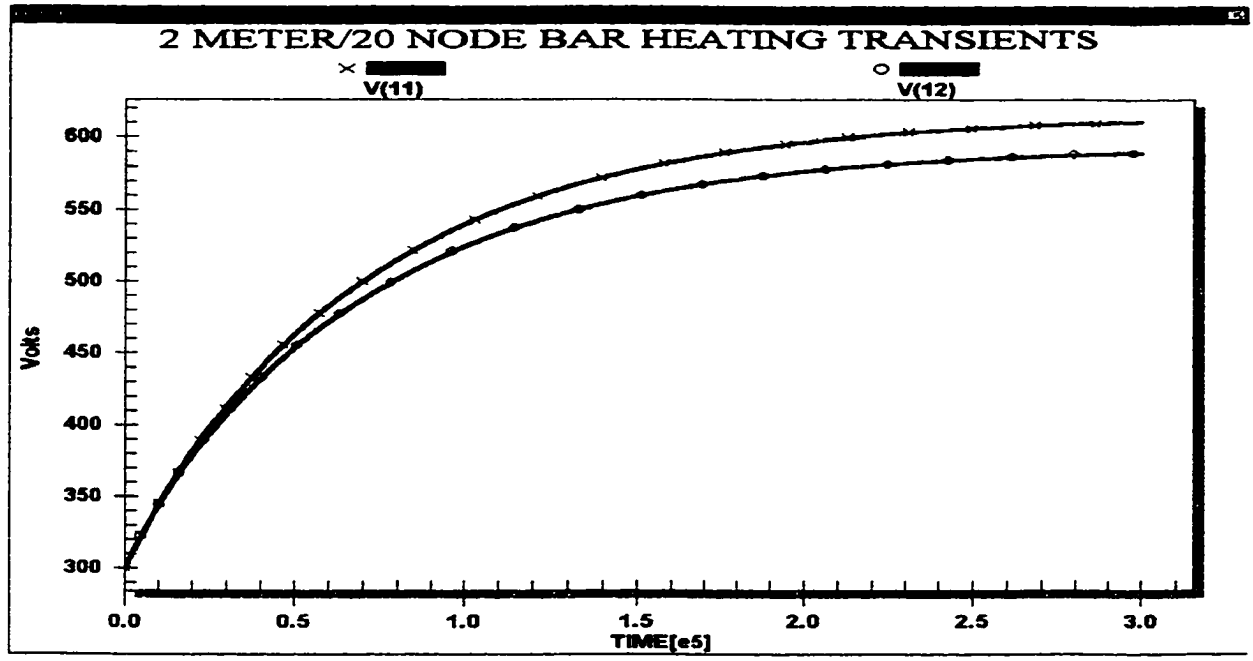

Figure 3-23: Voltage nodes 11 & 12 charging transients.

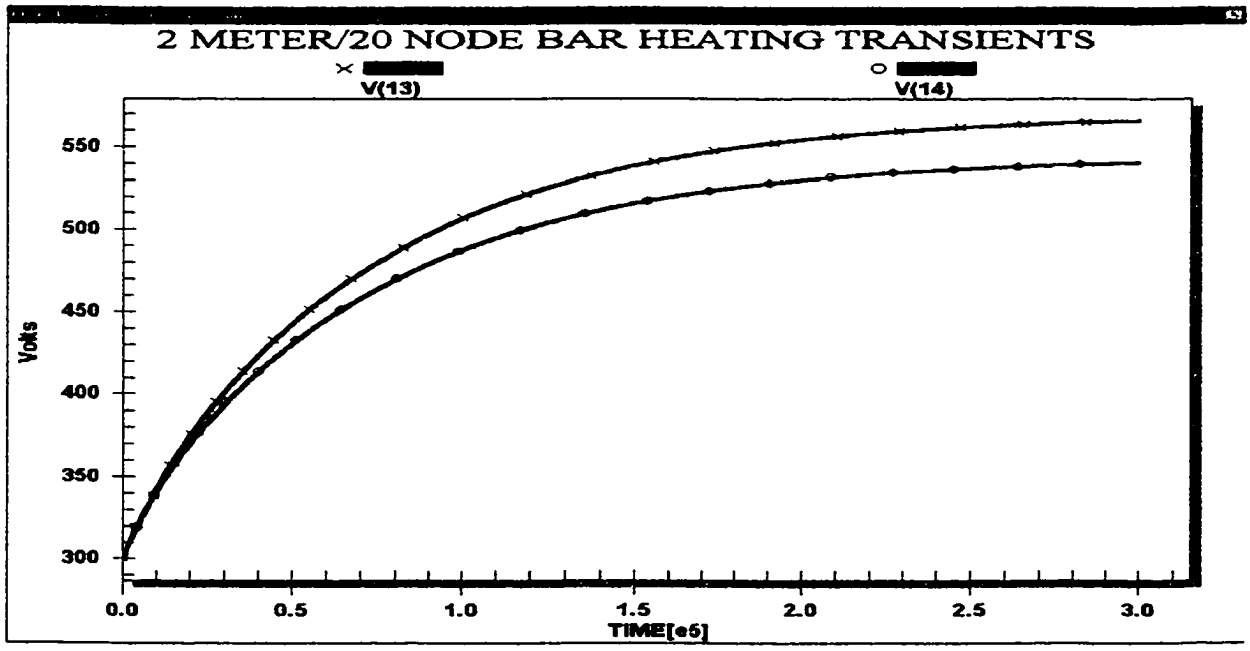

Figure 3-24: Voltage nodes 13 & 14 charging transients.

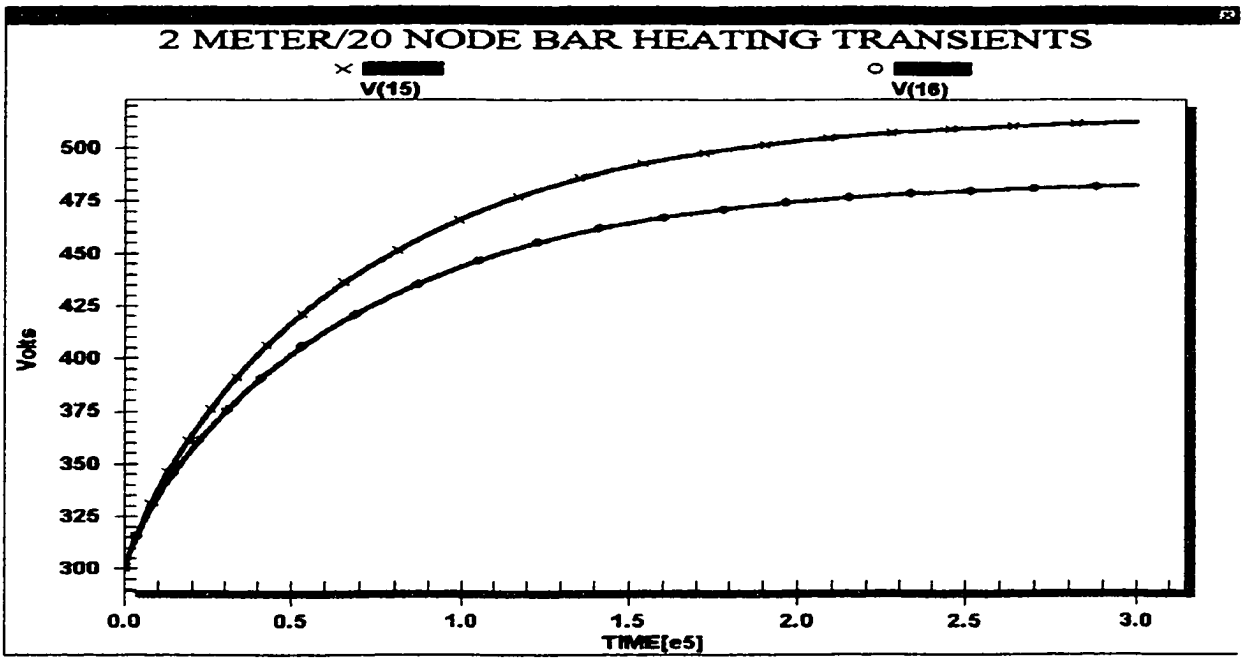

Figure 3-25: Voltage nodes 15 and 16 charging transients.

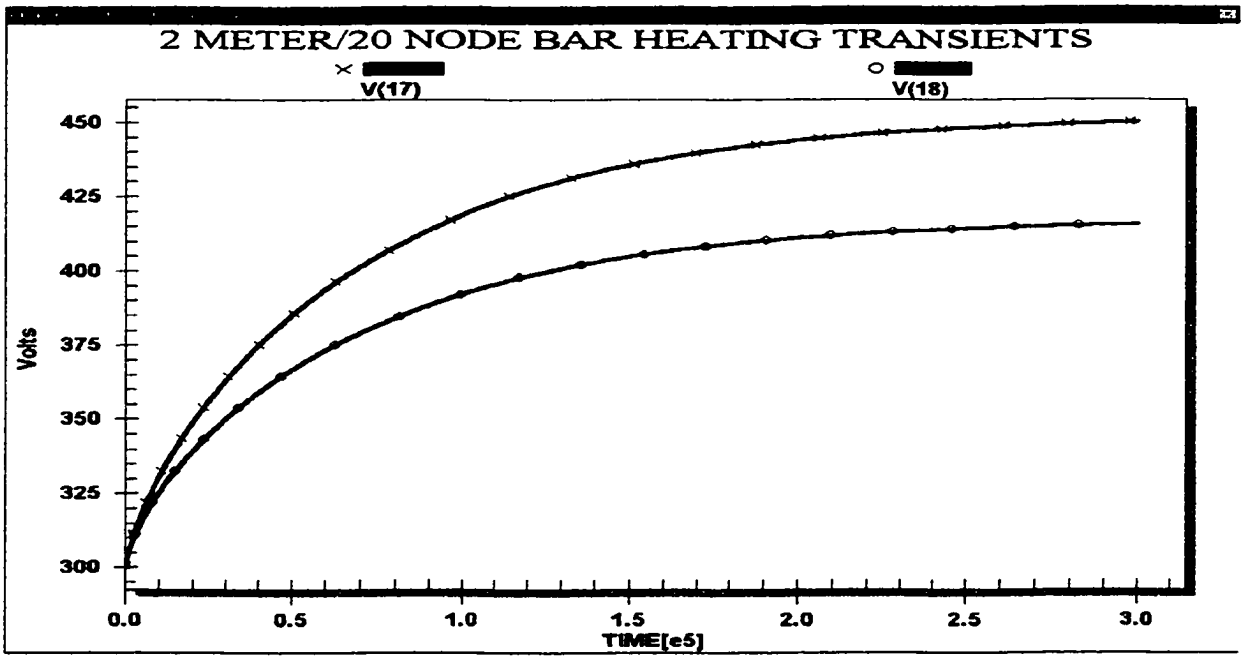

Figure 3-26: Voltage nodes 17 and 18 charging transients.

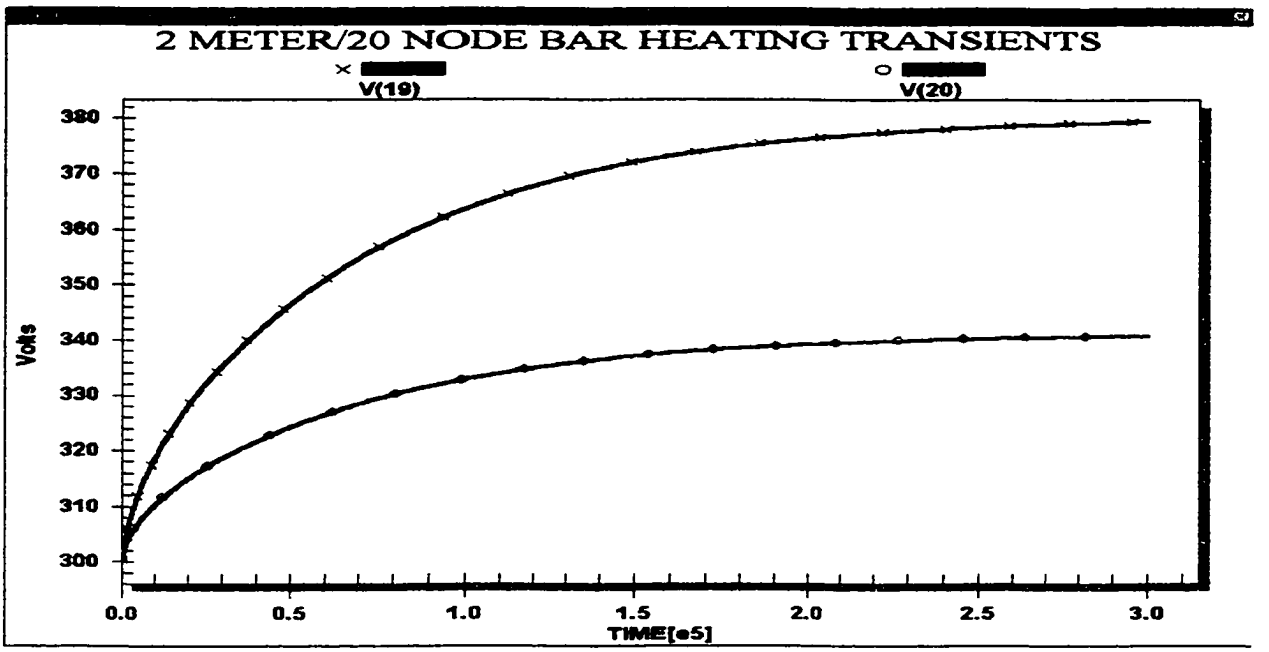

Figure 3-27: Voltage nodes 19 and 20 charging transients.

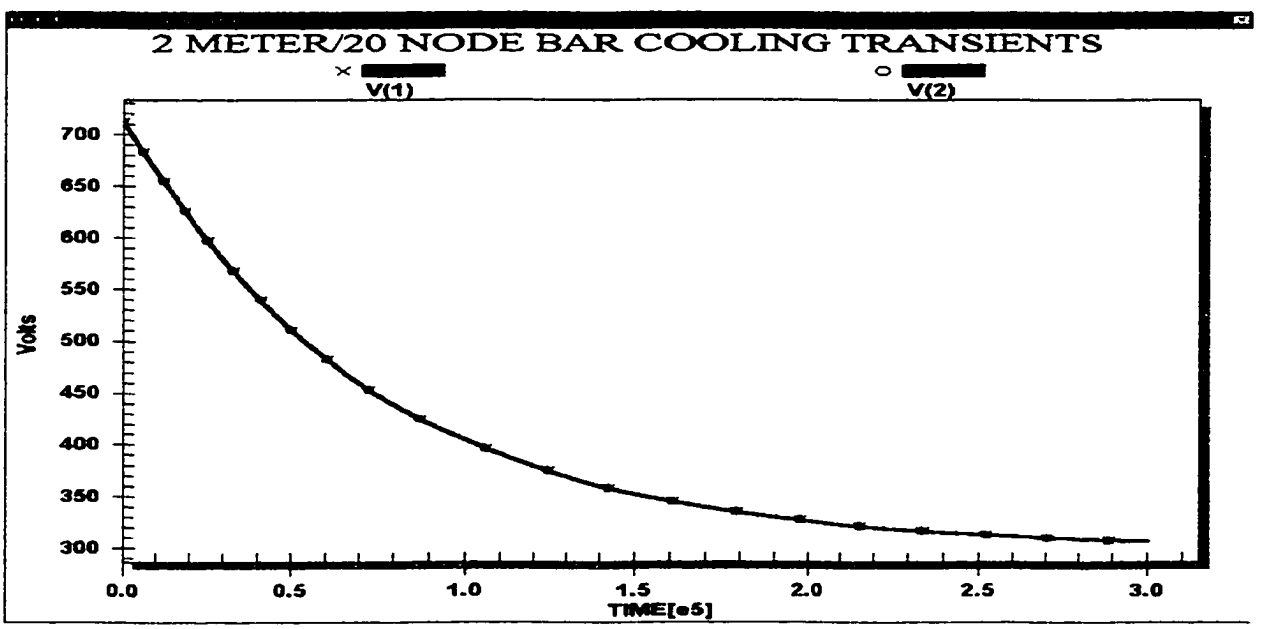

Figure 3-28: Voltage nodes 1 and 2 discharge transients.

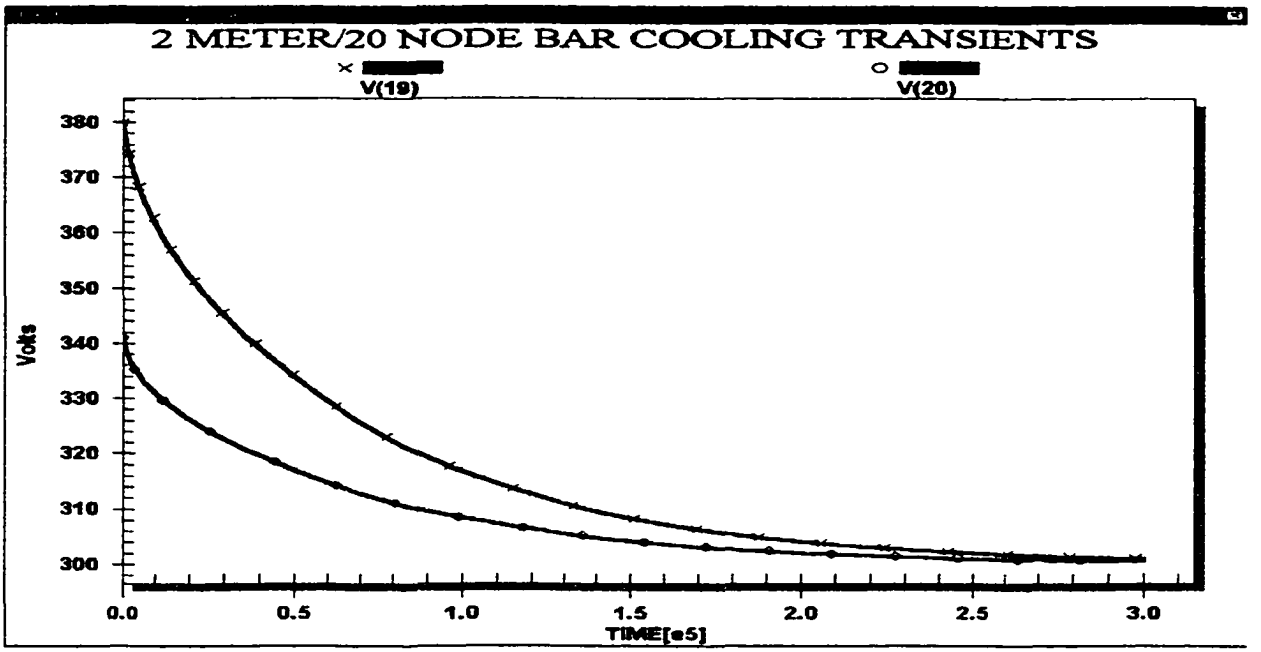

Figure 3-29: Voltage nodes 19 and 20 discharge transients.

3.8 CONCLUSION ON SIMULATIN ACCURACY

Based on the numerical simulation results presented in the previous section, the following conclusions can be drawn.

(i) The electrical equivalent analog developed in this thesis, provides a good physical representation of the actual thermal system. The nodal voltages (and hence, nodal temperatures) and currents all had the correct qualitative trend and behavior.

(ii) The SPICE-based implementation is accurate. Errors of less than 5 % between the SPICE results and those of an exact thermal solution were obtained for a 10-segment analysis. This maximum error decreased to less than 2.4 % by doubling the number of internal grid points.

(iii) The close agreement between the SPICE-based result and the exact analytical solution validates the present model. Since both heating- cooling-transients as well as steady state analysis was performed the comparisons made were careful and detailed.

(iv) The reliability (i.e., 100 % - error%) for the 20-node electrical model approached a beta distribution as depicted in figure 3-30 below.

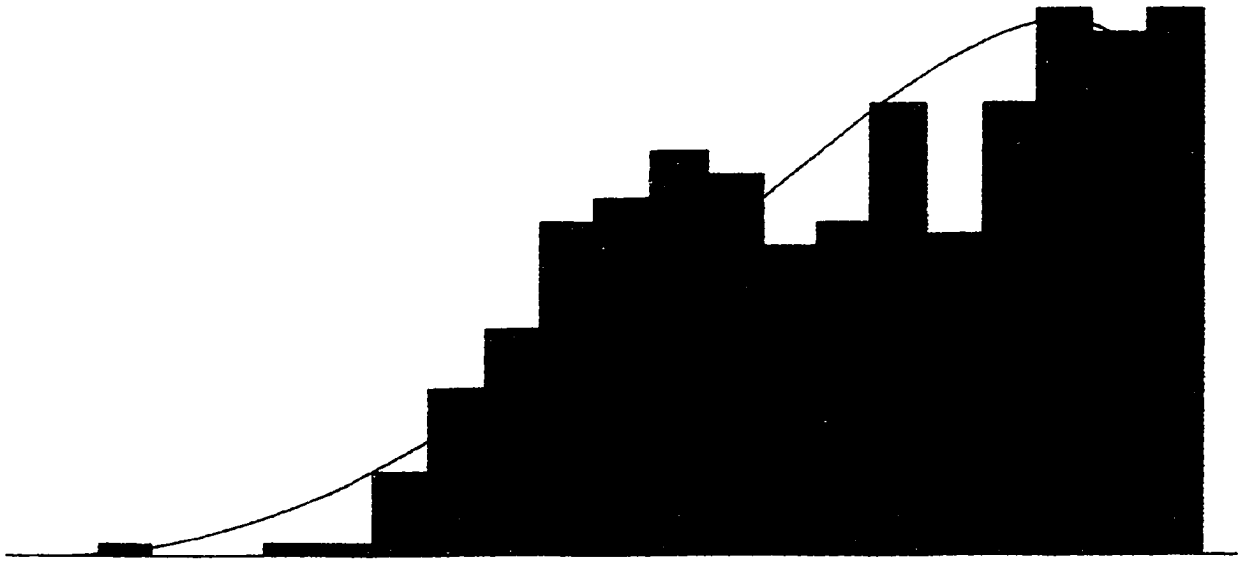

Figure 3-30: Distribution function for reliability of a 20-node model.

Reliability of the electrical model ranges in magnitude between 96.9 to 100 percent. The mean reliability of the electrical model is 99 percent with a standard deviation of 0.664 percent. A 100 percent correlation exists between both models at steady-state ambient temperature and varies during transient and steady state heated conditions.

(v) The reliability for the 10-node bar also approaches a beta function with reliabilities in the range of 94.4 to 100 percent. This function has a mean reliability of 99.3 percent with a standard deviation of 1.27 percent. Although this function has a higher mean accuracy, the range of error and standard deviation are greater than that for the 20-node analysis verifying greater probability for error with an increase in sub-section size. The beta distribution function for the 10-node bar is illustrated as figure 3-31 below.

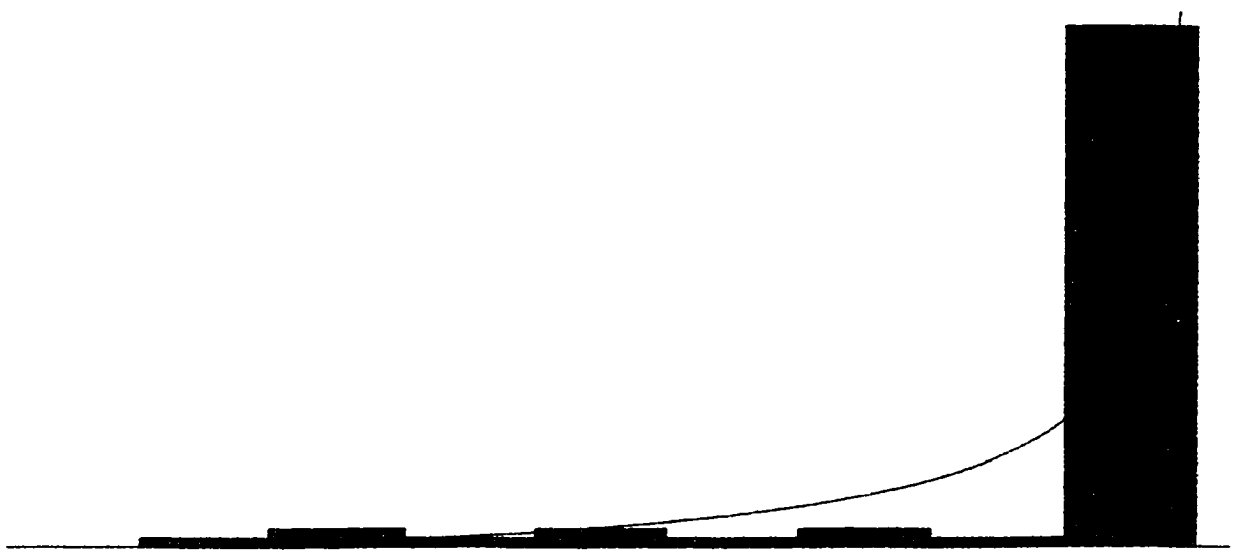

Figure 3-31: Distribution function for reliability of a 10-node model.

3.9 TEMPERATURE DEPENDANT MODEL TRANSIENT ANALYSIS

Circuit behavior for the heating and cooling of the 1D bar (corresponding to the charging and discharging of the capacitors in the electrical circuit analogue) were similarly carried out upon the temperature-dependent thermal conductivity model. In this case, voltage-controlled resistors were suitably used.

3.9.1 INITIAL STEADY-STATE CONDITION

Initially, all of the capacitors are fully charged and no current flows. All voltage nodes remain at a constant 300V. Figure 3-32 illustrates this state at equidistant locations along the length of the bar.

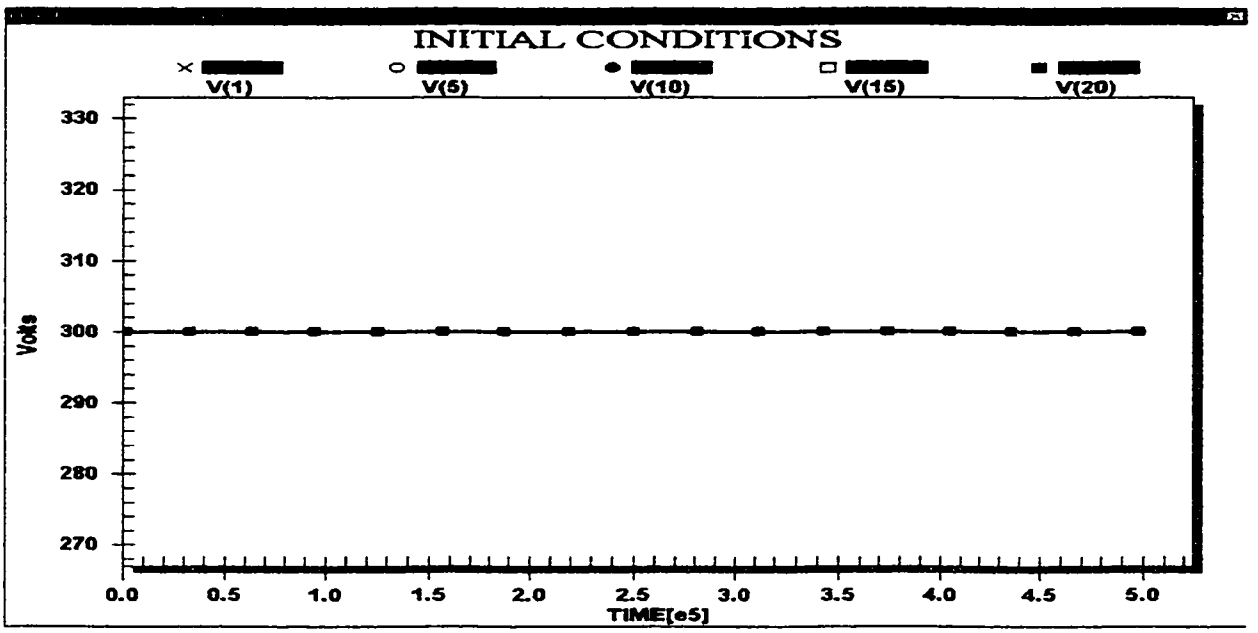

Figure 3-32: Initial state voltages for the variable thermal conductivity model.

3.9.2 HEATING TRANSIENT ANALYSIS

With the inclusion of the voltage-controlled resistors between the nodes, the charging time constants and maximum voltages are altered with respect to the constant-conductivity situation. As the capacitors charge, the associated nodal voltages increase, thereby raising the sub-section resistances. As the resistances increase, the maximum steady-state node voltage rises to a higher magnitude and at a faster rate. The heating curves for the variable thermal conductivity model and the comparison to the constant k model are presented in figures 3-33 and 3-34, respectively.

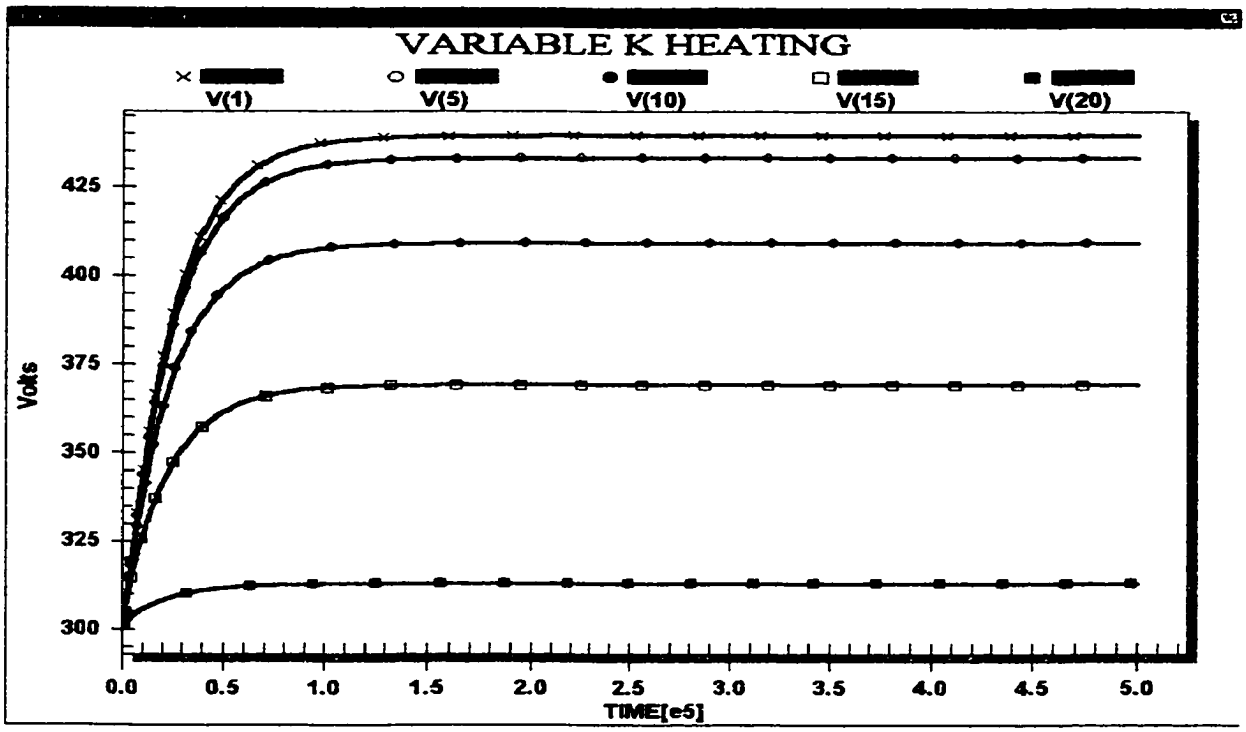

Figure 3-33: Variable thermal conductivity heating transients.

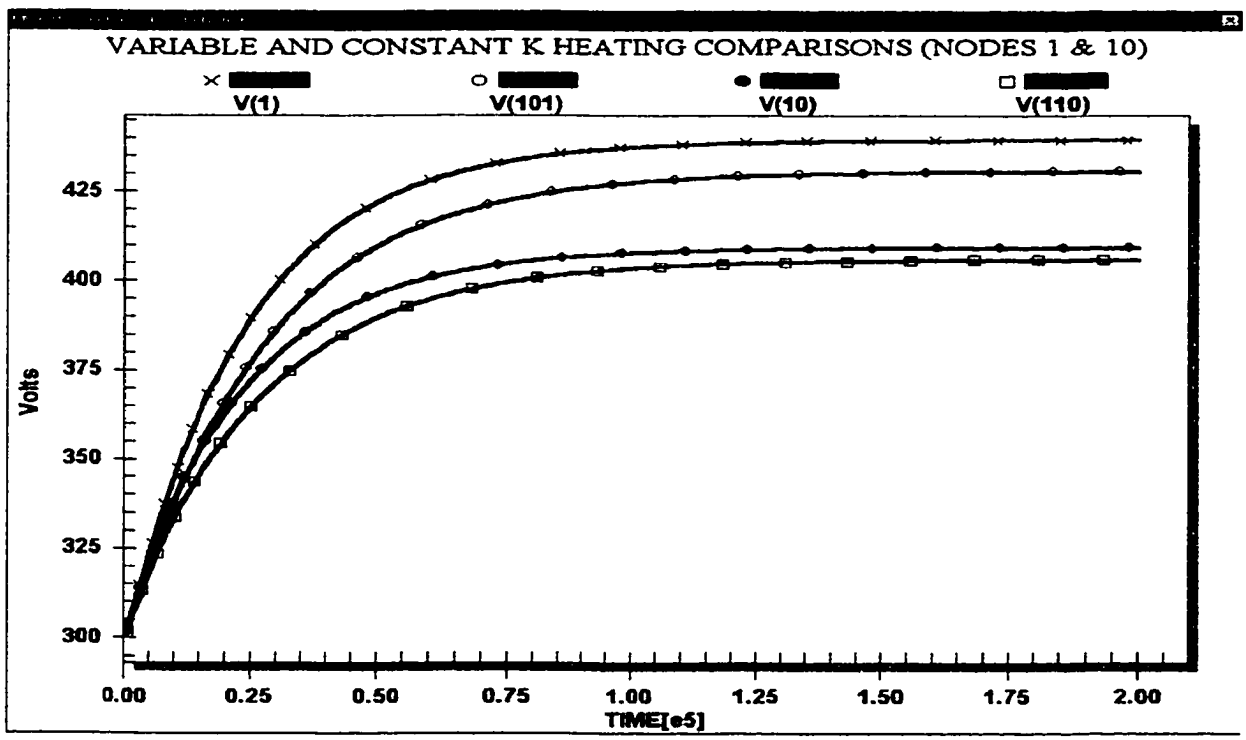

Figure 3-34: Heating transient behavior comparison between models.

The nodal voltages V(1) and V(10) correspond to nodes 1 and 10 of the variable thermal conductivity model. The constant thermal conductivity model depicts nodal voltages 1 and 10 as V(101) and V(110), respectively, in Fig. 3-34. A comparison of the heating curves in Figure 3-34 indicates that the variable thermal conductivity model reaches a higher steady-state voltage than when it remained constant. This behavior corresponds to the ideal expected analytical behavior. As the temperature within the bar rises, its thermal conductivity decreases. With a decrease in thermal conductivity, heat travels slower to the heat sink and builds up at the site. This buildup of heat increases the temperature at the location creating a more rapid heat up rate and a higher steady-state temperature.

3.9.3 COOLING TRANSIENT ANALYSIS

Once the heat source is removed (current sources turned off) the capacitors begin to discharge. As the capacitors discharge, the nodal voltages decrease. This decrease in nodal voltage potential causes the sub-section resistors to also lower in value, causing the capacitors to discharge faster. Even though the initial voltages at the nodes are higher for the variable thermal conductivity model, it cools faster than the constant thermal conductivity model due to the decreasing resistor values. Cooling curves for the variable thermal conductivity model and the comparison to the constant k model are plotted in figures 3-35 and 3-36, respectively.

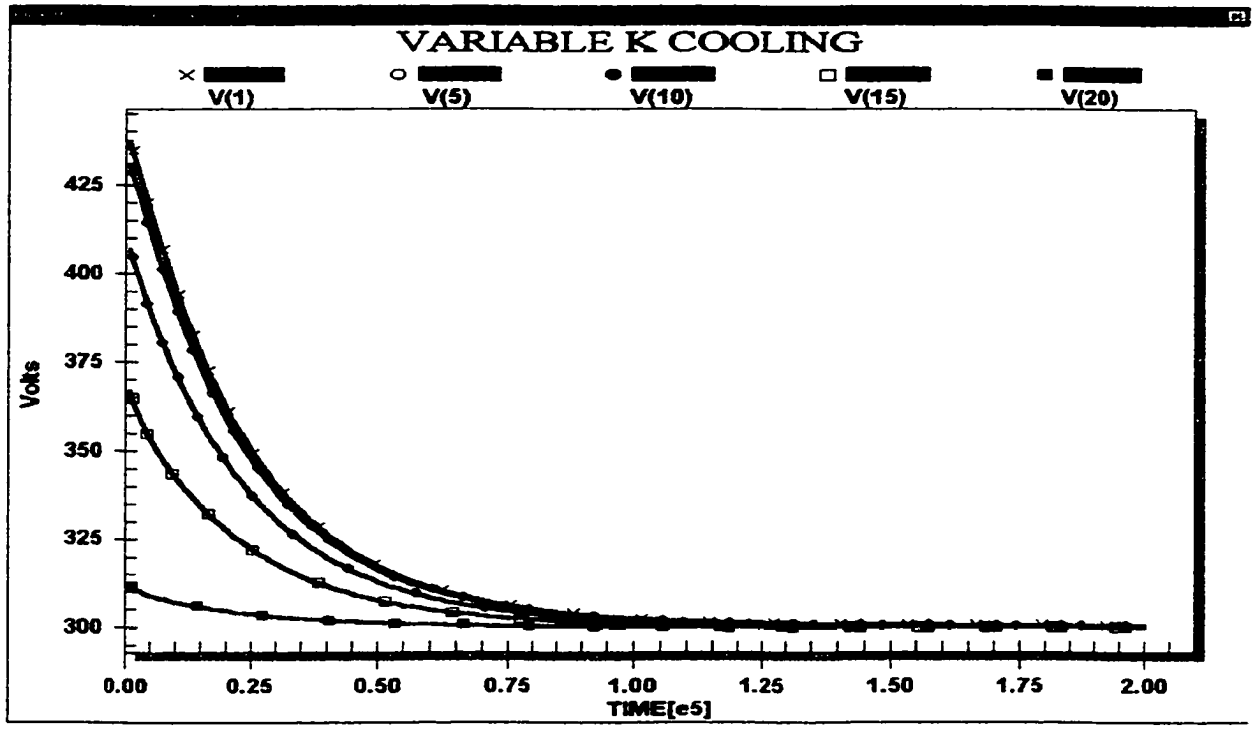

Figure 3-35: Variable thermal conductivity cooling transients.

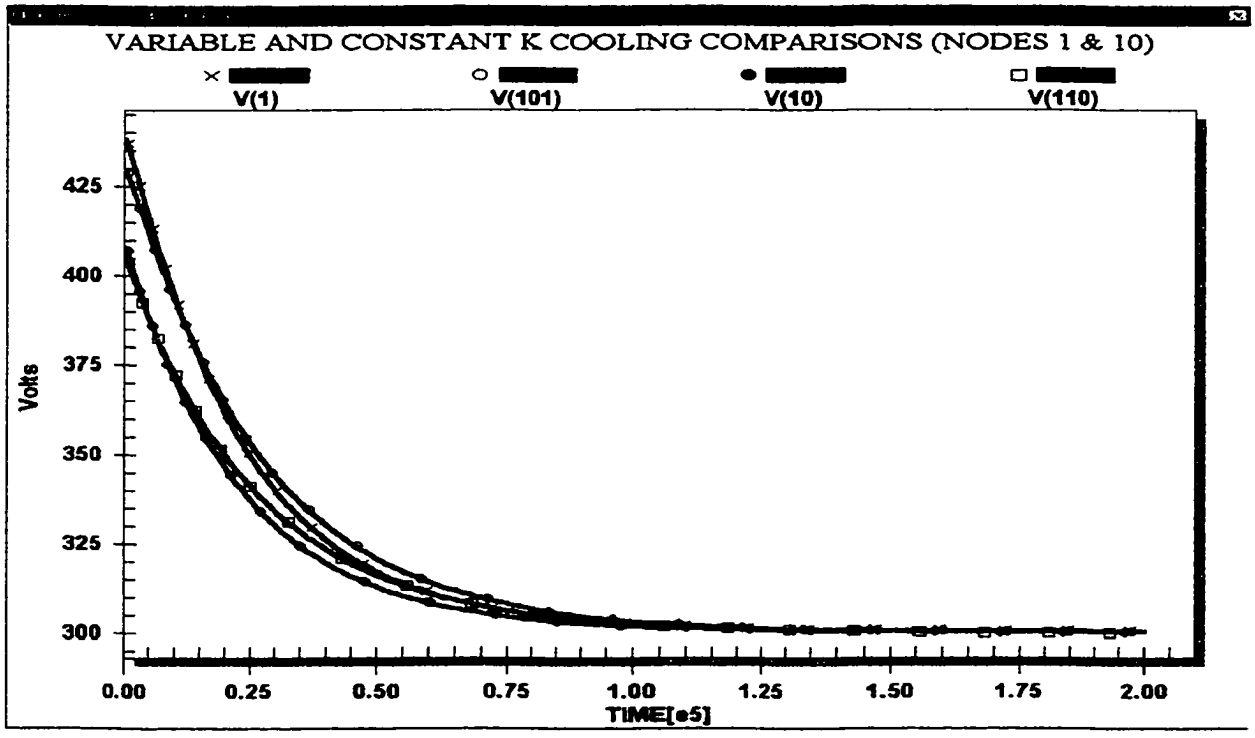

Figure 3-36: Cooling Transient behavior comparison between models.

3.9.4 FINAL STATE

The final state for the variable thermal conductivity model is identical to the initial state and occurs after 125,000 seconds after removal of the heat source. This once again demonstrates the validity of the model, the correctness of its implementation, and the accuracy of the physical results.

CHAPTER IV

RESULTS FOR THE THERMAL DIAGNOSTIC PROBLEM

4.1 INTRODUCTION

This chapter begins by introducing the possibility of applying the SPICE-based method for non-intrusive thermal diagnostic analysis. Non-intrusive thermal diagnostic (NITD) is a useful and increasingly popular tool to sense and detect material failures, cracks, and structural imperfections. NITD is generally carried out by subjecting the samples under test to pulsed thermal stimuli. Based on the signatures of the transient heating response within the sample, predictions can be made regarding its uniformity and homogeneity. Deviations from expected behavior, in terms of delays in the heat signal or amplitude variations indicate damage or internal imperfections. In order to obtain quick evaluations, it becomes desirable to scan the samples quickly, and yet obtain good spatial resolution. This has become possible with the advent of pulsed lasers, which are being used to locally heat sections of the samples under test.

A case is made here for utilizing the current SPICE-based numerical technique to accurately predict and model such heating transients and spatially resolved signatures for NITD. The next section presents a brief discussion of NITD. It is shown that NIDT will require the analysis of transient heating and cooling curves at various sections of a sample when it is subjected to external laser pulses to induce heating. Next, SPICE-based results for the response of a focused single and multiple traveling heat pulses are presented for one-, two-, and three-dimensional cases. Initially, the transient behavior of the traveling focused heat source is discussed and verified for a pure sample in the absence of any defects. Next, material defects are introduced to gauge the differences in

the thermal transient signal. It is shown that the differences can be used to detect defects and aberrations in homogeneity in samples through differential thermal analysis simulations.

4.2 THERMAL DIAGNOSTICS – APPLICATIONS AND SCOPE

Nondestructive testing and diagnostics are beginning to play an increasingly important role in reliability analysis, component wear-out testing, life-cycle estimates, and safety inspections [36]. Critical areas of nondestructive and non-intrusive testing for safety include: crack detection in airplane structures (especially the wings), fatigue in heavy machinery, and load-bearing rotating components and equipment. In general, structural components subjected to cyclic and/or random loads can develop cracks [37]. Corrosion can accelerate this failure process. Once a crack initiates, it can grow during subsequent load cycles leading to catastrophic failure and hazardous consequences. Therefore, it is important to be able to detect such cracks, fractures, and stress-related inhomogeneities for preventive maintenance. In this regard, a variety of techniques have been proposed for such monitoring and nonintrusive diagnostics [38-41]. These techniques are required since it is not easy or practical to dismantle equipment during the testing process, and care must be taken to ensure that no damage results in the diagnostic procedure itself. The ever-increasing demand for early detection of fatigue damage is fueled by the fact that small cracks are found to grow at unexpectedly high rates well below the "large-crack thresholds" in aluminum and titanium materials [42].

The detection of surface-breaking defects is important because stresses arising from strain are often maximized at the structure surface so that any surface-breaking

defect is particularly prone to growth. Significant work has already been devoted to the detection, location, and sizing of surface-breaking defects [43]. Ultrasound is an important method due to its convenience, reliability and efficient propagation in metals [44, 45]. In this area, there are two main kinds of detection methods: (a) those based on Rayleigh wave interaction with surface-breaking cracks [46-48], and (b) those based on the time-of-flight diffraction (TOFD) technique [49-51]. The latter is also used to detect subsurface defects by conventional ultrasound. The TOFD method uses the arrival time of ultrasound diffracted from the tip of the crack to determine the size of the defect in a through-thickness direction. It has the advantage that amplitude information from the received signal is not employed directly for defect sizing, but instead, the time of arrival of the signal is used.

Positive identification of small fatigue cracks and material inhomogeneities, presents a challenging problem since it is important to first distinguish them from the primary geometric features and secondary irregularities (such as caused by uneven machining, mechanical wear, and corrosion). Under laboratory conditions, a great variety of nondestructive evaluation techniques have been developed for detection of defects and material characterization. These include: acoustic emission [52-54], linear and non-linear ultrasonics [40, 43, 45], eddy-current inspection [55-57], x-ray imaging [58], and thermal sensing [59, 60]. Optical methods that include the use of microscopes and dye penetrants have also been used. However, the optical techniques are often not well-suited either because the affected areas are not accessible, or the defect dimensions are below the resolution limits of the microscopes. Most recently, three new techniques, namely, holographic interferometry, structural integrity monitoring, and laser ultrasound

inspection, which allow the simultaneous detection of multiple cracks, have been proposed [61]. Of these the laser method is being recognized as the most promising due to its remote and noncontacting nature, high speeds, and superior spatial resolution.

From the above discussion, it becomes clear that laser-based techniques are likely to be the superior choice for nondestructive evaluation (NDE). It also seems possible to combine the thermal aspects with laser excitation for a variety of potential benefits. The laser source would provide the energy for localized and directed thermal heating. Analysis of the thermal conduction and the temporal- and spatially-resolved signatures of the temperature characteristics would provide spatial resolution. In general, advantages of such a laser based thermal technique would include: (i) High speed by using the fast laser scanning and/or ultra-short laser pulses. (ii) Good spatial resolution arising from the narrow laser spot size. (iii) The ability to magnify cracks and defects by facilitating a reopening of pores and cracks as the result of a thermal expansion process. This feature is absent from all of the other techniques. (iv) Transients, repetitive frequency spans, and continuous mode operation would all be possible. (v) Analysis along both the lateral dimensions (i.e., surface analysis) and along the depth of the sample. Since thermal attenuation is relatively mild (as compared to electromagnetic or optical signals), study of thicker samples would be possible.

Given the possibility of laser-based thermal sensing of defects, cracks, and material inhomogeneities, it becomes germane to examine the role of the SPICE-based method for temperature analysis in samples containing defects. The overall analysis and resulting interpretation for the nondestructive evaluation of a complex sample is expected to be a difficult and complicated task. Such an endeavor is beyond the scope of this

thesis. However, the possibility of applying the SPICE-based equivalent electrical analog simulation technique will be probed here. Some simple test cases of samples containing defects are discussed in this chapter. The results are presented in later sections of this chapter, and potential applications for NDE brought out.

4.3 RESULTS FOR A SINGLE PULSED INPUT

4.3.1 ONE-DIMENSIONAL ANALYSIS

As demonstrated in the previous chapter, the SPICE-based method can be used to solve for the time and position dependent temperatures T(x,t). It requires the construction of an appropriate equivalent electrical circuit. For heat uniformly applied and distributed along the sample, current sources of equal magnitude at each sub-section simulate this process. Every current source is turned on or off in accordance with the switching of the heating source.

We now intend to focus all of the external heat at a particular point along the length of the bar for a 1-D analysis. If the applied heat intensity remains constant, only one large current supply is activated at a specified node and the other current sources are either turned off or are non-existent. This process effectively simulates a focused heating condition, such as a laser beam focusing all of its energy at a specific point.

The switching of the heat source is accomplished through the use of a voltage-controlled current source. Every current source is controlled independently at each node by a voltage pulse and an associated load resistor as depicted in figure 4-1.

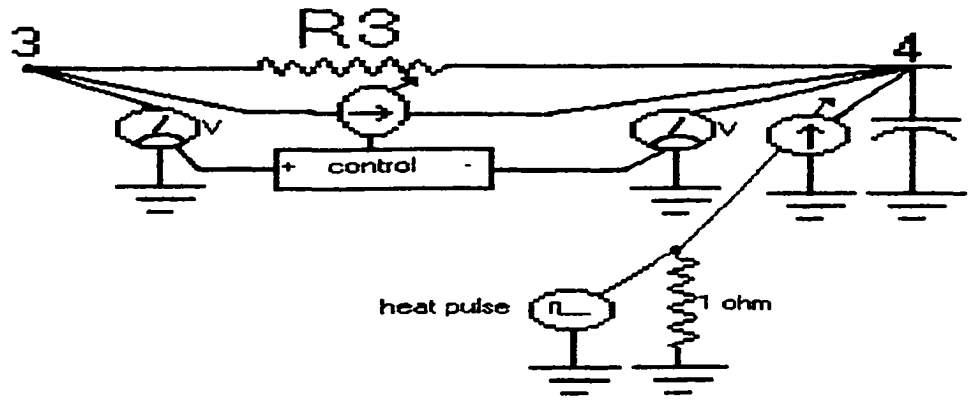

Figure 4-1: Voltage-controlled heating source.

During the time that the external heating does not occur, the heat pulse is zero and the associated current supply is turned off. For a concrete example, the laser was assumed to be focused directly at a point 0.5 meters from the free end. Thus, the node 5 current supply was switched on at time 12,000 seconds. It is obvious that the peak temperature (voltage) at each point should be directly proportional to the duration of the heating pulse. At time 15,000 seconds, the laser was turned off (electrically equivalent to turning off the current source at node 5), and the temperature at each point along the bar cooled to the ambient temperature. The numerical results are shown in figure 4-2 for equidistant positions along the length of the bar. These results are intuitive and in keeping with the expected qualitative behavior. The SPICE-based analysis is thus appropriate and valid.

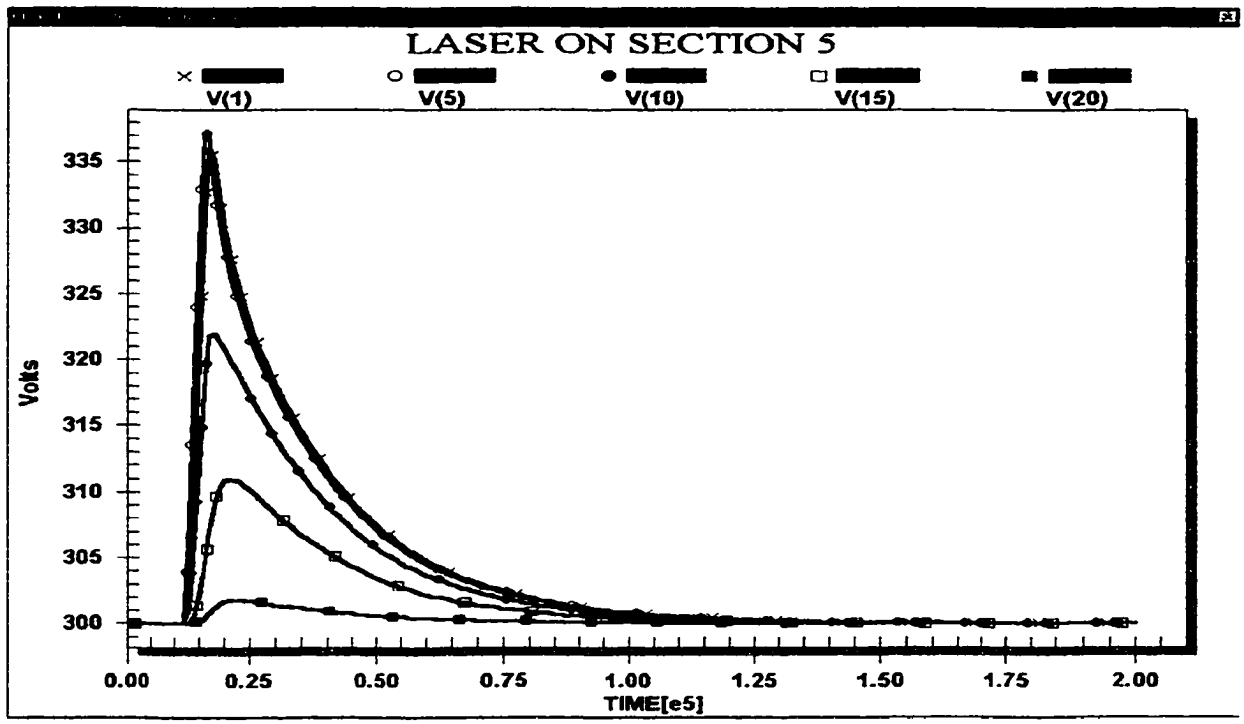

Figure 4-2: Transient behavior of a heating pulse directed at node 5.

4.3.2 TWO-DIMENSIONAL (2-D) ANALYSIS

To test the transient results for a 2-D sample, the plane is first sectioned into nine individual pieces as shown in figure 4-3.

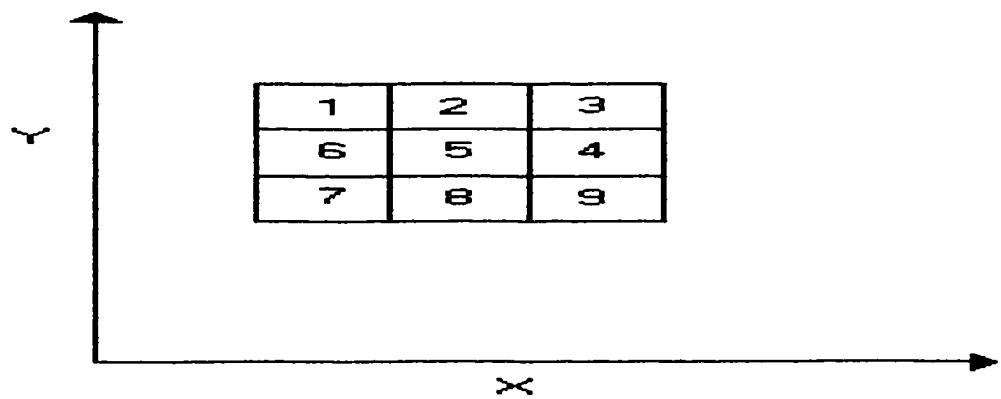

Figure 4-3: Separating the two-dimensional sample into individual sections.

The nodes corresponding to the corners of each plane are as given in table 4-1.

Plane	Voltage nodes
1	1, 2, 5, 6
2	2, 3, 6, 7
3	3, 4, 7, 8
4	7, 8, 11, 12
5	6, 7, 10, 11
6	5, 6, 9, 10
7	9, 10, 13, 14
8	10, 11, 14, 15
9	11, 12, 15, 16

Table 4-1: Individual plane voltage nodes.

A simulation was carried out for the transient response with section 5 being heated. The validity of this test will form a basis for understanding the transient behavior when other sections are heated. It was assumed that the laser was first positioned over section 5, heating that area from time 0 to 20,000 seconds. During this time the current sources at nodes 6, 7, 10, and 11 were correspondingly turned on in the model, to simulate the heat input of the laser. One expects the entire surface to warm, as is seen in figures 4-4 through 4-7 showing an increase in voltage at every node. At approximately 10,000 seconds the surface temperature (referenced by the voltage nodes) reaches steady-state conditions.

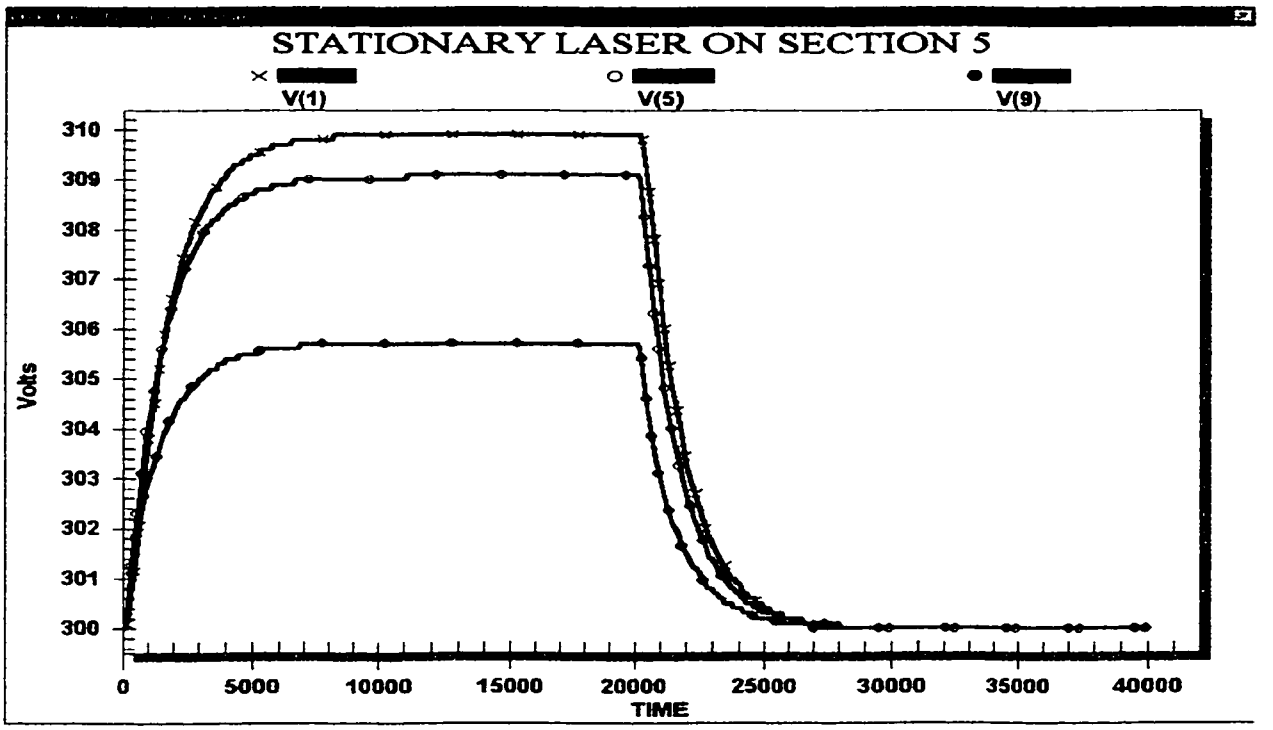

Figure 4-4: Transient response of nodes 1, 5, and 9 with stationary laser on section 5.

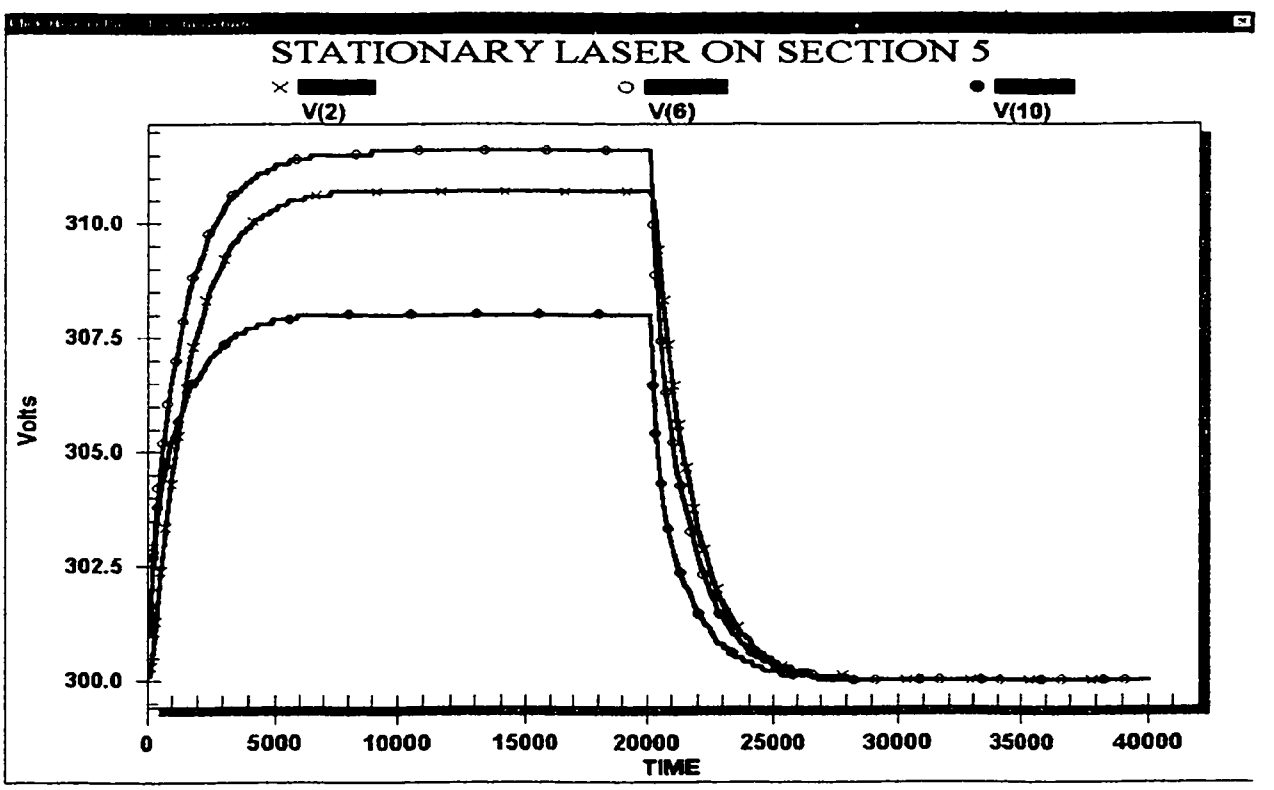

Figure 4-5: Transient response of nodes 2, 6, and 10 with stationary laser on section 5.

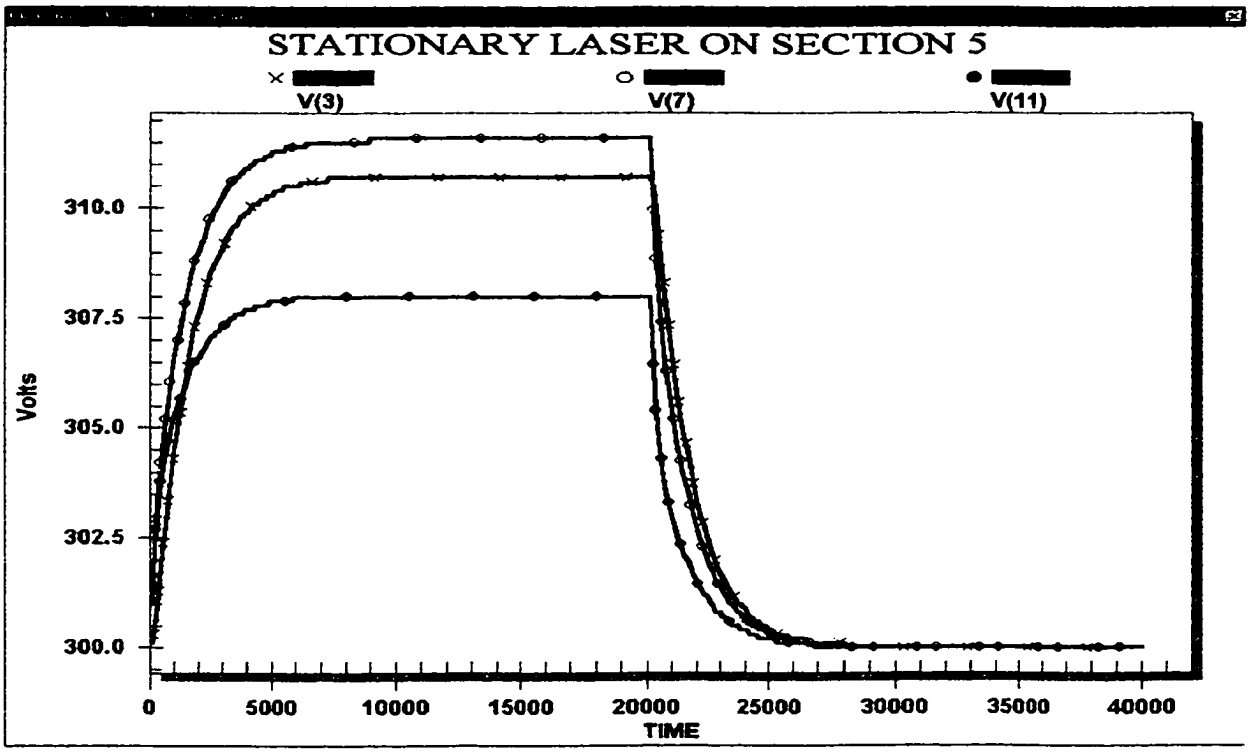

Figure 4-6: Transient response of nodes 3, 7, and 11 with stationary laser on section 5.

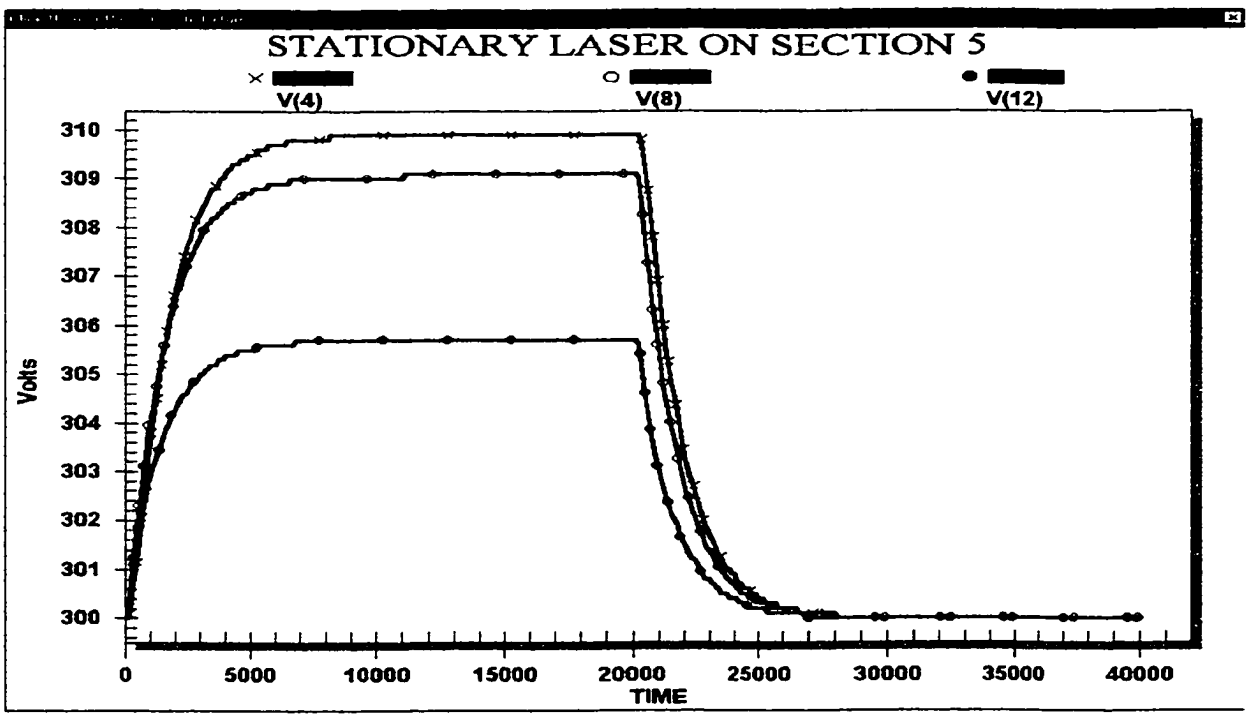

Figure 4-7: Transient response of nodes 4, 8, and 12 with stationary laser on section 5.

A close inspection of the voltages results reveals the following features: (i) The greatest temperature difference occurs between the heat sink (voltage nodes 13 through 16) and the sub-section junctions adjacent to it (voltage nodes 9 through 12). This situation occurs because the heat cumulates at each sub-section junction (voltage node) as it flows towards the heat sink. (ii) A symmetry about the x-axis is evident. Since both x-axis ends are insulated and are equal in distance (but opposite in direction) from the heating point, temperature dissipates evenly in both directions causing equidistant points to be at the same temperature. (iii) Finally, when adjacent sub-section junctions (voltage nodes) are heated, the temperatures at both junctions along the x-axis are the same. This situation occurs because there is an equal distance and thus equal heat dissipation along the x-axis to the insulated ends. With both temperatures at the same magnitude, no temperature difference occurs between the junctions causing the heat to remain stationary between those points.

These statements are summarized by the following set of equations:

$$V_1 = V_4,\ \Delta V_{2,1} = \Delta V_{3,4} \tag{4.1}$$
$$V_5 = V_8,\ \Delta V_{6,5} = \Delta V_{7,8} \tag{4.2}$$
$$V_9 = V_{12},\ \Delta V_{10,9} = \Delta V_{11,12} \tag{4.3}$$
$$V_2 = V_3,\ V_6 = V_7,\ V_{10} = V_{11} \tag{4.4}$$
$$\Delta V_{9,13} > \Delta V_{5,9} > \Delta V_{1,5} \tag{4.5}$$
$$\Delta V_{10,14} > \Delta V_{6,10} > \Delta V_{2,6} \tag{4.6}$$
$$\Delta V_{11,15} > \Delta V_{7,11} > \Delta V_{3,7} \tag{4.7}$$
$$\Delta V_{12,16} > \Delta V_{8,12} > \Delta V_{4,8} \tag{4.8}$$

Equations (4-1) through (4-3) verify equal heat dissipation along the x-axis. No heat flow due to equal temperatures between adjacent junctions is verified by equation (4-4). Finally, equations (4-5) through (4-8) represent heat flowing down the y-axis to the heat sink. At time 20,000 seconds, the heat source was removed and the entire surface began to cool. The cooling continues following the conditions of equations (4-1)-(4-8) until the

sample reaches steady-state ambient temperature (300K) at approximately 30,000 seconds.

4.3.3 THREE-DIMENSIONAL ANALYSIS

Any single heat pulse focused on the top surface of a three-dimensional sample will respond with similar characteristics similar to those of the two-dimensional analysis. The only difference would be that on the bottom surface the temperatures would be lower in magnitude and slower in response due to heat dissipation and transit time through the material. Results demonstrating the above were obtained, but are not shown here for simplicity.

4.4 RESULTS FOR MULTIPLE PULSED INPUTS

4.4.1 ONE-DIMENSIONAL ANALYSIS

The transient behavior associated with multiple heat pulses is now examined and discussed. As shown previously, once a heat source is activated, the temperature rises along each point of the bar for the duration of the heat pulse. If the next heating pulse (at any point) occurs before a complete cool-down of the bar, the temperature at every point along the bar will transition from a cooling cycle to a heating cycle. This behavior is revealed in figure 4-8 with a heating pulse (delay = 12,000 seconds, pulse width = 3,000 seconds, and period = 50,000 seconds) directed at node 5. An analysis of the simulation results of figure 4-8 corroborate that the first heating pulse occurs 12,000 seconds from the start. The heating then occurs at periodic increments of 50,000 seconds, changing the situation from a cooling to a heating transient. This results in an increasing initial

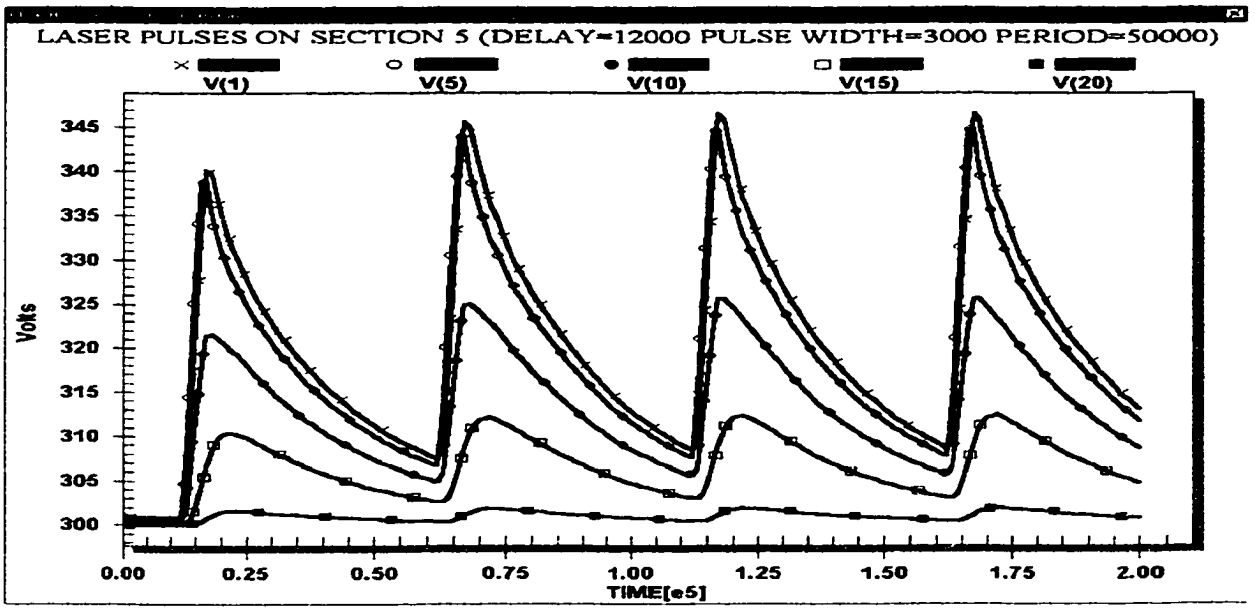

Figure 4-8: Transient response of simulated cyclic heat pulse directed at node 5.

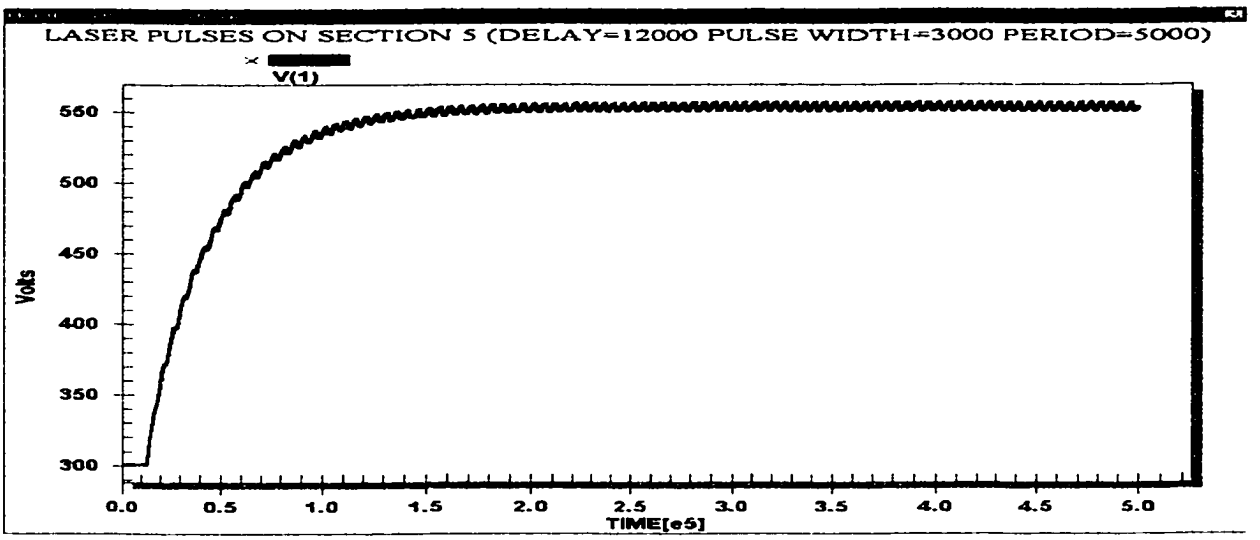

Figure 4-9: Transient voltage of node 1 for multiple current pulses at node 5.

temperature for each heating pulse and thus a higher peak temperature until steady state is eventually obtained. Figure 4-9 displays the transient heating behavior at the free end of

the bar (node 1) with a heating pulse (current pulse) 0.5 meters from the free end (node 5) having the following characteristics:

Delay = 12,000 seconds, Pulse width = 3,000 seconds, and Period = 5,000 seconds.

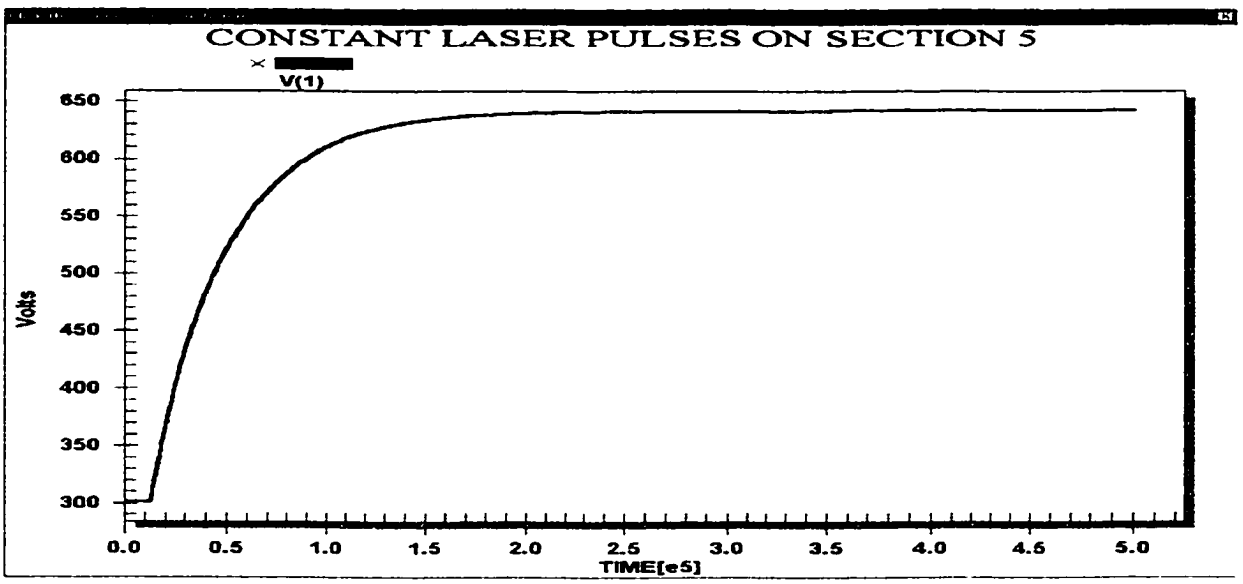

Figure 4-10: Transient voltage of node 1 for a constant current pulse at node 5.

On comparing the voltage transient results for the pulsating current source as shown in figure 4-9 with that of the constant pulse of figure 4-10, it is evident that the charging rate and steady-state voltages are identical. During the charging transient, the voltage oscillations exceed that for the constant heating model. This occurs due to the increase in initial temperature for each charging pulse. After the node reaches steady-state conditions, the peak voltage oscillations never exceed the magnitude of the constant heating model.

We now expand upon the previous test simulations to analyze the effects of a traveling heat source. This action can physically model a traveling laser that is capable of

localized heating within a given spot size, moving along the length of a 1-D bar from the location x = 0 to x = L. At each sub-section junction the laser remains stationary for 3,000 seconds applying heat to that specific point. It is then taken to travel to the next junction. This process is electrically equivalent to activating a current source at the corresponding node for 3,000 seconds and then turning it off while simultaneously activating the next succeeding current source, and so on.

This procedure incorporates characteristics of both focused single and multiple heating pulses. As witnessed earlier, activating a current source at any node causes the voltage to rise at every point along the bar. Once the current source is turned off at a particular node, the capacitor begins to discharge causing the nodal voltage to lower (simulating the cooling of the sub-section junction). But this cooling action is of extremely short duration because, once the adjacent current source is activated, the same node begins to charge again. As we continue this simulated heating process down the length of the bar, the effects of distant heating pulses contribute a smaller effect on the change in temperature at the prior heating points. Hence, eventually the nodes all begin to cool.

This process is now analyzed in detail for a 2-meter, 20 sub-section bar. The laser begins at x = 0 (node 1) at t = 0 and heats (i.e., turns on the node 1 current supply) the point for 3,000 seconds. Heating at this point then ceases (the node 1 current supply is turned off), and the laser moves to the next sub-section junction at x = 0.1m (node 2). This section begins its heating cycle at time 3,000 seconds and remains at this point for an additional 3,000 seconds heating the bar at x = 0.1m. This action is simulated electronically by activating the current source at node 2 from time 3,000 to 6,000 seconds

before turning it off. This action is continued at every sub-section junction (node) until the entire length of the bar is heated in succession. Results shown in figures 4-11 through 4-14 illustrate this complete procedure.

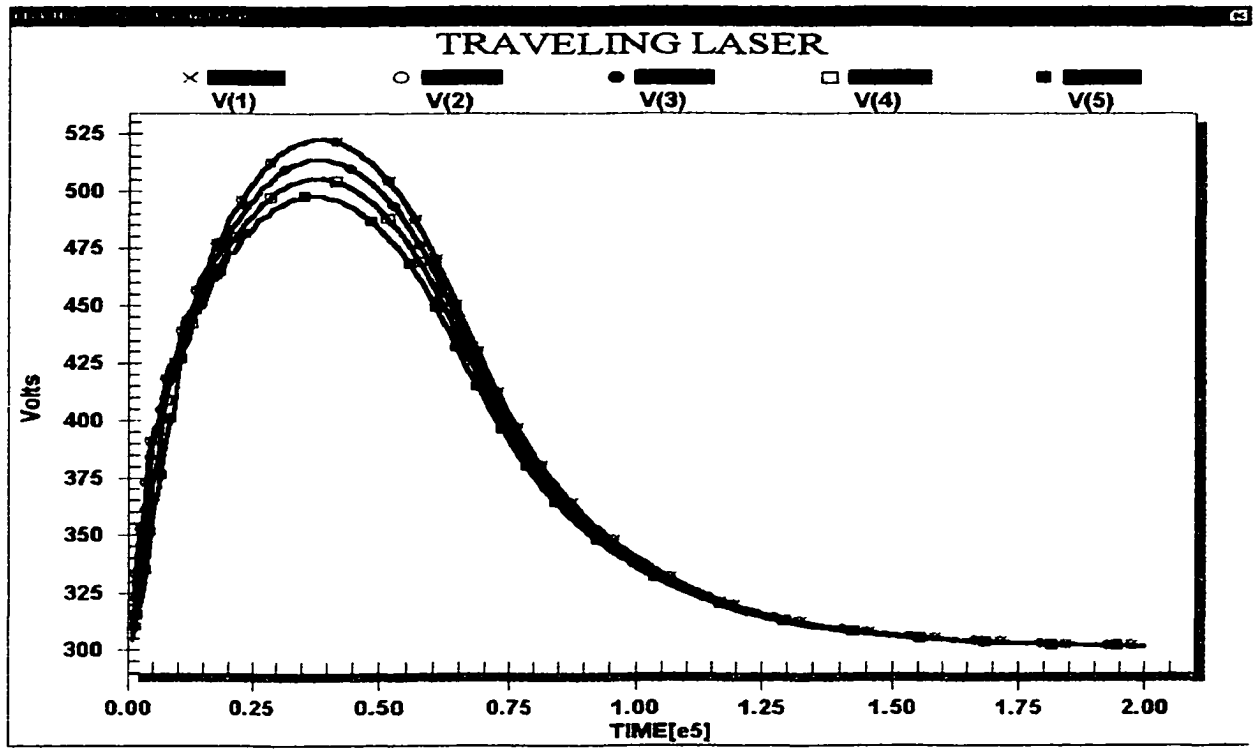

Figure 4-11: Transient behavior of nodes 1-5 for the traveling laser analysis.

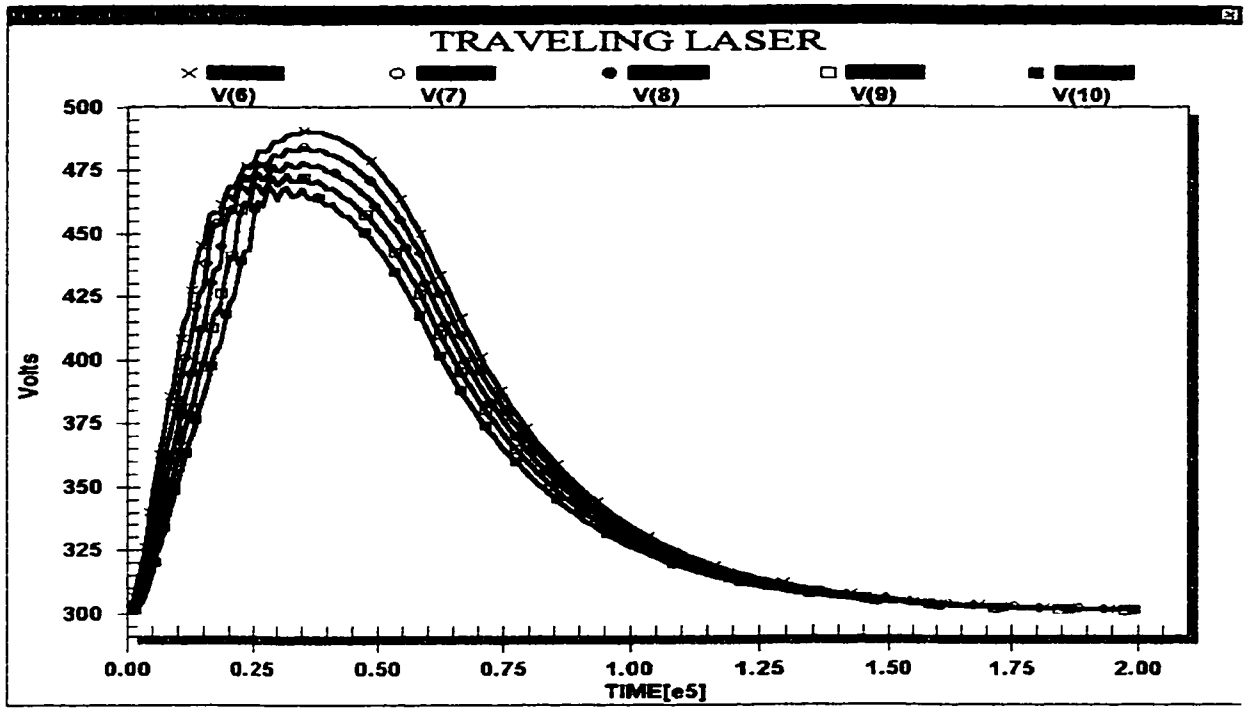

Figure 4-12: Transient behavior of nodes 6-10 for the traveling laser analysis.

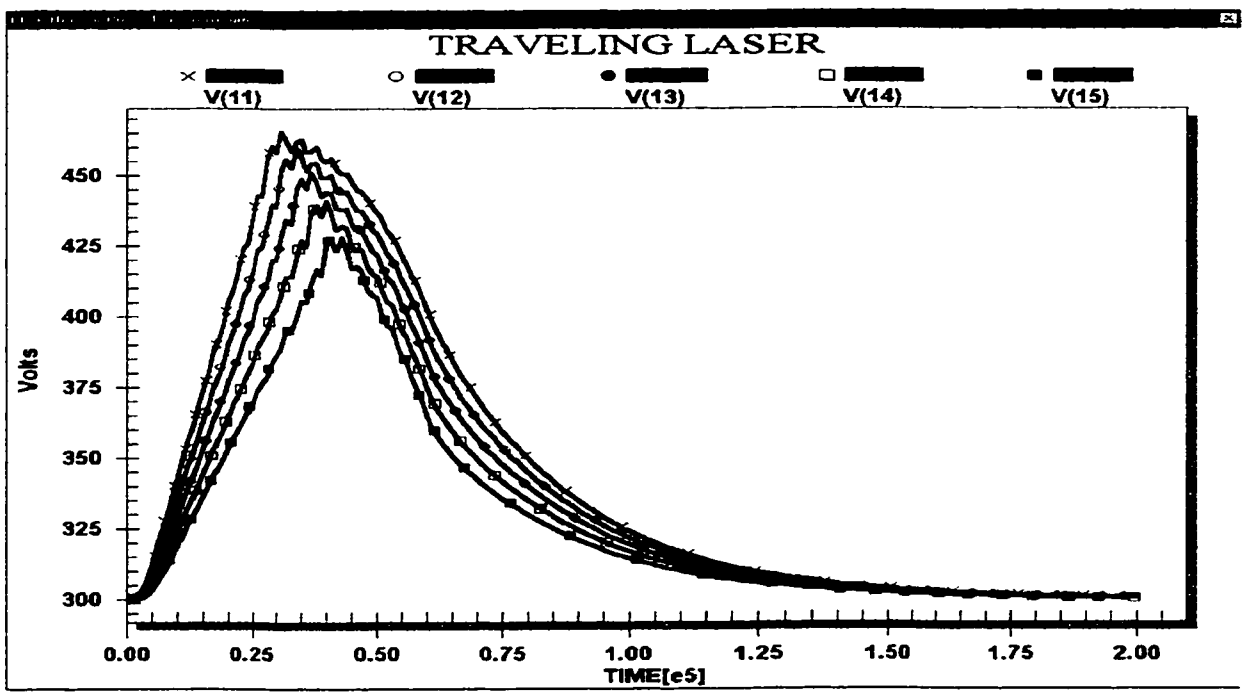

Figure 4-13: Transient behavior of nodes 11-15 for the traveling laser analysis.

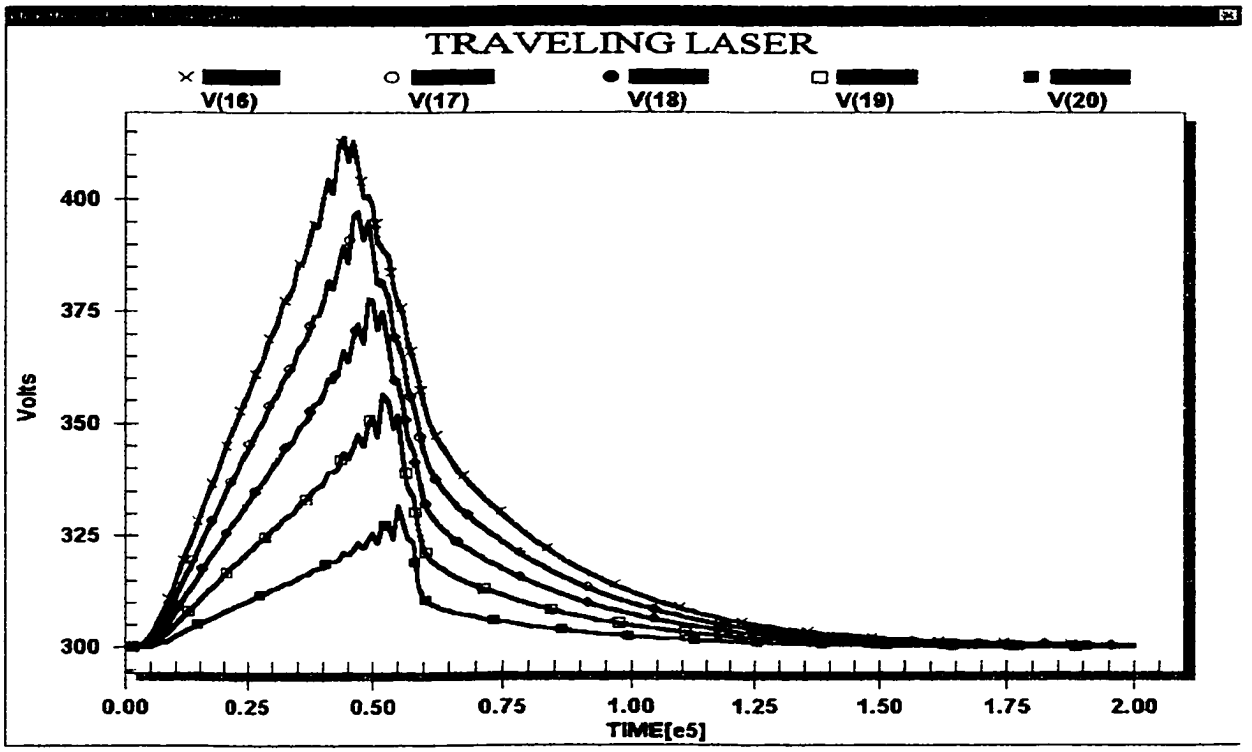

Figure 4-14: Transient behavior of nodes 16-20 for the traveling laser analysis.

A comparison of figure 4-14 with figure 4-11 reveals that the initial heating pulses have the greatest effect on nodes 1 through 5 and the lowest at nodes 16-20. This is to be expected due to the large resistance (and corresponding length) between these points. Therefore, every heating pulse at any section along the bar produces a temperature rise throughout the bar, but the magnitude of its effect decreases with an increase in distance between the points.

4.4.2 TWO-DIMENSIONAL ANALYSIS

Scanning the two-dimensional sample is accomplished in a fashion similar to the 1-D traveling laser concept. Physically, this can be achieved by mounting the laser on a two-axis movable arm so that every section of the two-dimensional plane may be heated

sequentially. Thermocouples could be placed on the surface of the sample (at the voltage nodes) on the same side of the laser to measure the temperature transients.

The movement of the laser follows a continuous motion such that adjacent sections are heated in succession. Heating of the sample begins in the upper-left hand corner of the sample (section 1) and remains stationary at that point for 3,000 seconds heating that section. The laser then travels to the next section along the sample's width (section 2) and repeats this procedure. When the laser has traveled to the last section along the x-axis (section 3), the laser then moves to the section below it (section 4) and heats that section. Heating of the material now continues toward the left end of the sample (from location 4 to location 6). Sections 7 through 9 are not heated because of their close proximity to the heat sink. Heating those areas would send too much heat to the sink leaving very little to heat the sample.

Once any section is heated, the temperature is dispersed across the entire surface area, having a decreased effect at a point more distant from the heating source. The voltage (temperature) at a particular node (sub-section junction) is equal to the summation of the instantaneous voltage at each node. The transient waveforms for this procedure are depicted in figures 4-15 through 4-19 for a few select nodes. Of these results, the node 1 curve will be analyzed in detail. Initially, node 1 (and every other voltage node) is at ambient temperature (300K). From time 0 to 3,000 seconds the laser is on section 1, heating the entire surface from that location. Figure 4-15 illustrates this behavior for node 1 as a rising voltage transient during this time. At time 3,000 seconds, the laser travels to section 2 and heats that area. During this time interval, the cooling rate of voltage node 5 is greater than the heat generation by the laser located on section 2.

Hence, the temperature decreases from time 3,000 to 6,000 seconds at node 1. The laser then travels to and heats section 3 from time 6,000 to 9,000 seconds. With the increased distance from node 1, the heating of section 3 has a diminished effect on section 1, and so node 1 continues to cool. The cooling transients of nodes 2 and 5 govern the behavior of node 1 during this cycle. Another cooling cycle at node 1 occurs as the laser heats section 4 from time 9,000 to 12,000 seconds. A cooling cycle occurs during this duration because the neighboring (nodes 2 and 5) cooling transients exceed the low heating effect of the more distant section 4. During time 12,000 to 15,000 seconds, node 1 remains steady in response to the heating of section 5. Finally, node 1 once again heats up during the heating cycle of section 6 from time 15,000 to 18,000 seconds. The magnitude of this transient is mainly attributed to the combined heating of nodes 5 and 6.

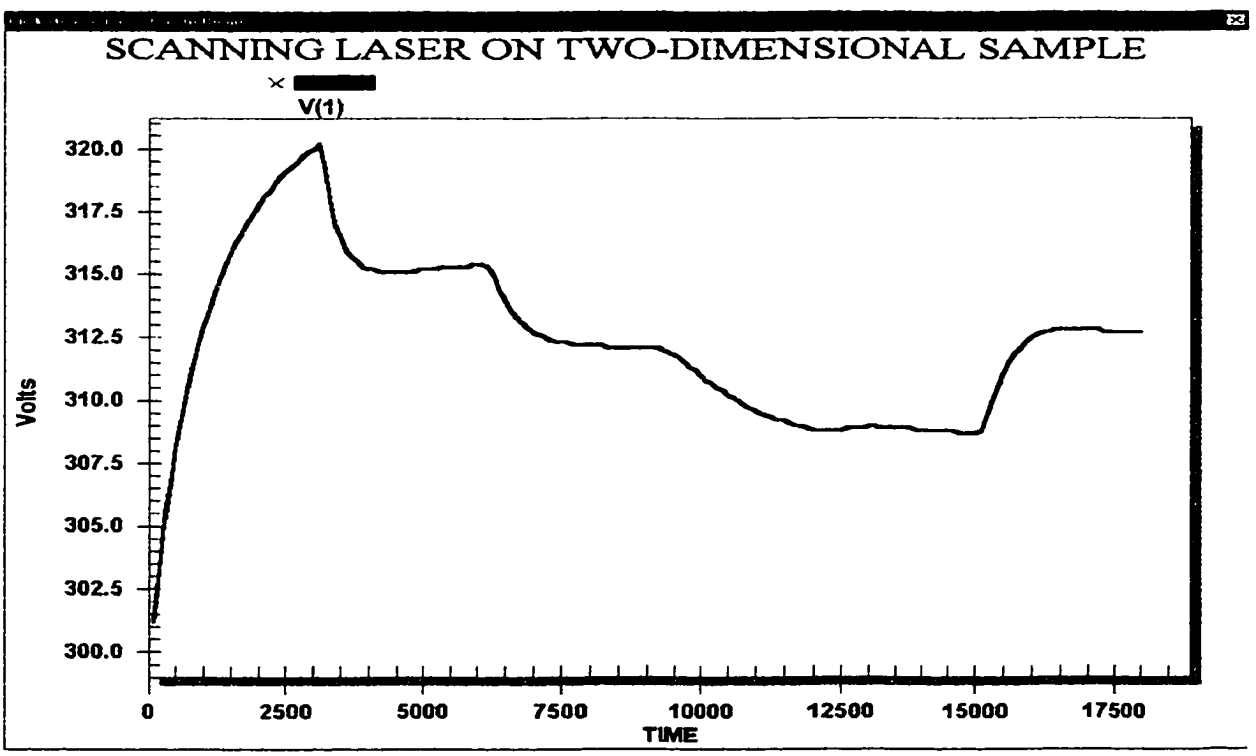

Figure 4-15: Voltage node 1 for two-dimensional simulations.

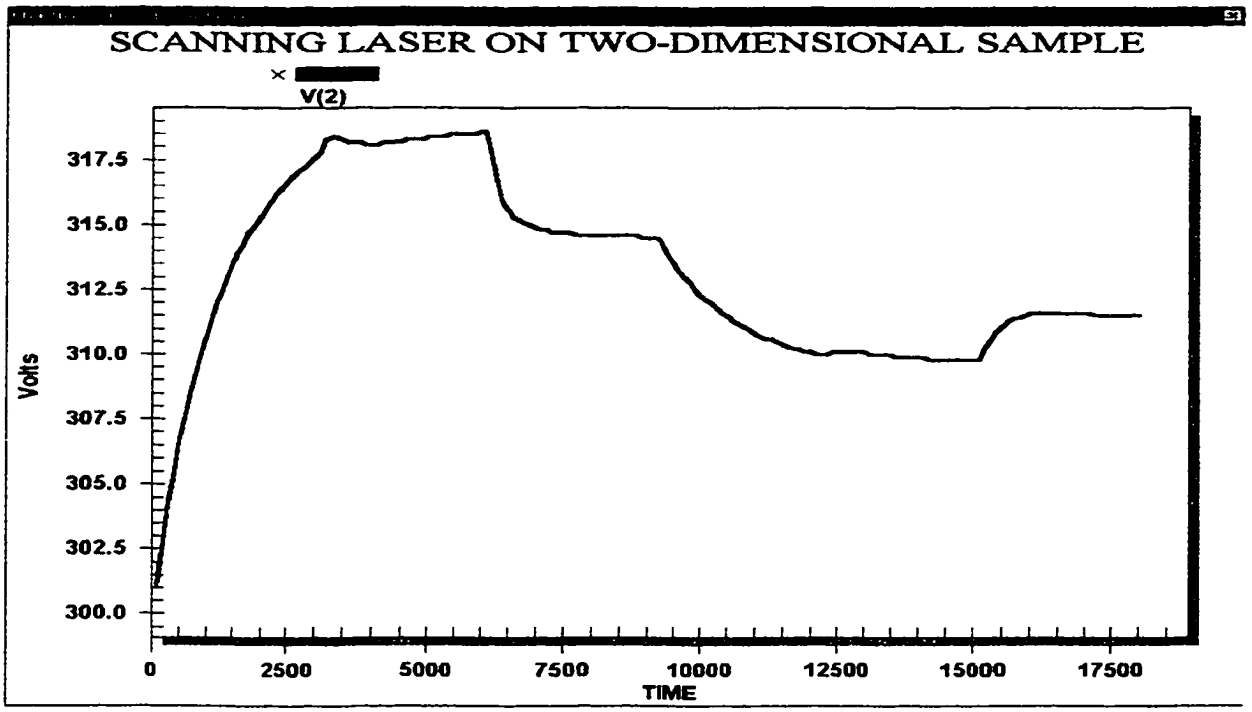

Figure 4-16: Voltage node 2 for two-dimensional simulation testing.

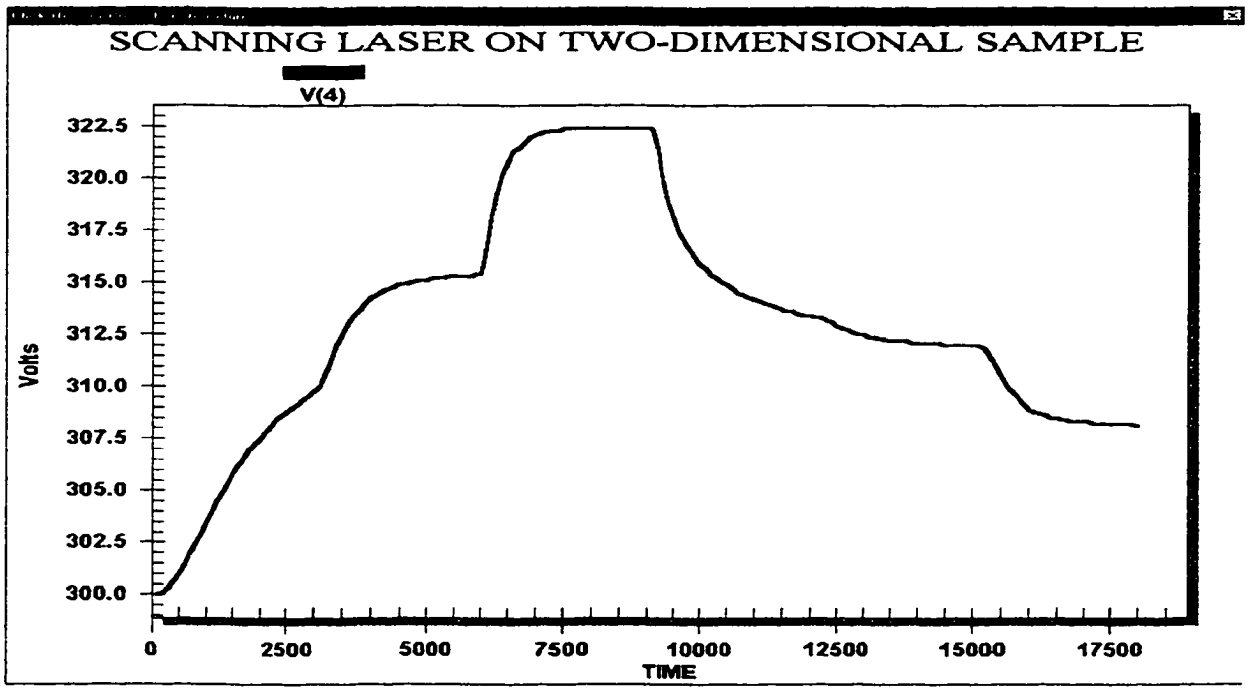

Figure 4-17: Voltage node 4 for two-dimensional simulations.

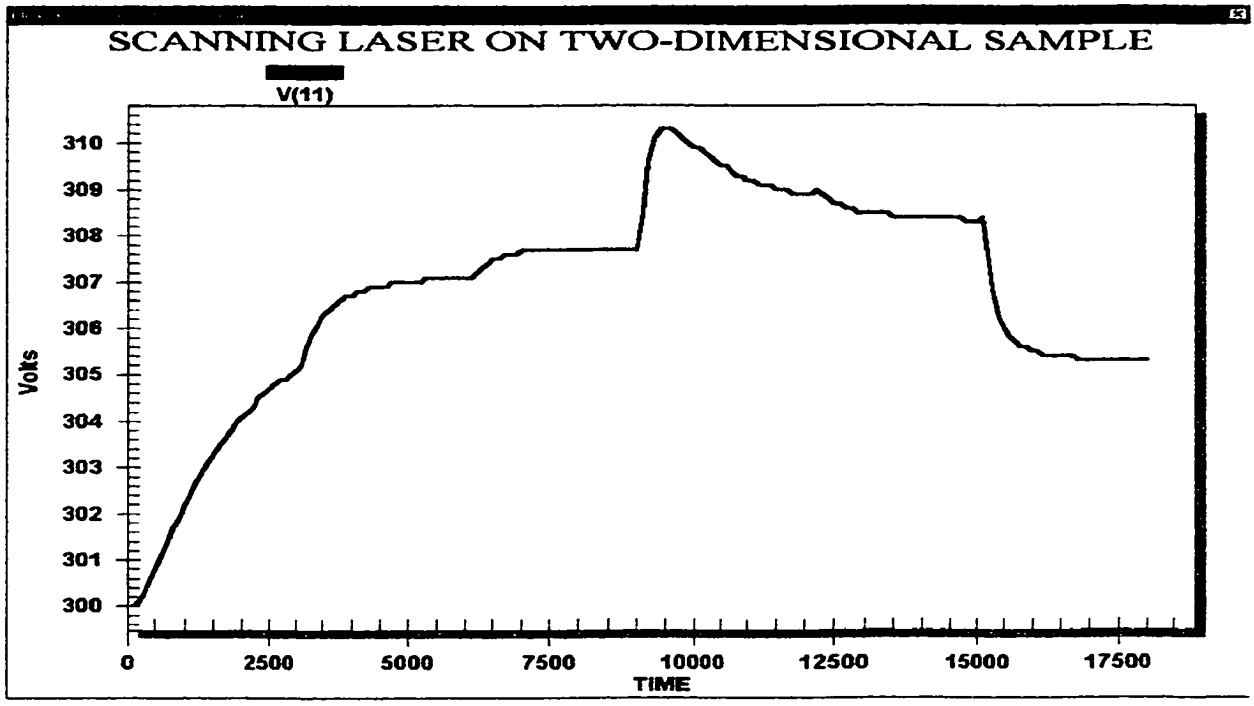

Figure 4-18: Voltage node 11 for two-dimensional simulations.

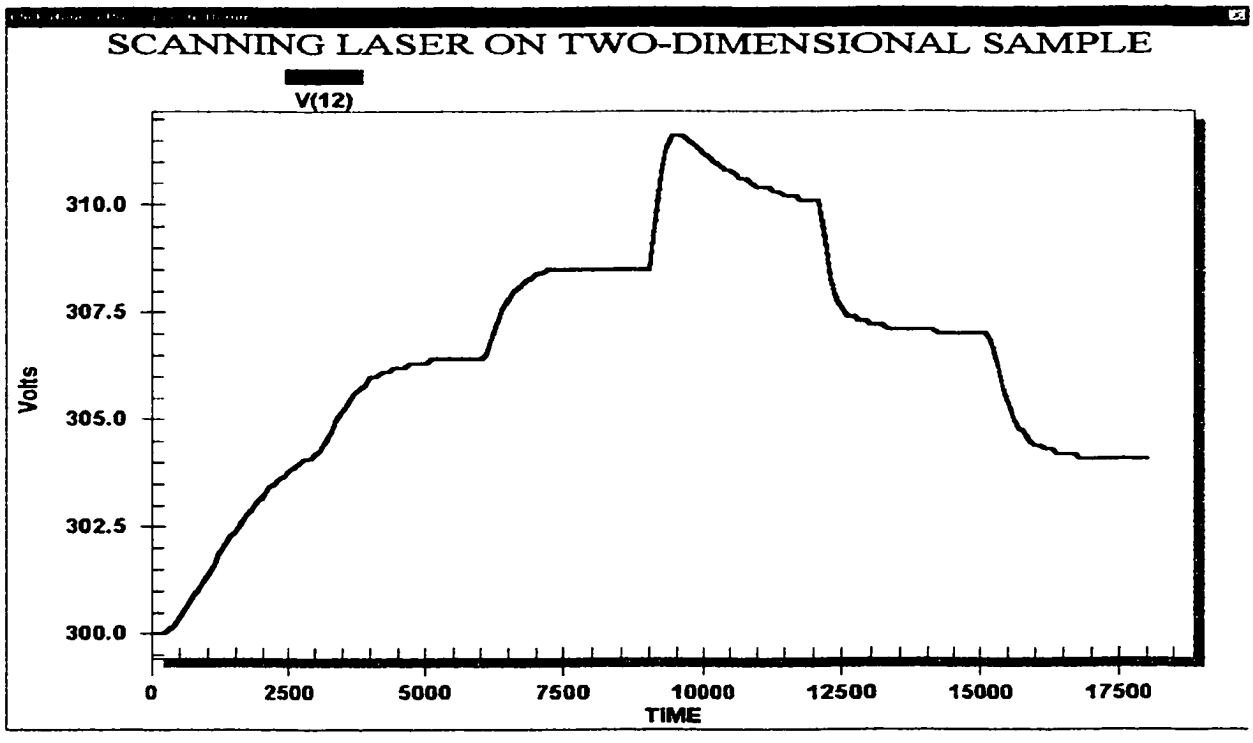

Figure 4-19: Voltage node 12 for two-dimensional simulation testing.

4.4.3 THREE-DIMENSIONAL (3-D) ANALYSIS

Simulation testing for a traveling heat source was similarly carried out for a 3-D sample. The heating and cooling transients were calculated for locations on opposite faces. Thus, one was the incident surface of the incoming laser, while the other was taken to be the back-surface furthest from the incident face. As is expected, the temperatures (i.e., voltages) should be less on the opposite side, since dissipation occurs through the material during the heat flow process. Also, since heat requires a finite amount of time to travel through the material, a delay is expected for transient the back-surface temperature response characteristic.

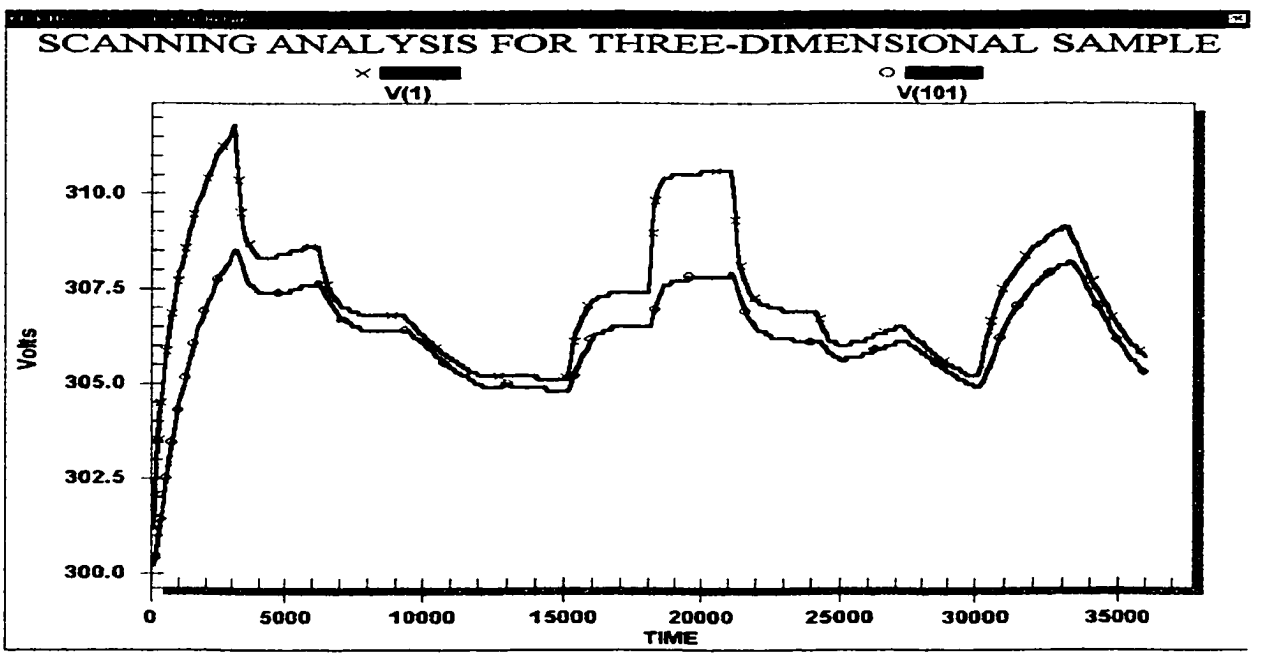

Figure 4-20: Temperature profile of node 1 for a three-dimensional sample.

Figure 4-20 displays both the top (node 1) and bottom surface (node 101) response for the same scanning scenario as used in the previous 2-D case. The result is in

keeping with the expected behaviors. The response of the remaining locations (nodes) was similar, and so is not shown here.

4.4.4 SIMULATING SURFACE CRACKS

A crack upon the surface of a body is simulated as a high sub-section resistance at the location of the defect. The greater resistance offers an increased opposition to current flow in the electrical circuit simulating a corresponding hindrance to heat flow in the thermal model. This behavior shall be examined using the schematic of figure 4-21 representing the electrical equivalent model of a 0.7m square sample of silicon.

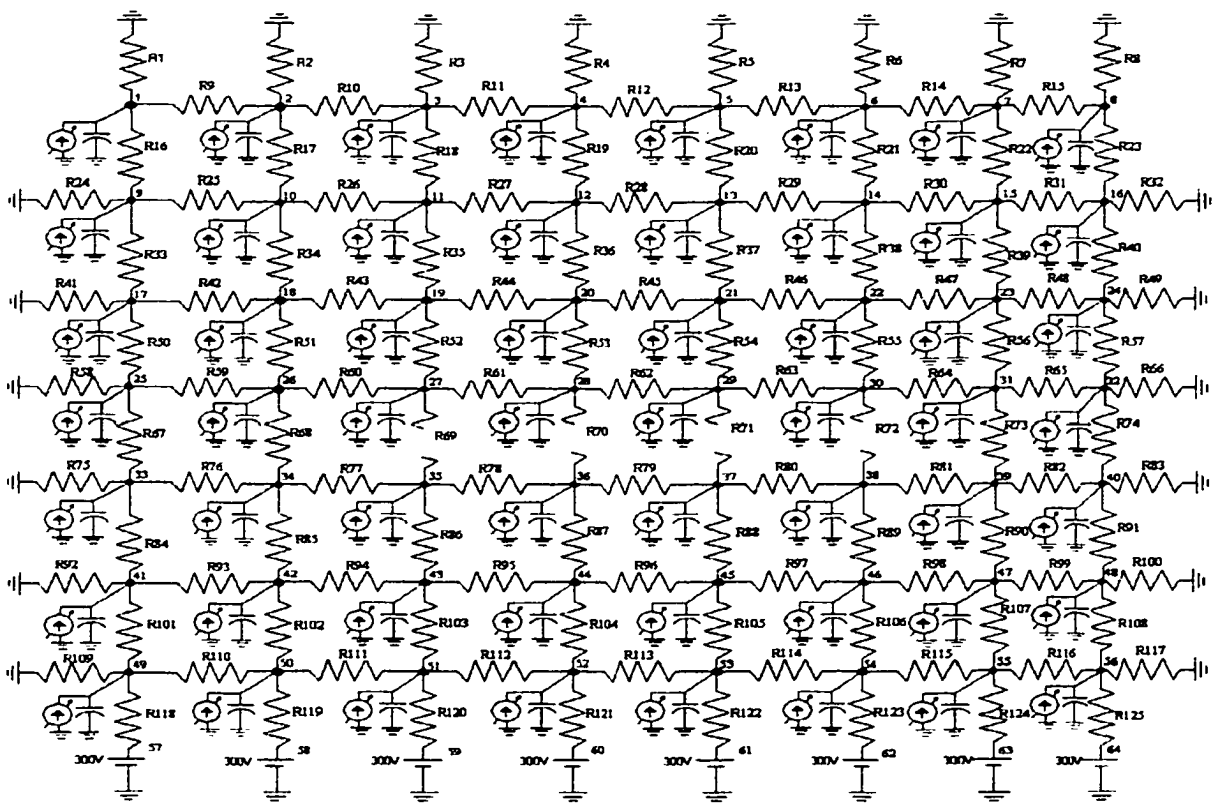

Figure 4-21: Electrical equivalent model of a 0.7m square sample of silicon.

The crack exists as a 0.5m x 0.1m void lying in the middle of the sample and occupies the locations of R69, 70, 71, and 72 (illustrated as open resistance values) in the electrical model. As witnessed previously, once any heating pulse strikes a pure two-dimensional plane, heat travels at the same magnitude to every point across its surface. This situation changes, however, for a plane with a cracked surface. A cracked surface presents a discontinuity to heat flow causing the heat to travel around the defect creating a delay in response on the side opposite from the heat source. Also, since the heat takes a non-direct path to the other side (across the crack), greater heat is dissipated during its travel causing the resulting temperatures to also be of lower magnitudes than what would occur if the sample had no defect.

This scenario has been simulated based upon the electrical model by activating the current sources at nodes 12, 13, 20, and 21 (representing a focused laser beam upon the associated plane). The resulting voltage (temperature) response at this location is depicted in figure 4-22.

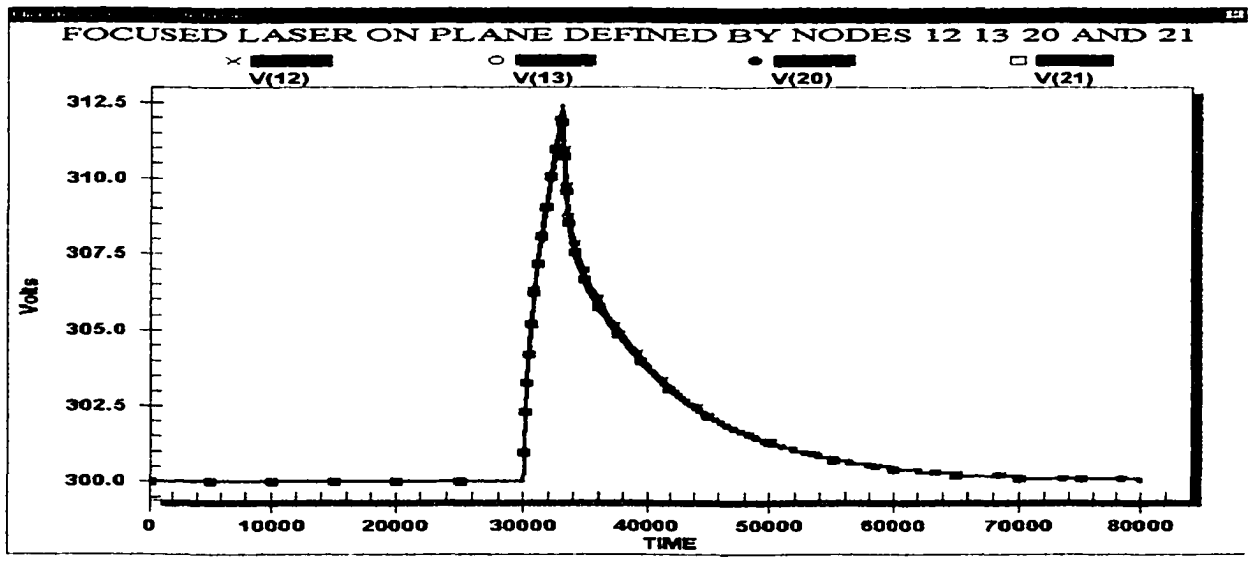

Figure 4-22: Simulated heat pulse upon a cracked two-dimensional sample.

The resulting voltage (temperature) profiles on the side opposite of the crack shall be analyzed for the plane defined by nodes 44, 45, 52, and 53. Since this plane lines in the center of the x-axis, heat is distributed evenly as it travels outwards towards the insulated ends causing the voltages at nodes 44 and 45 to be equivalent. This same situation occurs as well at nodes 52 and 53; hence, only nodes 44 and 52 will be discussed.

Figures 4-23 and 4-24 compare the results for a pure test sample (nodes 244 and 252) with that of the simulated cracked surface (nodes 44 and 52) at nodes 44 and 52 respectively for figure 4-21.

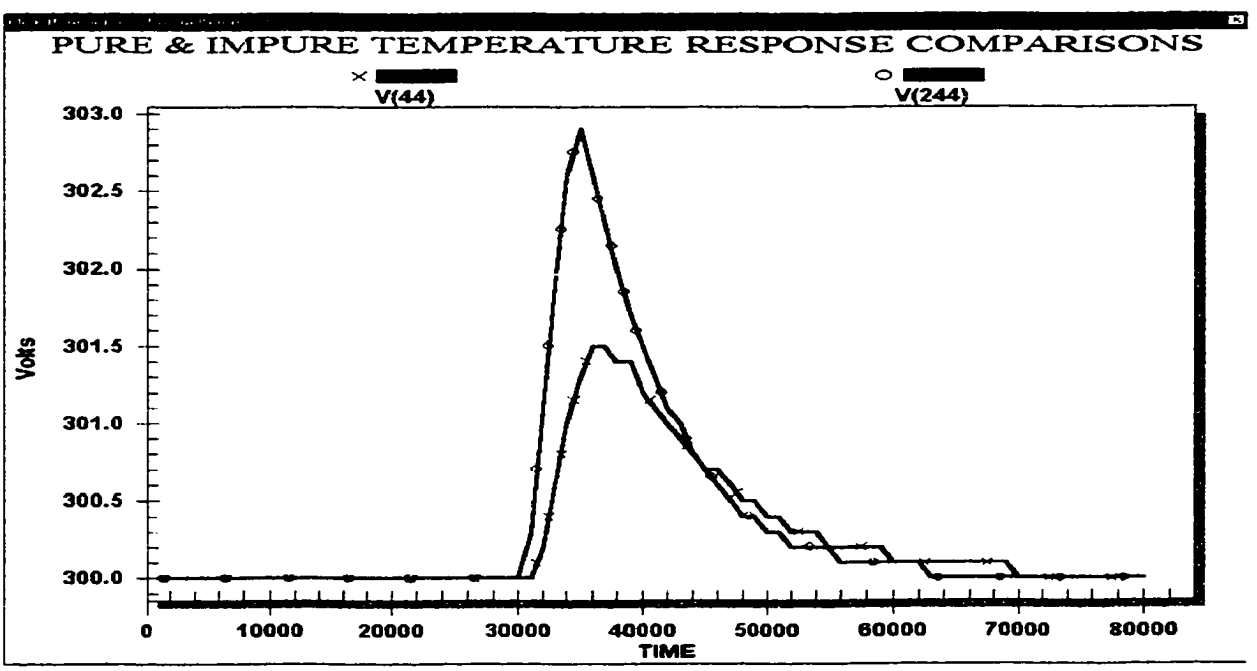

Figure 4-23: Node 44 voltage comparisons for a pure and a cracked surface.

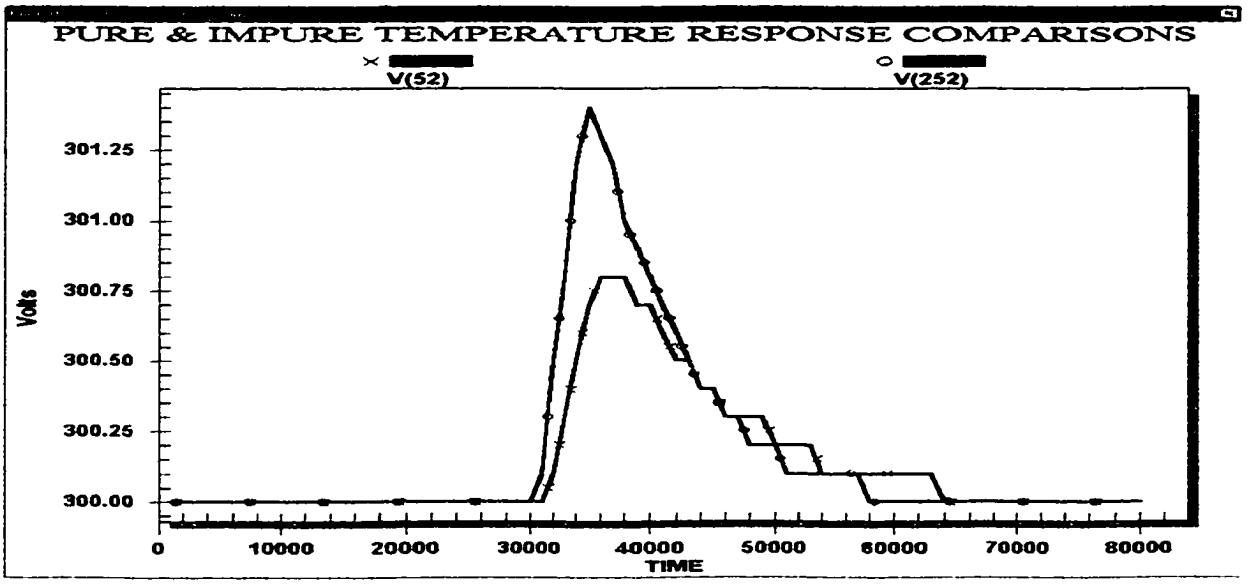

Figure 4-24: Node 52 voltage comparisons for a pure and a cracked surface.

Comparisons between the voltage (temperature) transients verify that the voltages for the simulated crack defect are delayed and possess lower magnitudes than would occur for a pure sample. These behavior relationships between the electrical and thermal models verify that inhomogenities can be simulated and detected electrically. Furthermore, differences between the pure and cracked samples are highest at nodes situated near the physical location of the cracks. Hence, observing differences in temperature patterns would reveal the presence of defects. Also, for a given impure sample, time delays and temperature differences between nodes lying near the edges of cracks also occur. For example, the voltage (i.e., temperature) transients between nodes 34 and 36 of the cracked sample are different. Consequently, the laser-excited transient heating technique would work for crack detection, even when there were no "pure" samples available for relative comparison. This technique will be discussed for the crack example by performing an analysis upon nodes 34 and 36 as depictured in figure 4-25.

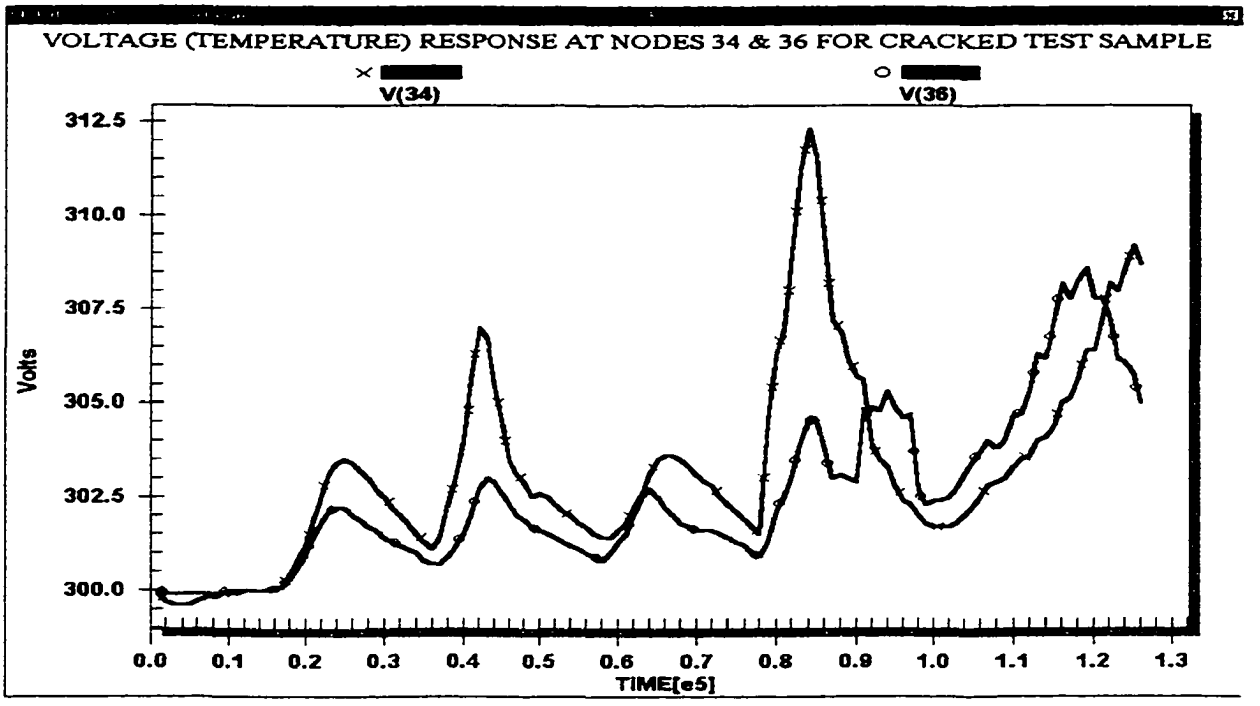

Figure 4-25: Voltage (temperature) response at nodes 34 and 36 for the simulated crack.

By analyzing the transient voltage (temperature) upon a time domain analysis, the location and type of defect may be detected. For the simulated heating scenario of the first row, (time periods of 0 to 21,000 seconds) the temperatures at nodes 34 and 36 remain approximately constant at 300K, indicating a discontinuity (crack) upon the surface at a great distance from the first row (since the induced heating dissipates to zero at these points). During the time periods of 21,000 to 42,000 and 42,000 to 63,000 seconds, the second and third row sections respectively, are simulated as being heated by the laser. For these time periods, node 34 attains greater temperatures and responds at a faster rate (leads) node 36 as the scan advances in row position, indicating a reduction in distance to the defect. Since the voltages (temperatures) occurring for this time period always have the node 34 voltage greater than that at node 36, it is apparent that the discretized resistance of the section at node 34 is less than that occurring at node 36; thus,

it may be concluded that node 34 represents the edge and node 36 the center of the crack defect. As the scan procedure travels to the fourth row, node 36 advances to the leading position due to the close proximity of this node to the simulated laser position. This condition exists for the next 3,000 seconds (time period between 63,000 to 66,000 seconds). For the next 12,000 seconds (time periods between 66,000 to 78,000 seconds) it is assumed that the simulated laser beam is focused within the void of the crack defect and contributes no thermal energy to the surface; thus, both nodes begin to cool. This task is accomplished by not activating the current sources at nodes 26-30 & 35-38 for the required scan cycle. Node 34 once again assumes the leading position due to the activation of the node 34 current source to simulate the heated corner of the next four scanned sections (time periods of 78,000 to 90,000 seconds). For the time period between 90,000 to 120,000 seconds, node 36 assumes the lead of node 34 due to the proximity (and associated lower resistance) of the heated section to the referenced node. Finally during the simulated heating of the last two sections (time periods of 120,000 to 126,000 seconds), node 34 returns to the leading position as the articulated laser more closely approaches the associated node. The voltage (temperature) transients are now in correct response for a second scan. This same procedure may be repeated at node 39 to identify the other edge of the crack defect.

4.4.5 THE DIFFERENTIAL THERMAL ANALYZER (DTA) SIMULATOR

A material may be tested for surface defects by comparing the thermal transient results against those for a known, pure sample. From the standpoint of a simulation, this can be carried out by obtaining numerical results from two 2D electrical equivalent

circuits simultaneously. In the model, the reference sample would have no defects, and the test sample would need to have the same dimensions and bulk material characteristics as the reference standard. In the simulation (or an actual test, if implemented), the position and movement of the external laser would move on the reference standard in unison with that of the test sample. Each point (as a function of time) of the test sample would then be compared with the corresponding point (and time) of the reference standard to determine if the test sample possessed surface defects. Thus, in a sense, a SPICE modeled difference amplifier would result.

For concreteness, such a difference amplifier simulation with a pure and an impure sample was carried out. The fifty six-node circuit of figure 4-21 was used. The output voltage of interest was set equal to the voltage difference between the corresponding nodes of the two samples. For example, the difference output voltage for node 1 may be expressed as:

$$V_{\text{node 1 difference}} = V_{\text{node 1 of sample}} - V_{\text{node 1 of reference standard}}. \quad (4.9)$$

The difference outputs for nodes 1 through 56 were obtained from nodes 401 through 456, respectively. Under ideal conditions, a perfect test sample compared with a reference standard should have voltages (temperatures) of equal magnitude per instant of time. Thus, in our simulations, the differential voltage between the two samples was zero. A mismatch between difference voltages at any instant is indicative of a defect in the sample. The error signal at node 44 for the previously discussed surface crack example is presented in figure 4-26.

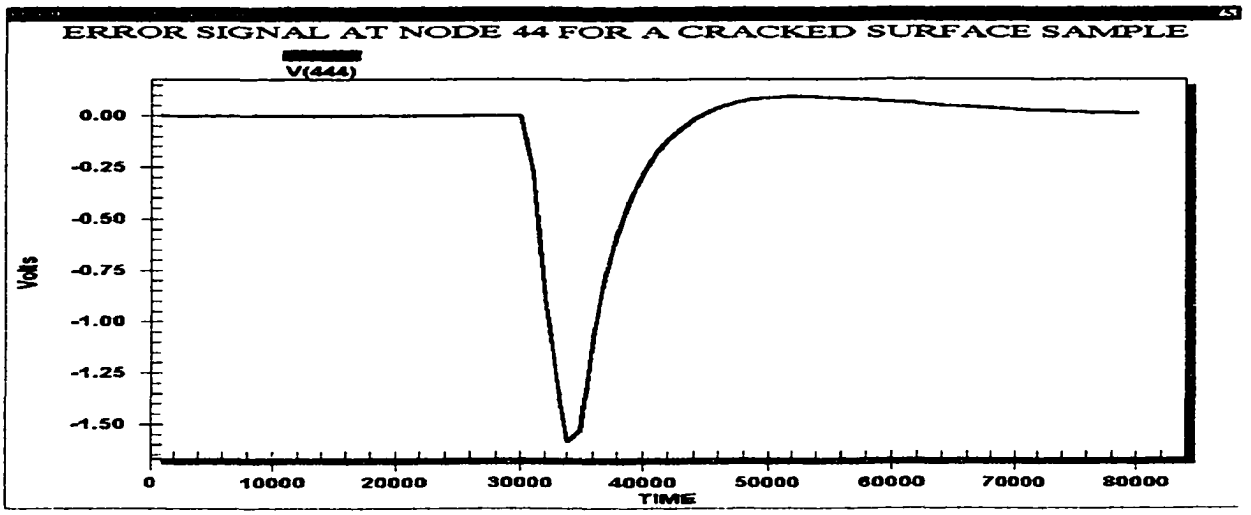

Figure 4-26: Error signal at node 44 for the cracked surface example.

An analysis of this error signal reveals that no difference exists between the test sample and the reference standard prior to activation of the current sources (at time 30,000 seconds). Upon activation of the current sources, the error signal at this node goes sharply negative indicating a cooler test sample than that of the reference standard. The error signal than performs a slight positive excursion at 44,000 seconds as the reference standard cools at a faster rate than that of the test sample. Finally, both samples return to ambient temperature at approximately 80,000 seconds and the error signal returns to zero.

4.4.6 ERROR DETECTION USING THE DTA

Now that the principles of error signals and the traveling laser technique for a two-dimensional scan have been demonstrated and analyzed, both techniques were combined to design a two-dimensional thermal differential analyzer simulator for locating and detecting surface defects. The scanning sequence was taken to follow the

same procedure as before. It originated in the upper left hand corner and simulated heating (by activating the corresponding nodal current sources) each section for 3,000 seconds before advancing on to the next section to the right. Once the right-most section was heated for the row, the laser was taken to hit the right-most section of the row below, before continuing towards the left-most section of the new row. This zigzag pattern continued across the surface of the plane until the final section (that defined by nodes 41, 42, 49, and 50) was activated during the time periods of 123,000 to 126,000 seconds. For periodicity, the entire process was repeated at the starting section.

In discussing of this simulation, it would be too cumbersome to display every error signal at each node for analysis. Hence, only 20 nodes were analyzed for simplicity. It will be shown that this number of nodes is sufficient to accurately locate and identify the test surface defect. The results obtained for the traveling scan technique for the differential thermal analyzer simulator are presented as figure 4-27.

Figure 4-27: Error signal of difference thermal analyzer simulator for an impure sample.

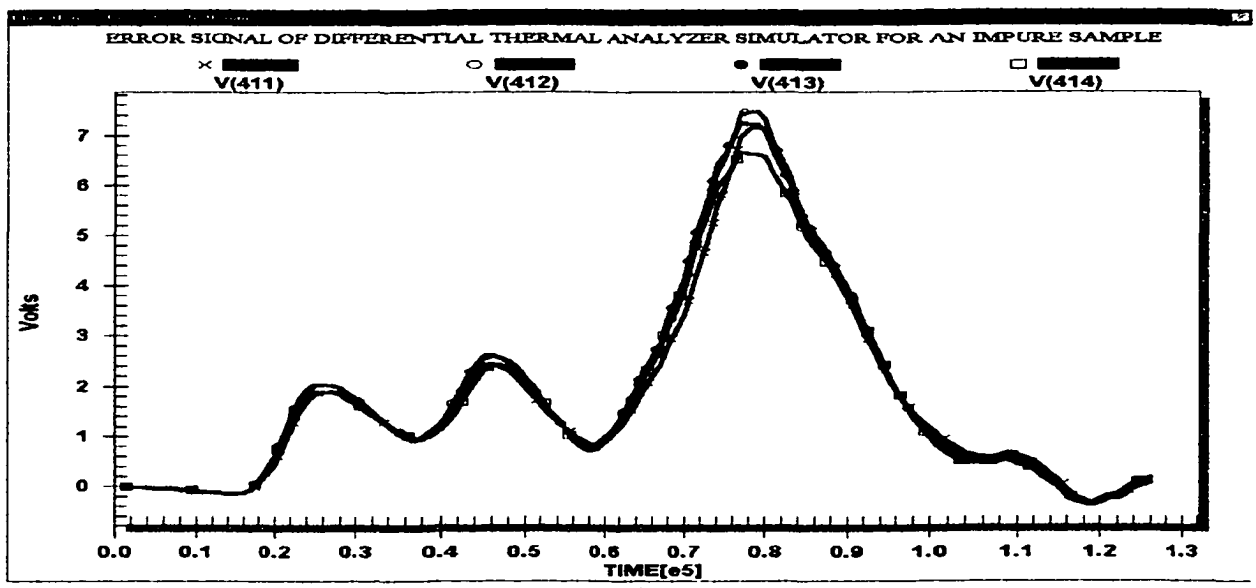

(A)

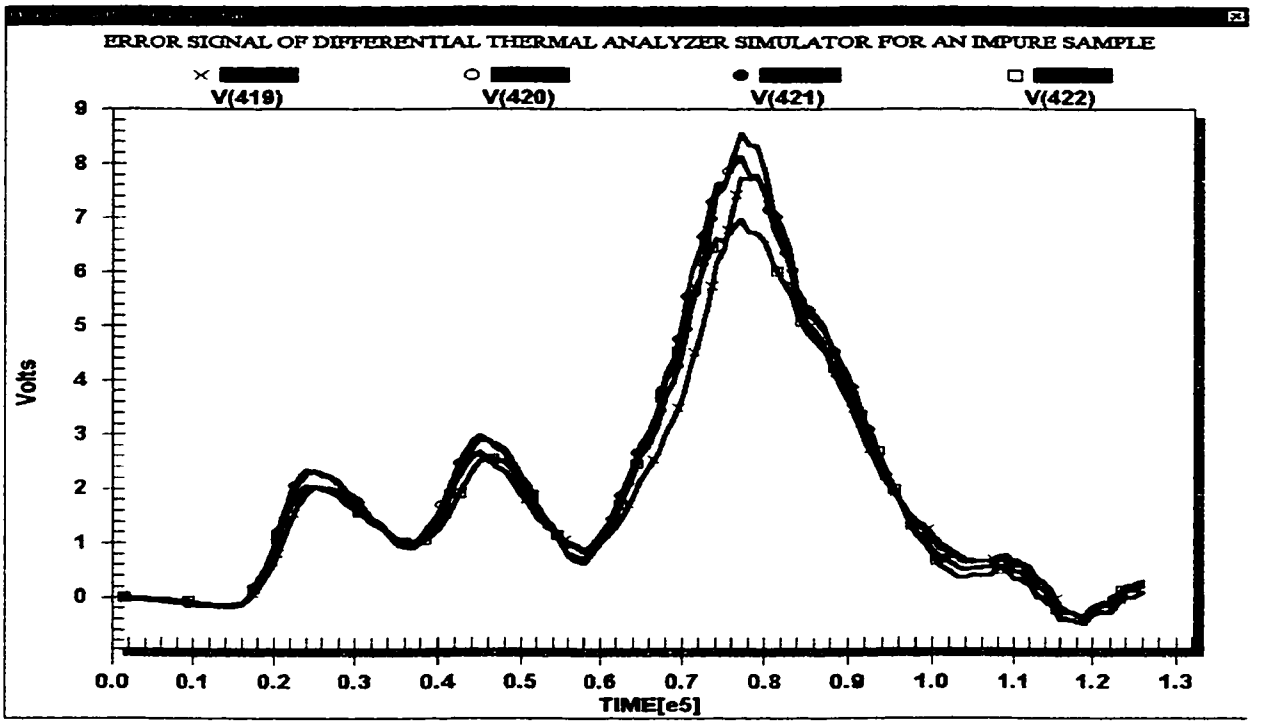

(B)

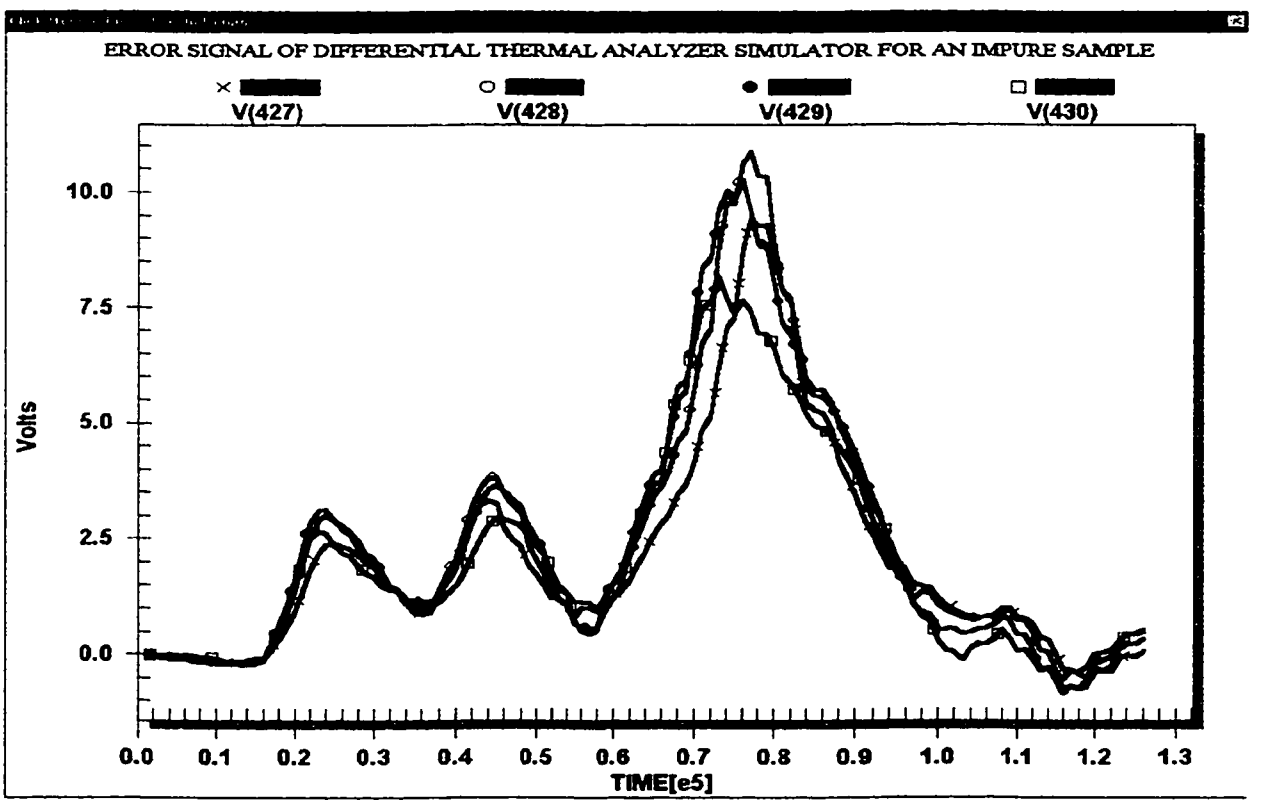

(C)

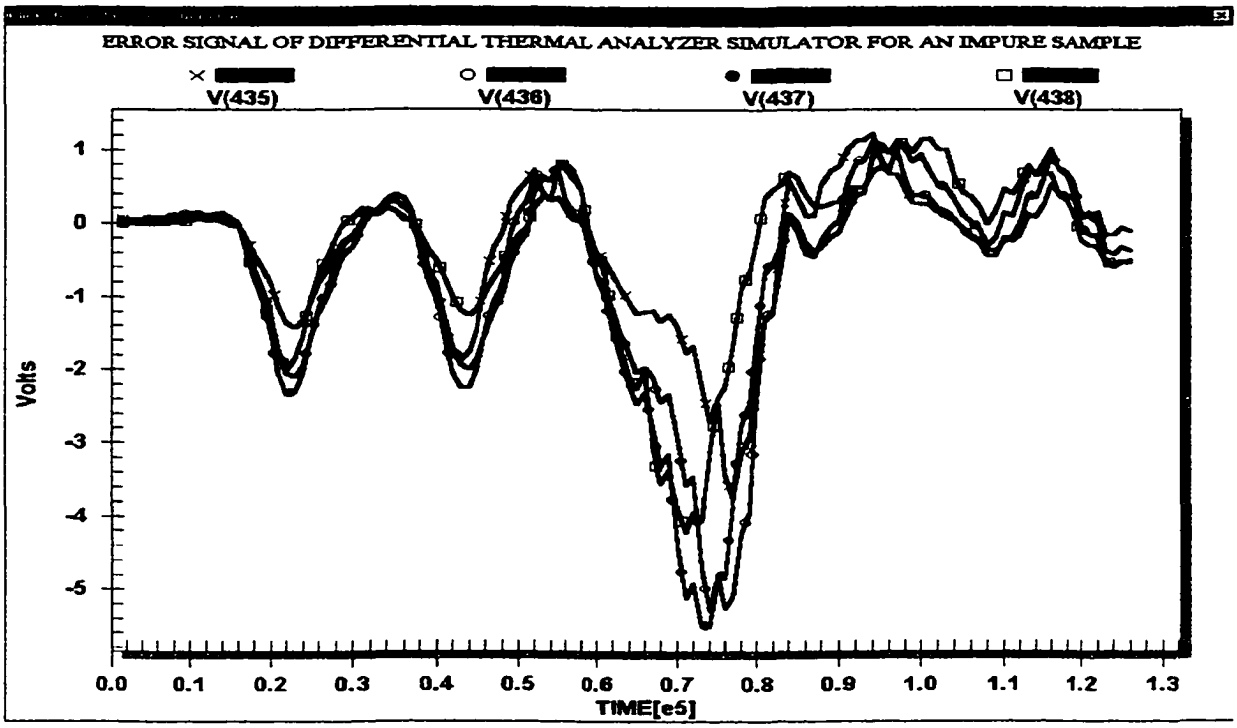

(D)

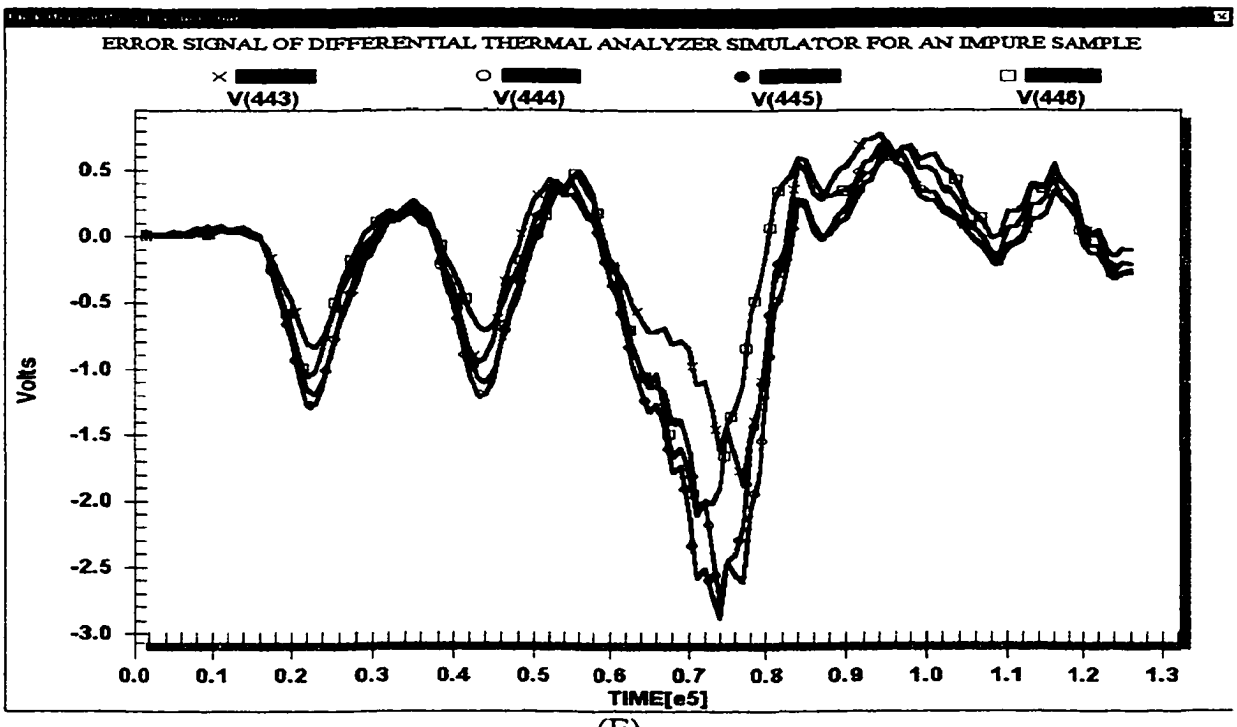

(E)

Upon comparing the results of figure 4-26, it becomes evident that the error of greatest magnitude occurs between 60,000 to 105,000 seconds. This time period corresponds to the simulated heating of the sections defined by nodes 22-39 which reveal the location of the defect. Further, the analysis shows that this error is positive in magnitude for nodes less than 430, and negative in value for nodes greater than 435. This response matches the behavior observed earlier for a surface crack. Measurement points (nodes) existing on the same side of the heating source heat faster and thus obtain a positive error voltage. Temperatures (voltages) on the surface opposite of the crack and heating source experience a delay in transit time (and thus a negative error) around the crack defect, as well as temperature dissipation during its travel. The temperature dissipation may be observed by noticing that the magnitude of error in figures 4-26 (A)-(C) is greater than that occurring in figure 4-26 (D)-(E). In a practical situation, these results can be used as crude indicators of potential defect sites. The rough locations indicated can subsequently serve as the guide to examine the area more closely by focusing the laser more narrowly on the physical sample.

4.5 COMMENTS AND DISCUSSION OF RESULTS

A detailed analysis of the single and multiple focused heat pulses provided the framework for ensuring the validity of the traveling laser heat source. Simulations of this traveling focused heat source technique was applied to ideal one-, two-, and three-dimensional samples and verified from a thermal viewpoint to ensure an appropriate and valid behavior existed between the models.

Surface cracks existing upon a two-dimensional sample present a large opposition to heat flows in the thermal model. Placing a large value resistor at the location of the crack easily simulated this scenario. The resistor offered such a large opposition to electrical current flow (representing conduction heat transfer) that the current had to travel around the defect creating a delay in the response function and a reduction in the peak temperature. These changes experienced the greatest delay on the locations directly opposite the simulated cracked region. These behavior patterns were shown to qualitatively correspond very well with the expected behavioral trends for both pure and cracked surface samples. By analyzing the transient voltages (temperatures) upon a time domain analysis, the location and type of defect were accurately detected without reference to a pure test sample.

The differential thermal analyzer (DTA) simulator operated two identical two-dimensional electrical circuits simultaneously to model heating of a test structure and a reference sample, concurrently. An analysis between the magnitude of the error voltages and the time that they occurred verified proper electro-thermal relationships for the differential thermal analyzer simulator and generated the error voltages indicative of a physical crack. These results, in themselves, would be sufficient to isolate the location of defects in materials.

CHAPTER V

CONCLUSIONS

5.1 OVERVIEW

The heat transport mechanisms and thermal conduction models were all effectively simulated on the basis of electrical equivalents. Specifically, only DC sources, resistors, and capacitors were shown to be sufficient to model the thermal system completely. Voltage magnitudes in the electrical model corresponded exactly with the temperatures of the thermal system representing a valid relationship and equivalence between the two transport models.

The one-dimensional model compared the transient and steady state response of both systems to ensure an accurate representation. Here, verification was proven by comparing the behavior of the electrical model to that of the thermal model as a function of time. Validation of the model was implemented by comparing the voltage and temperature magnitudes at various times. It has been shown that the accuracy (and hence, the validity) of the electrical model increased with a reduction in sub-section size.

Two- and three-dimensional models were constructed through simple geometric combinations of one-dimensional circuits. The transient and steady state behavior of these models were analyzed from both an electrical and thermal viewpoint to verify a correct representation.

Material defects were introduced as large sub-section resistances at the location of the discrepancy to simulate surface cracks upon the physical sample. The results for the simulated scanning heat source upon the electrical model corresponded identically with

the expected behavior of both a pure and a cracked physical sample, verifying sound simulation procedures for the model.

A differential thermal analyzer simulator was also developed for possible application to non-intrusive diagnostics. It was applied to a test sample containing a defect and a reference standard simultaneously. The aim was to evaluate the magnitude and time delays (if any) for a difference voltage generated at each node as a function of time. By observing the temperature differences between the sample and the reference standard, it was shown that material defects could be correctly located.

5.2 SUMMARY

This thesis research focused on heat and thermal conduction and their role in the electrical engineering field. The self-heating of electronic devices and thermal management issues are of prime importance in integrated circuit technology. Temperature increases produced by the internal heat generation affect several parameters of electronic devices that collectively alter their overall response characteristics. These internal temperature increases need to be taken into account for all device optimization and design procedures.

Computer simulations provide a method to study the response and behavior of real world systems through numerical evaluations based on software that is designed to mimic the system's operational behavior or characteristics. The simulations employed in this thesis analyzed thermal transport and heat flow, both under transient and steady state conditions for a physical sample.

A model allows the analyst to experiment with a representation of the system and produce safe and cost effective results. An electrical analogue model was constructed and analyzed with the SPICE circuit simulator to represent the thermal system. This equivalent model offered the benefits of improved efficiency and computational speed for analyzing the thermal system with parameter alterations.

The five general techniques for analyzing thermal modeling self-heating problems include the following: Computer Aided Finite Difference Techniques, Computer Based Finite Element Techniques, The Transmission Line Matrix Method, Thermal Analysis Using The SPICE Circuit Simulator, and Analytical Techniques and Fourier Series Solutions.

The Computer Aided Finite Difference Technique assumes that heat flow may be adequately represented by a non-linear diffusion equation in accordance with Fick's law. Although this technique is simple in concept, it is neither a very fast nor accurate method. As compared to the finite-element method, a larger number of nodes are required for comparable accuracy. This increase in the matrix size for accuracy then increases the computational burden. Also, since the final solution is not explicitly expressed in terms of an equation, the technique does not provide physical insight and is not very intuitive. There is a more serious problem with this technique for simulations of power pulses of high magnitude and short durations. Using a smaller time step in the equation may minimize this problem, but it also significantly increases the computation time.

Computer Based Finite Element Techniques are based upon variational approximations of the heat equation. This technique may be applied if rigorous solutions to complicated geometric structures are desired. The primary difficulty with the FE

method is that it requires a great deal of expertise and experience to decompose the geometry into finite elements and set up trial solutions.

The Transmission Line Matrix (TLM) method analyzes a discretized segment of a semiconductor material as a differential element of a transmission-line circuit. In this procedure, the heat flow problem is transformed into an equivalent problem of evaluating the time dependent propagation of voltage waveforms across the nodes of a distributed transmission line network.

The advantage of the TLM method is that it provides an exact time-domain solution for the network by considering the propagation of delta pulses from the various source nodes. The disadvantage of this method is that it is not very well suited for steady state thermal analysis.

The equivalence between the thermal system of equations and the variables of circuit theory, immediately suggests the use of circuit simulators for the solution of the thermal problem. This technique compares a differential element of volume within a semiconductor material denoting a unit cell for the thermal problem to an equivalent electrical building block. This equivalent electrical network could be solved for a given set of current (representing thermal) excitations, using the commercially available SPICE simulator yielding all node voltages (representing temperatures) as a function of time.

This approach can easily be generalized to include the temperature dependence of the thermal conductivity and specific heat by employing voltage controlled resistor and capacitor elements. The added advantage is that in addition to time-domain analysis, this technique would easily furnish the frequency response characteristics based on the built-in capability of the SPICE simulation tool.

Analytical Techniques and Fourier Series Solutions are the least intensive computationally and provide closed form expressions for the internal device temperature. Quantities of interest such as the thermal resistance and peak surface temperatures can easily be obtained. However, most of these methods are intended for analysis under steady state operating conditions.

Electro-thermal modeling began with simulating the heat transfer mechanisms of conduction, convection, and radiation. Conduction heat transfer occurs when heat travels from warmer to cooler objects. The physical model for this transport mechanism analyzed a bar with constant cross sectional area divided into discretized sections. A constant heat source existed at the left end of the bar and the right end was held constant at ambient temperature.

The electrical model for heat conduction represented each section of the bar as an electrical resistance and the temperatures as proportional voltage sources. Resistance values were computed according to the length and material properties of the corresponding section. The magnitudes of these resistances assured the proper distribution of the potential difference between Vheat and Vambient at the voltage nodes (representing the section junctions) validating the model for steady state thermal conduction.

Convection heat transfer occurs between a solid boundary and fluid in motion along its surface. The heat in the thermal model traveled from the gas to the left side of the cylinder wall (convection heat transfer), through the cylinder wall (conduction heat transfer), and from the right side of the cylinder wall to the coolant (convection heat transfer).

In order to model this heat transfer mechanism electrically, a series resistance circuit was created. The temperatures of the gas and coolant were modeled as proportional DC voltage sources. Series connected resistors modeled the thermal resistance for the gas layer, cylinder wall, and coolant.

Thermal radiation is energy emitted by matter as a result of changes in the electron configuration of the atoms or molecules. The mathematical model computes emitted radiation as a result of surface temperature and magnitudes for absorption, reflection, and transmission by their respective coefficients.

A series-parallel electrical network simulated this mechanism. The potential difference across each resistor related directly to the amount of radiation transferred by that means.

A one-dimensional model was constructed to simulate unidirectional heat flow along a single axis. This model was constructed using voltage and current sources, resistors, and capacitors. These component values were derived from physical properties of the thermal model. The voltage source was used to represent the ambient temperature reference. Current sources were used to simulate the heat generated from a laser beam. Specific heat of the thermal system was modeled electrically as capacitance. Finally, resistors were used to represent the thermal conductivity of the physical model.

The initial state, heating transient, steady-state, cooling transient, and final state of the thermal model was compared behaviorally and quantitatively with the response of the electrical model to prove verification and validation between the models. This procedure was conducted for two models to derive a relationship between sub-section size and

accuracy. A comparison of the results revealed that an increase in accuracy occurred with a reduction in sub-section size.

One-dimensional analysis then continued with temperature dependant features. An in-depth investigation of how the electrical and thermal models responded with a temperature dependant thermal conductivity was presented in this section. This feature was modeled electrically as voltage controlled resistors and increased both the rate of heating and cooling of the sample and also the maximum temperature attained.

Finally, one-dimensional analysis concluded with analyzing the results obtained from a focused heat source (which heats the sample at a particular point on the sample), a cyclic heat source, and a traveling focused heat source.

A two-dimensional sample was constructed of several intersecting one-dimensional models lying parallel to the x- and y- axis, forming a geometric plane. This plane was divided into nine equivalent square sections. The corners of each section existed at a voltage node. When a particular section was simulated as being heated physically with a laser, the corresponding current sources at the corners were activated to simulate the introduction of heat. The transient behavior of a traveling laser, heating each section in succession was analyzed and compared to the electrical model to verify the relationship between the models.

The three-dimensional model was constructed as a combination of two two-dimensional models with several intersecting one-dimensional circuits. In this representation, it was found that the voltage upon the bottom surface of the sample responded slower and reached a lower magnitude from that of the top surface. This

action relates to the physical model in that the heat dissipates and is delayed at the bottom due to transit time incurred through the material.

Non-intrusive thermal diagnostic (NTID) testing is generally conducted by subjecting the samples under test to pulsed thermal stimuli. This has become possible with the advent of pulsed lasers, which are being used to locally heat sections of the samples under test. It has been shown that NIDT requires the analysis of transient heating and cooling curves at various sections of a sample when it is subjected to external laser pulses to induce heating. Initially, the transient behavior of the traveling focused heat source is discussed and verified for a pure sample in the absence of any defects. Next, material defects are introduced to gauge the differences in the thermal transient signal.

The laser source provided the energy for localized and directed thermal heating. In general, advantages of the laser based thermal technique included: (i) High speed by using the fast laser scanning and/or ultra-short laser pulses. (ii) The ability to magnify cracks and defects by facilitating a reopening of pores and cracks as the result of a thermal expansion process.

A crack upon the surface of a body is simulated as a high sub-section resistance at the location of the defect. The greater resistance offers an increased opposition to current flow in the electrical circuit simulating a corresponding hindrance to conduction heat flow in the thermal model. This surface discontinuity causes heat to travel around the defect creating a delay in response on the side opposite from the heat source. Also, since the heat takes a non-direct path to the other side (across the crack), greater heat is dissipated during its travel causing the resulting temperatures to be of lower magnitudes

than what would occur if the sample had no defect. It has been proven through simulations that the voltages existing at the nodes upon the surface of a two-dimensional electrical circuit corresponds behaviorally and quantitatively with the temperatures of the thermal system (at the same reference points) for the simulated crack defect.

By analyzing the results of the two-dimensional scanning simulation, the location and type of defect may be detected by analyzing the transient voltage (temperature) at selected locations upon a time domain analysis. This process may be simplified with the aid of a differential thermal analyzer (DTA) simulator.

The differential thermal analyzer simulator was used to probe a sample for surface defects by comparing the thermal transient results against those from a known, pure sample. Each point (as a function of time) of the test sample was compared with the corresponding point (and time) of the reference standard to determine if the test sample possessed surface defects. The output voltage of interest was set equal to the voltage difference (termed the error voltage) between the corresponding nodes of the two samples. Using this technique, the location and type of defect was discovered by observing the location and time at which the greatest error voltage signal occurred.

5.3 SCOPE FOR FUTURE WORK

This thesis served as an introduction to electro-thermal modeling and differential thermal analysis simulation. The basic concept of using an electrical equivalent model to represent a physical material was presented. The work, however, is far from complete. Much more study of the material is required to advance and perfect this technique. Thermal analysis may be conducted in the laboratory to validate the conclusions made in

this research. It would be interesting to also work in reverse, by constructing the SPICE model using a thermal plot of the material. Other ideas to explore include heating and cooling durations for the heat source, variations in dielectric properties, and discontinuities in thermoelectric potentials. The results of corrosion resistance, changes in specific heat, and decomposition effects may also be investigated and simulated.

Further analysis may explore the results of multiple defects on or within (using the 3D circuit) the sample as well as quantifying the defect from error voltage and time delay magnitudes.

Improvements in the electrical model may include more available nodes (so that sub-section size may be minimized) to improve the accuracy of the model as well as varactors (voltage-controlled capacitors) to model temperature (voltage) dependant specific heat.

It is my hope that this research is continued such that more advanced models are constructed with ever widening practical applications.

REFERENCES

[1]. G. K. Wachutka, "Rigorous Thermodynamic Treatment of Heat Generation and Conduction in Semiconductor Device Modeling," *IEEE Trans. Comp. Aided Design*, Vol. 9, pp 1141-1149, 1990.

[2]. W. Liu and B. Bayraktaroglu, "Theoretical Calculations of Temperature and Current Profiles in Multi-Finger Heterojunction Bipolar Transistors," *Solid St. Electr.*, Vol. 36, pp 125-132, 1993.

[3]. D. de Cogan, "Propagation Analysis for Thermal Modeling," *IEEE Trans. Component, Packaging and Manufacturing Technol. A*, Vol. 21, pp 418-423, 1998; and references therein.

[4]. F. Profumo, A. Tenconi, S. Facelli, and B. Passerini, "Instantaneous Junction Temperature Evaluation of High-Power Diodes During Current Transients," *IEEE Trans. Pcwer Electr.*, Vol. 14, pp 292-299, 1999.

[5]. M. Fan, A. Christou, and M. Pecht, "Two Dimensional Thermal Modeling of Power Monolithic Microwave Integrated Circuits," *IEEE Trans. Elec. Dev.*, Vol. 39, pp 1075-1079, 1992.

[6]. V. Ramamurthy, P. K. Chaturvedi, and D. Kakati, "Temperature Rise in Microwave p-i-n Diodes: A Computer Aided Analysis," *Solid St. Electr.*, Vol. 24, pp 445-453, 1981.

[7]. H. F. Cooke, "Thermal Effects and Reliability," in *High Power GaAs FET Amplifiers*, John Walker, Ed., Boston: Artech House, 1993, pp 227-261.

[8]. R. D. Lindsted and R. J. Surty, "Steady-State Junction Temperatures of Semiconductor Chips," *IEEE Trans. Elec. Dev.*, Vol. 19, pp 41-44, 1972.

[9]. W. Zhou, S. Sheu, J. J. Liou, and C. I. Huang, "Analysis of Non-Uniform Current and Temperature Distributions in the Emitter Finger of AlGaAs/GaAs Heterojunction Bipolar Transistors," *Solid St. Electr.*, Vol. 39, pp 1709-1721, 1996.

[10]. P. Donzelli, G. Ghione, and C. U. Nldi, "Thermal Models for Low and High Power Gas MESFET Devices," *GaAs Applications Symp. Conf. Proc.*, April 1990, pp 120-127.

[11]. R. Anholt, in *Electrical and Thermal Characterization of MESFETs, HEMTs and HBTs*, Boston: Artech House, 1995.

[12]. F. T. Wenthen, "Computer Aided Thermal Analysis of Power Semiconductor Devices," *IEEE Trans. Electr. Dev.*, Vol. 17, pp 765-770, 1970.

[13]. G. Liebmann, "The Solution of Transient Heat Flow and Heat Transfer Problems by Relaxation," *Brit. J. Appl. Phys.*, Vol. 6, pp 129-135, 1955.

[14]. A. Ammous, S. Ghedira, B. Allard, H. Morel, and D. Renault, "Choosing a Thermal Model for Electrothermal Simulation of Power Semiconductor Devices," *IEEE Trans. Power Electr.*, Vol. 14, pp 300-307, 1999.

[15]. P. B. Johns, " A Simple Explicit and Unconditionally Stable Numerical Scheme for the Solution of the Diffusion Equation," *Int. J. Numer. Methods Engg.*, Vol. 11, pp 1307-1328, 1977.

[16]. A. M. Lohse, P. B. Johns, and A. Wexler, "Computer Graphics for Transient Fields," *IEEE Trans. on Education*, Vol. E-20, pp 64-68, 1977.

[17]. P. B. Johns and R. L. Beurle, "Numerical Solution of Two-Dimensional Scattering Problems Using a Transmission-Line Matrix," *Proc. Inst. Elec. Eng.*, Vol. 118, pp 1203-1208, 1971.

[18]. S. Akhtarzad and P. B. Johns, "Three-Dimensional Transmission-Line Matrix Computer Analysis of Microstrip Resonators," *IEEE Trans. Microwave Theory Tech.*, Vol. MTT-23, pp 990-997, 1975.

[19]. F. J. Auerbach, G. Meiendres, R. Muller, and G. J. E. Scheller, "Simulation of Thermal Behavior Flow Sensors by Equivalent Electrical Circuits," *Sensors and Actuators A*, Vol. 41-42, pp 275-278, 1994.

[20]. S. Ravi Kiran and G. Karunasiri, "Electro-thermal Modeling of Infrared Microemitters Using PSPICE," *Sensors and Actuators A*, Vol. 72, pp 110-114, 1999.

[21]. M. Necati Özisik, in *Heat Conduction* (Wiley, New York, 1993).

[22]. C. Kittel and H. Kroemer, in *Heat Conduction* (W. H. Freeman, San Francisco, 1980).

[23]. F. J. Auerbach, G. Meiendres, R. Muller, and G. J. E. Scheller, "Simulation of Thermal Behavior Flow Sensors by Equivalent Electrical Circuits," *Sensors and Actuators A*, Vol. 41-42, pp 275-278, 1994.

[24]. S. Ravi Kiran and G. Karunasiri, "Electro-thermal Modeling of Infrared Microemitters Using PSPICE," *Sensors and Actuators A*, Vol. 72, pp 110-114, 1999.

[25] J. Callaway, Phys. Rev. **113**, 1046 (1959); J. Callaway, Phys. Rev. **122**, 787 (1961).

[26] J. Callaway and H. C. von Baeyer, Phys. Rev. **120**, 1149 (1960).

[27] C. Herring, Phys. Rev. **95**, 954 (1954).

[28] P. G. Klemens, in *Encyclopedia of Physics*, edited by S. Flugge (Springer Verlag, Berlin, 1956), Vol. 14, p. 198.

[29] W. J. de Haas and T. Biermasz, Physica **5**, 619 (1938).

[30] R. Berman, Proc. Roy. Soc. (London) **A208**, 90 (1951).

[31] P. G. Klemens, in *Solid State Physics*, edited by F. Seitz and D. Turnbull (Academic Press, New York, 1958), Vol. 7, p. 1.

[32] R. Peierls, Ann. Physik **3**, 1055 (1929).

[33] G. A. Slack and S. Galginaitis, Phys. Rev. **133**, A253 (1964) ; C. J. Glassbrenner and G. A. Slack, Phys. Rev. **134**, A1058 (1964).

[34] W. B. Joyce, "Thermal Resistance of Heat Sinks With Temperature-Dependent Conductivities," *Solid State Electronics*, Vol. 18, pp 321-322, 1975.

[35] C. Y. Ho, R. W. Powell, and P. E. Liley, in *Thermal Conductivity of the Elements: A Comprehensive Review*, New York: American Chemical Society and American Institute of Physics, 1975.

[36]. J. D. Achenbach, "Measurement Models for Quantitative Ultrasonics," *J. Sound Vibr.*, Vol. 159, pp 385-401, 1992.

[37]. E. Welsch, "Photothermal Surface Deformation Technique: A Goal for Nondestructive Evaluation in Thin-film Optics.," *Journal of Modern Optics*, Vol. 38, pp 2159-2176, 1991.

[38]. J. Z. Pan, "Detecting Small Fatigue Cracks by Acoustic Microscopy," *Fatigue and Fracture of Engineering Materials & Structures*, Vol. 16, pp 1329-1337, 1993.

[39]. S. Suresh, in *Fatigue of Materials*, (Cambridge University Press, Cambridge, 1991.)

[40]. H. Xiao and P. Nagy, "Enhanced Ultrasonic Detection of Fatigue Cracks by Laser-Induced Crack Closure," *J. Appl. Phys.*, Vol. 83, pp 7453-7460, 1998.

[41]. I. Mostafa, S. Hailu, G. Welsch, D. Hazony, and G. R. Halford, "Detection and Measurement of Fatigue Crack in HLSA Steel with a Dedicated Ultrasonic Pulse Transmission Method," *Intl. Journ. Of Fracture*, Vol. 85, pp 99-109, 1997.

[42]. R. P. Gangloff, R. S. Piascik, D. L. Dicus, and J. C. Newman, Jr., "Fatigue Crack Propagation in Aerospace Aluminum Alloys," *J. Aircraft*, Vol. 31, pp 720-726, 1994.

[43]. For example, Q. Shan and R. J. Dewhurst, "Surface-breaking Fatigue Crack Detection Using Laser Ultrasound," *Appl. Phys. Lett.*, Vol. 62, pp 2649-2651, 1993.

[44]. J. Krautkramer and H. Krautkramer, in *Ultrasonic Testing of Materials*, (Springer, Berlin, 1990).

[45]. C. B. Scruby and L. E. Drain, in *Laser Ultrasonic: Techniques and Applications*, (Hilger, Bristol, 1990), pp. 335-350.

[46]. J. A. Cooper, R. J. Dewhurst, and S. B. Palmer, "Characterization of Surface Breaking Defects in Metals With the Use of Laser Generated Ultrasound," *Philos. Trans. Roy. Soc.*, Vol. A 320, pp. 319-328, 1986.

[47]. R. J. Dewhurst, A. D. W. McKie, and S. B. Palmer, "Further Evidence of Two-Component Surface Acoustic Wave Reflections from Surface Breaking Slots," *Appl. Phys. Lett.*, Vol. 49, pp. 1694-1695, 1986.

[48]. D. A. Hutchins, F. Nadeau, and P. Cielo, "A Pulsed Photoacoustic Investigation of Ultrasonic Mode Conversion," *Can. J. Phys.*, Vol. 64, pp. 1334-1340, 1986.

[49]. J. A. Ogilvy and J. A. Temple, "Diffraction of Elastic Waves by Cracks: Application to Time-of-Flight Inspection," *Ultrasonics*, Vol. 21, pp. 259-269, 1983.

[50]. F. A. Ravencroft, K. Newton, and C. B. Scruby, "Diffraction of Ultrasound by Cracks: Comparison of Experiment with Theory," *Ultrasonics*, Vol. 29, pp. 29-37, 1991.

[51]. M. G. Silk, in *Research Techniques in Non-Destructive Testing*, edited by R. S. Sharp (Academic, N. York, 1977), Vol. 4.

[52]. M. N. Bassim, M. Dudar, R. F. Rifaat, and R. Roller, "Application of Acoustic Emission for Nondestructive Evaluation of Utility Inductive Reactors," *IEEE Transactions on Power Delivery*, Vol. 8, pp. 281-287, 1993.

[53]. H. Nayeb-Hashemi, P. Kisnomo, and N. Saniei, "Nondestructive Evaluation of Fiberglass-Reinforced Plastic Subjected to Localized Heat Damage Using Acoustic Emission," *Journal of Acoustic Emission*, Vol. 15, pp. 3342-3348, 1997.

[54]. M. Ohtsu, M. Shigeishi, Y. Sakata, "Nondestructive Evaluation of Defects in Concrete by Quantitative Acoustic Emission and Ultrasonics," *Ultrasonics*, Vol. 36, pp. 187-196, 1998.

[55]. T. Chady, M. Enokizono, and R. Sikora, "Crack Detection and Recognition Using an Eddy-Current Differential Probe," *IEEE Trans. On Magnetics*, Vol. 35, pp. 1849-1852, 1999.

[56]. T. Takagi, M. Uesaka, and K. Miya, in *Electromagnetic Nondestructive Evaluation*, edited by T. Takagi (IOS Press, N. York, 1997.), pp. 9-14.

[57]. R. Albanese, G. Rubinacci, and F. Villone, "An Integral Computational Model for Crack Simulation and Detection via Eddy-Currents," *Journ. Comput. Physics*, Vol. 152, pp. 736-755, 1999.

[58]. W. J. Baxter, "Imaging Short Fatigue Cracks with the Gel Electrode," *Journal of Testing and Evaluation*, Vol. 18, pp. 430-435, 1990.

[59]. R. L. Thomas, L. D. Favro, and P. K. Kuo, "Thermal Wave Imaging of the Temperature Distributions Around Propagating Cracks in Polymers," *Journal de Physique IV*, Vol. 4, pp. C4:595-601, 1994.

[60]. R. L. Thomas, L. D. Favro, and P. K. Kuo, "Thermal Wave Imaging of Propagating Cracks in Polymers," *Review of Progress in Quantitative Nondestructive Evaluation*, Vol. 13, pp. 1641-1656, 1994.

[61]. P. K. Sharp, D. E. Rowlands, and G. Clark, in *Technical Report DSTO-TR-0366*, (Defense Science and Technology, Melbourne, 1996).

CURRICULUM VITA
for
Michael Stelzer

DEGREES:

Master of Science (Electrical Engineering),
Old Dominion University, Norfolk, Virginia, August 2001

Bachelor of Science (Electrical Engineering Technology),
DeVry Institute of Technology, Columbus, Ohio, October 1990

SCIENTIFIC AND PROFESSIONAL SOCIETIES MEMBERSHIP:

Electronics Technician Association

HONORS AND AWARDS:

General Radiotelephone Operator's License with Radar Endorsement, 1999
Senior Certified Electronic Technician, Electronics Technician Association, 1998
Naval Nuclear Power Training Course, U.S. Navy, 1993
Honors Society, DeVry Institute of Technology, 1990
Who's Who Among American High School Students,
Celina Senior High School, 1985 and 1986